



UNIVERSIDAD DE CHILE
FACULTAD DE CIENCIAS FÍSICAS Y MATEMÁTICAS
DEPARTAMENTO DE INGENIERÍA MECÁNICA

**FABRICATION AND MECHANICAL CHARACTERIZATION OF
 $BA_{1-x}LA_xFE_{1-y}NB_yO_3$ ($0 \leq X$ AND $Y \leq 0.1$) MIEC PEROVSKITES**

MAGÍSTER EN CIENCIAS DE LA INGENIERÍA, MENCIÓN MECÁNICA

SAGARKUMAR ANILBHAI ZALAVADIYA

PROFESOR GUÍA:
DR. ALI AKBARIFAKHRABADI

MIEMBROS DE LA COMISION:
DR. VIVIANA ISABEL MERUANE NARANJO
DR. RODRIGO ESPINOZA GONZÁLEZ

SANTIAGO DE CHILE

2022

RESUMEN DE LA TESIS PARA
AL GRADO DE MÁSTER EN
INGENIERO MECÁNICO CIENCIA
POR: ZALAVADIYA SAGARKUMAR ANILBHAI
FECHA: 2022
PROFESOR GUÍA: ALI AKBARI-FAKHRABADI

**FABRICATION AND MECHANICAL CHARACTERIZATION OF
 $BA_{1-X}LA_XFE_{1-Y}NB_YO_{3-}$ ($0 \leq X$ AND $Y \leq 0.1$) MIEC PEROVSKITES**

La clase de compuestos que tienen una estructura de red cúbica o estructura cristalina ABX_3 se denominan perovskitas y la estructura se conoce como estructura de perovskita. Las características electroquímicas y eléctricas del óxido de perovskita pueden alterarse con la selección adecuada de los elementos del sitio A y del sitio B (o combinaciones de elementos) y, finalmente, hacerlos más adecuados como materiales de componentes de SOFC y membranas de separación de gases. El óxido de ferrita de bario ($BaFeO_{3-\delta}$), un óxido de perovskita de membrana de electrodo rico en hierro, se utiliza ampliamente en las SOFC debido a la rápida cinética de intercambio superficial y a su elevada actividad electrocatalítica. En condiciones severas, presenta una buena estabilidad térmica y química y se ha utilizado ampliamente en muchas aplicaciones. Las capacidades de estas membranas de perovskita integradas aún no se han desarrollado del todo, aunque existen múltiples ventajas asociadas a estas membranas como el bajo coste de la energía en comparación con la producción de oxígeno convencional. En el caso del óxido de ferrita de bario $BaFeO_{3-\delta}$ (BFO), que suele existir como un compuesto multifásico, existe un desajuste de radio iónico entre el Ba y el Fe. Recientemente se están llevando a cabo muchas investigaciones para estabilizar la estructura de la red cúbica, centrándose en los efectos del dopaje del sitio B con elementos metálicos altamente cargados como el lantano (La) y el niobio (Nb) y en la optimización de las estrategias de dopaje. La mayor parte de los trabajos se centran en el rendimiento de los nuevos materiales desarrollados y en sus propiedades de conducción, por lo que la bibliografía asociada a las propiedades mecánicas y a la caracterización basada en ellas es limitada, lo que define completamente el objetivo del trabajo. En este trabajo, $BaFeO_{3-\delta}$ dopado con La en el sitio A y Nb en el sitio B utilizando el método sol-gel para la síntesis de polvos. La estructura cristalina de los materiales preparados se estudió mediante XRD, que mostró que el dopaje del BFO con La estabiliza la estructura cúbica y el dopaje con Nb estabiliza la estructura tetragonal. El efecto del dopaje con La y Nb sobre la microdureza y las curvas de tensión-deformación se analizaron mediante ensayos mecánicos cíclicos.

RESUMEN DE LA TESIS PARA
AL GRADO DE MÁSTER EN
INGENIERO MECÁNICO CIENCIA
POR: ZALAVADIYA SAGARKUMAR ANILBHAI
FECHA: 2022
PROFESOR GUÍA: ALI AKBARI-FAKHRABADI

**FABRICATION AND MECHANICAL CHARACTERIZATION OF
 $BA_{1-X}LA_XFE_{1-Y}NB_YO_{3-}$ ($0 \leq X$ AND $Y \leq 0.1$) MIEC PEROVSKITES**

The class of compounds having a cubic lattice structure or ABX_3 crystal structure are called perovskites and the structure is known as perovskite structure. The electrochemical and electrical characteristics of the perovskite oxide can be altered with the appropriate selection of A-site and B-site elements (or element combinations) and eventually making them more suitable as SOFC components materials and gas separation membranes. Barium ferrite oxide ($BaFeO_{3-\delta}$), a perovskite oxide of iron-rich electrode membrane is widely used in SOFCs due to fast surface exchange kinetics and its high electrocatalytic activity. Under severe conditions, it exhibits good thermal and chemical stability and has been widely used in many applications.

The capabilities of these integrated perovskite membranes are not fully developed yet, even though there are multiple advantages associated with these membranes like low cost of energy when compared to the conventional oxygen production. In the case of barium ferrite oxide $BaFeO_{3-\delta}$ (BFO) which usually exists as a multi phase compound, there is an ionic radius mismatch between Ba and Fe. Recently many investigations are happening to stabilize the cubic lattice structure focusing on the effects of B-site doping with Ferro active highly charged metal elements like Lanthanum (La) and Niobium (Nb) and on the optimisation of doping strategies. Most of the work emphasises on the performance of newly developed materials and its conduction properties, and hence there are only limited literature's associated with mechanical properties and characterization based on its which completely defines the purpose of the work. In in this work, $BaFeO_{3-\delta}$ doped with La in A site and Nb in B site using sol-gel method for synthesis of powders. The crystal structure of prepared materials were studied by XRD, which showed that doping BFO with La stabilise cubic structure and doping with Nb stabilise tetragonal structure. The effect La and Nb doping on microhardness, stress-strain curves were analysed by cyclic mechanical testing.

Table of Content

1. Introduction	1
1.1. Perovskites Preparation Methods	3
1.2. Doping of ABO_3 Perovskites	4
1.3. Applications of Perovskites	5
1.4. Perovskites in SOFC	7
1.5. B site doping of $BaFeO_3$	10
1.6. Mechanical Properties	11
2. Literature Review	15
2.1. $BaFeO_{3-\delta}$ based cathode for SOFCs	15
2.2. Lanthanum doping of $BaFeO_{3-\delta}$	18
2.3. Niobium doping of $BaFeO_{3-\delta}$	20
2.4. Mechanical Properties of perovskites based oxides	23
2.5. Perovskite Applications in Membrane	25
2.6. Miscellaneous applications	28
3. Methodology	31
3.1. Materials	31
3.2. Sol-Gel Method	31
3.2.1. Principle	31
3.2.2. Fabrication of BFO	32
3.2.3. Fabrication of La-doped-BFO	32
3.2.4. Fabrication of Nb-doped-BFO	32
3.3. Calcination and Sintering	33
3.4. XRD (X-RAY DIFFRACTION)	34
3.4.1. Principle	34
3.4.2. XRD experiments	35
3.5. Thermogravimetric Analysis / Differential Thermal Analysis	36
3.6. Scanning Electron Microscope (SEM)	36
3.6.1. Principle	36
3.6.2. Applications	37
3.7. Mechanical Testing	37

3.7.1. Sample Preparation	37
3.7.2. Uniaxial Compression Test	37
3.7.3. Micro hardness test	39
4. Results And Discussion	40
4.1. Structural Characterisation	40
4.2. SEM Results	43
4.2.1. SEM results for BFO	43
4.2.2. SEM results for BFNbO:	47
4.3. Compression Tests	49
4.3.1. Microhardness Test	51
4.3.1.1. Effect of La and Nb doping on Micro Hardness and fracture toughness of BFO	51
5. Conclusion	55
Bibliography	56

Index of Tables

2.1.	Electronic conductivity, Ionic conductivity and CTE values of La based perovskite materials	21
2.2.	Fracture toughness and hardness of different perovskite oxides	26
3.1.	Materials components and their terminology	31
3.2.	List of Precursor and Quantity for BFO	32
3.3.	List of Precursor and Quantity for BLFO	32
3.4.	List of Precursor and Quantity for BFNbO	33
3.5.	A heat treatment plan for calcination and sintering	34
4.1.	Crystal structure of BFO	41
4.2.	Crystal structure of BLFO	42
4.3.	Crystal structure of BFNbO	43
4.4.	Micro-hardness measurements for BFO, BLFO and BFNbO	53

Index of Figures

1.1.	a) Unit cell of a cubic ABO_3 perovskite structure and b) framework of an ABO_3 perovskite structure where corner-shared oxygen octahedral extending in three dimensions)[9]	1
3.1.	(a) Dissolving metal nitrites in distilled water and (b) Dried gel	33
3.2.	(a) Drying in oven, (b) Calcination in heat treatment furnace, (c) Calcined powder and (d) Disc shaped Sintered sample	35
3.3.	Stages of XRD	35
3.4.	Schematic diagram of SEM	37
3.5.	Experimental setup for compression test	38
3.6.	(a) Sample specimen before applying speckle pattern	38
3.7.	(b) Specimen with speckle pattern by matte paint	39
4.1.	XRD Patterns of BFO powders calcined at Various Temperatures for 5 hours.	40
4.2.	XRD Patterns of BLFO powders calcined at Various Temperature for 5 hours.	41
4.3.	XRD Patterns of BFNbO powders calcined at Various 1000 °C for 5 hours.	42
4.4.	SEM images of BFO captured at (a) 330x at 200 μm (b) 980x at 80 μm by BSD	43
4.5.	SEM images of BFO captured at (a) 680x at 100 μm (b) 2900x at 20 μm by BSD	44
4.6.	SEM images of BFO captured at (a) 1450x μm at 50 (b) 2900x at 92.6 μm by SED	44
4.7.	SEM images of BLFO captured at (a) 20x μm at 12.1mm (b) 330x at 811 μm by SED	45
4.8.	SEM images of BLFO captured at (a) 780x at 344 μm (b) 1900x at 141 μm by BSD	45
4.9.	SEM images of BLFO captured at (a) 1900x at 141 μm (b) 1900x at 141 μm by BSD	46
4.10.	SEM images of BLFO captured at (a) 1950x at 138 μm (b) 1950x at 138 μm by BSD	46
4.11.	SEM images of BFNbO captured at (a) 1450x μm at 50 (b) 2900x at 92.6 μm by SED	47
4.12.	SEM images of BFNbO captured at (a) 1450x μm at 50 (b) 2900x at 92.6 μm by SED	47
4.13.	SEM images of BFNbO captured at (a) 1450x μm at 50 (b) 2900x at 92.6 μm by SED	48
4.14.	Strain vs Force for BFO	49

4.15.	Strain vs Force for BFO	49
4.16.	Strain vs Force for BFO	50
4.17.	Comparison of axial and lateral stress-strain curves of BFO, BLFO, BFNbO samples tested at room temperature.	50
4.18.	SEM images of indented BFO captured at (a) 1650x at 163 μm (b) 2150x at 30 μm by BSD	51
4.19.	SEM images of indented BLFO captured at (a) 1650x at 163 μm (b) 2150x at 30 μm by BSD	52
4.20.	SEM images of indented BFNbO captured at (a) 1650x at 163 μm (b) 2150x at 30 μm by BSD	52

Chapter 1

Introduction

Perovskites are a family of chemicals with a cubic lattice structure or an ABX crystal structure, where A and B are two distinct cations, and X is an anion that has a significantly different size. The rising attention on perovskites oxides has curtailed from their catalytic and electronic transport properties. [1][2] The doping in ABO_3 perovskites is found to be an effective strategy to augment its chemical stability [3] Doping of the A or B site of perovskite oxide highly influences the crystal structure which can be tailored from the hexagonal, orthorhombic, or rhombohedral phase to the cubic phase.[4] Doping in perovskites structures is modifiable which allows the catalytic properties to be optimized for sensor applications. [5] Perovskite oxides ABO_3 plays an important role in developing and providing sustainable energy through clean and efficient energy conversion from chemical to electrical energy, and membrane-based oxy-fuel combustion technology.[6] Apart from these, perovskites oxides also find application in photocatalysis owing to their electronic structure[7][8]

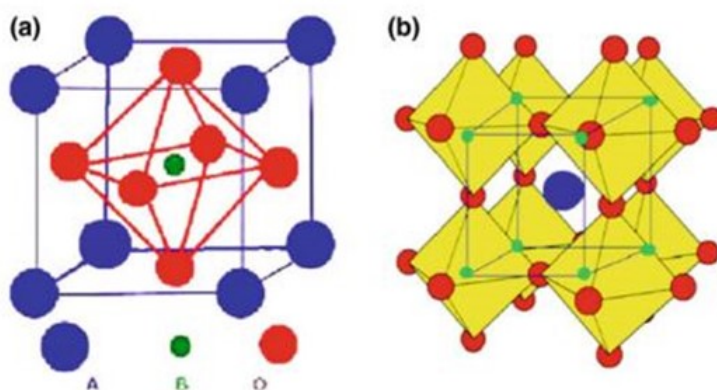


Figure 1.1: a) Unit cell of a cubic ABO_3 perovskite structure and b) framework of an ABO_3 perovskite structure where corner-shared oxygen octahedral extending in three dimensions)[9]

Perovskites with the general formula ABO_3 is constructed on the corner of the octahedron with shared layers and A cations located amidst these layers with a 12 fold site. Depending on the nature of the B site cation, these materials may demonstrate excellent magnetic or

electrical properties with potential oxygen vacancies. [8] [10] The main characteristics of ABO_3 perovskite are the corner shared octahedron assists in oxygen and electron transfer, and the larger A-site atoms in the perovskite structure stabilize it. Diverse categories of elements comprise the A- and B-site of ABO_3 perovskite owing to their requirements for the ionic radius. A-site cation has a larger size (1.10 - 1.80 Å) while B-site cation being medium in size (0.62 - 1.00 Å) on which the A-site cation is bounded by 12 oxygen anions and the B-site cation is enclosed by 6 oxygen anions. Alkaline earth, alkaline, and lanthanide ions in twelve-fold coordination constitute A-site cation, whereas B-site is primarily composed of transition metal ions in six-fold coordination with oxygen ions. [11] [12] [2] In addition to the A and B-site cation radius, the perovskite structure must have electrical neutrality, the sum of the charges of the A and B-site cations must correlate to the total charges of oxygen anions. Within the perovskite, partial substitution of A and B-site cations is thus feasible by doping with different cations of varied ionic radius and valency. Because of the perovskite structure's resilience to changes in its compositional ions, non-stoichiometry in perovskites is quite prevalent, resulting from either cation deficit in the A or B-site, anion deficiency, or anion excess [10][12]. Because of the stability of the BO_3 , A-site cations can be lost in the cation deficit scenario without causing the perovskite structure to collapse. In contrast, because of the significant variation in the structure formation and petite size of the B cations in perovskites, B-site cation vacancies are not energetically favoured. [1] [8].

The ideal and simple perovskite structure can be observed as a cubic close-packed structure in which the oxygen and the A-site cations are stacked along the cubic [111] direction in a cubic close-packing arrangement. The consequent octahedral holes are engaged by B-site cations [11]. The cubic phase has immense oxygen vacancy creation energy relative to the hexagonal phase [13]. In cubic structure, the vacancies are dispersed arbitrarily in the lattice which elevates the transport properties, making the cubic structure the most favourable [14]. The stability of cubic perovskite oxide is elucidated based on the tolerance factor given the symbol 't' which is defined by Liang et al 2013 [15]. If the tolerance factor is greater than 1 the perovskite oxide is found to be stable, the range is in the order of $0.75 < t < 1.0$ [2]. In a comparison of the two substitution sites, B-site substitution leads to rearrangement and restructuring throughout the crystal lattice which can lead to the formation of oxygen vacancy proportional to the substitution on A-site [16]. Since the B-site cations are the foremost accountable for the electrocatalytic activity of perovskite oxides. Hence, in order to refrain from the electrochemical properties, a suitable option of B-site ions is essential [17] [18] [19]. If the valence state is static for B-site ions, then the oxygen vacancies maintain electrical neutrality. It should be acclaimed that in certain circumstances the concentration of oxygen vacancy is not invariably proportional to the ionic conductivity [20]. Although the catalytic activity of perovskite oxides is directly connected to the B-site cation, modifying the A-site cation may result in a change of valence state and redox characteristics of the B-site cations vary the oxides catalytic activity [21]. The perovskite-type oxides, with general formula AB_3 , which are similar to the structure $CaTi_3$, act as a catalyst for hydrocarbon

oxidation owing to their thermal stability, and high activity. It is normally produced by ceramic methods which require high temperature and synthesize materials with surface area lower than $5\text{m}^2\text{g}^{-1}$ [22], which restricts its applications to a certain level. The application of perovskites in catalysis requires solids with an intense porous network. Voorhoeve et al (1976). has prepared a sequence of 20 perovskite oxides by ceramic method, in which the surface area is smaller than $1\text{m}^2\text{g}^{-1}$. Though it is easy to prepare, this method of preparation is considered as not attractive. The main disadvantage is the acquired solids have lack homogeneity, which is caused due to the unfinished reaction between the varied precursors [23]. High-temperature solid-state methods are gaining attention in the synthesis of perovskite phases with morphologies such as thin films and single crystals. The merits of these materials are their application in the current industry such as catalysts, fuel cells and optical devices [24]. Several perovskite oxide compounds synthesized by solid-state reaction shows polycrystalline structure. The obtained perovskite oxide materials by this synthesis method show weak chemical homogeneity, particle agglomeration and coarse particle sizes[6].

1.1. Perovskites Preparation Methods

Molten Salt Synthesis (MSS) is the simplest, flexible and cost-efficient technique to prepare perovskite oxide powders with uniform compositions, perfect structure and high purity [24]. Recently, Pb –based perovskite relaxors, Ba-based dielectric oxides, perovskite nanoparticles are produced by MSS methods [25] [26] [27]. Mechanical milling methods were also used to synthesize perovskite oxide nanoparticles such as BT, PT, PZ, and BST [28] [29]. Perovskite manganite $\text{Pr}_{0.7}\text{Ca}_{0.3}\text{MnO}_3$ nanopowders were prepared by ball milling method with the standard crystallite size of 29 nm [30]. When compared to the traditional ball–milling techniques, the Vibro-milling procedure has various merits such as finer particles, low cost, simple equipment, narrow size distribution, and pilot-scale manufacturing of nano powders[31]. Even though mechanical milling methods can produce nano particles at room temperature, it’s not applicable in large scale industries owing to the long processing time and its small batch sizes. Moreover, this intensive process creates critical impurities from the milling media. To overcome these issues and produce homogeneous and stoichiometric perovskite oxide powders, wet chemical methods such as sol-gel process [32], hydrothermal synthesis [33], microwave-hydrothermal synthesis [34], and microemulsion synthesis [35] have been developed. The sol-gel process is a wet-chemical technique to prepare several perovskite oxides. Here, the sol has dissolved metal-organic, metal alkoxide and metal inorganic salts which are followed by gel formation, calcination and sintering at high temperature. The perovskite oxides produced by the sol-gel process robustly depend on the initial precursor, pH and temperature. In the sol-gel process, the reacting species are homogenized at the atomic level, so diffusion distance is significantly reduced when compared to the solid-state reaction. As a result, the product could be obtained at a very low temperature. For example, multicomponent perovskite oxide nanopowders have been produced by the sol-gel process through meticulous stoichiometry [36] [37] [38]. Modified sol-gel methods such as the Pechini method, polymer complex solu-

tion and glycol-gel reaction have been developed to obtain the BFO nanoparticles. Flaschen (1955) first proposed an alkoxide hydroxide sol-precipitation method, that is majorly used to synthesize crystalline perovskite oxide nanopowders at lower temperatures and additional calcination is not mandatory at high temperatures. In this technique, hydrolysis and condensation are considered key inputs for crystal growth. By using this method, BT nanopowders could be produced at a lower temperature in the range of 80–100 °C by applying alkaline solution as an initial material [39] [40]. A hydrothermal method is also called the autoclave method and low-cost process, in which the preferred phases can be obtained when heating an aqueous insoluble salt suspension in an autoclave at modest temperature and pressure [41] [42]. This is method gives constant end products and restricts the impure phase’s formation which is mainly used to synthesize perovskite nanoparticles. The low-temperature solution combustion method is a proficient technique in chemical synthesis due to its less consumption of energy [43] [44]. This is integrated by heating the salt solution using citric acid, urea, and glycine [45] [46]. This technique has been used to produce perovskite oxide nanoparticles with a high surface area and plays a vital part in catalytic applications. Qi et al (2003) fabricated LaFeO_3 with a particle size around 30 nm using $\text{Fe}(\text{NO}_3)_3 \cdot 9\text{H}_2\text{O}$ and $\text{La}(\text{NO}_3)_3 \cdot 6\text{H}_2\text{O}$ as precursors and citric acid as combustion fuel at room temperature. The prepared LaFeO_3 has high coercivity, which indicates its capability to produce permanent magnets [47]. In the past decade, the microwave synthesis method has gained attention due to its significant properties such as retention time, environmentally friendly nature and energy efficiency [48] [49] [50]. This technique is integrated with other methods such as combustion, sol-gel, and hydrothermal to enhance its productivity [51]. Maggio Paul Pechini in 1967, first proposed the Pechini method, which is mainly related to the production of lead and alkaline-earth titanates and niobates [48] [52]. In this process, the formation of the complex between the metal ion and chelators takes place before it is dissolved in ethylene glycol, which is followed by heating, to synthesize polyester. This method has been considered as an alternative to the sol-gel method, also it is optimal for high purity perovskite oxides production [53].

1.2. Doping of ABO_3 Perovskites

ABO_3 perovskites can be doped with various A site and B site metal elements to form a ferromagnetic compound that improves their electrical and oxygen reduction reaction (ORR) activity and oxygen ionic conductivity [54]. This makes a useful mixed ionic electronic conductor (MIEC) that conducts both ions and electronic charge carriers (electrons and holes). An important function of ABO_3 perovskite oxides are as an electrode or an electrolyte component in solid oxide fuel cells (SOFCs), as oxygen separation membranes, and for membrane-based reactors [55] [56]. Electrodes manufactured from MIEC materials are used in state-of-the-art electrolysis cells (SOECs) and SOFCs [57] [58]. Alkaline earth (AE)-doped LaCrO_3 oxides are majorly used ceramic interconnects for high temperature owing to their tremendous electrical conductivity [59], high densification and chemical solidity in oxidation and reduction environment [60][61]. Pure LaCrO_3 is a p-type conductor that has less electrical conductivity,

but doping of Sr, Mg and Ca improve its electrical conductivity[62]. By doping in the A/B sites of ABO_3 perovskite oxides, enhances the ionic and electrical conductivity but also adjust the catalytic activity. Various studies have investigated the development of perovskite oxygen permeation materials by doping methodology, and various positive results were obtained [63] [55].

1.3. Applications of Perovskites

Perovskites find application in oxygen separators, solid oxide fuel cells, and membrane reactors which may be due to their ability to yield numerous perovskites oxide compositions and structures with hybrid properties [64]. A low-cost oxygen generation technique, according to energy scenario studies, might enable future technologists the production of clean energy on a techno-economic level. The potential of integrated perovskite membranes is not yet completely resolved, although it lowers energy costs compared to the conventional oxygen generation methods [65] [66]. Even though MIEC perovskites may be a viable option for membrane-based oxy-fuel plants, further improvements in membrane material and fabrication, process design, and external factors such as CO_2 penalties and energy legislation need to be explored to make this a promising technology in the near future [6] [14]. At present, photocatalytic HER is probably the best option concerned with sustainable energy. In the past decades, low cost, efficient and stable photocatalysts have gained popularity towards energy conversion. Perovskite type oxides are majorly studied by researchers for the production of H_2 through solar energy conversion due to their tunable structure and diversity of properties [67]. Moreover, computer simulation has been used to study the electronic structure and catalytic mechanism process. Fu et al (2012) reported that the amalgamation of TiO_2 and $SrTiO_3$ has altered the material electronic structure by creating vacancy (O, Sr), which boost the photovoltaic behaviour of $SrTiO_3$ for HER [68]. Chen et al (2012) evaluated the metal-doped $SrTiO_3$ photocatalytic activity by the DFT method and the results indicated that Rh-doped $SrTiO_3$ has shown the energy states near to the valence band level, which causes a reduction in the bandgap. This indicated that HER performance is amplified owing to the enhanced light absorption capability [7]. For photocatalytic HER, the niobate-based perovskites are widely studied [69]. Various single niobate-based perovskite oxides ($ANbO_3$), such as $NaNbO_3$, $KNbO_3$ [70] [71] and $AgNbO_3$ [72], have visible performance in HER in the presence of methanol as sacrificial agents. Moreover, pristine single niobate-based perovskite oxides cannot make H_2 generation effectively owing to their limitation such as broad bandgap, inadequate visible light absorption and less efficient charge separation. In addition, these materials have been modified through doping and loading methods to improve their photocatalytic HER activity [73] [74]. Among the various influencing factors, photo catalysts surface morphology has gained attention owing to its photocatalytic reaction on the surface. $NaNbO_3$ nanowires showed the utmost photocatalytic activity due to their crystallinity, surface-to-volume ratio, and anisotropic aspect [75]. Li et al (2008) have revealed that $NaNbO_3$ particle size is a significant factor than the surface morphology [76].

Zhou et al (2011) have stated that the porous $K_4Nb_6O_{17}$ microsphere has a porous structure and high surface area which shows significant activity for HER with an evolution rate of $30,000 \mu\text{molg}^{-1}\text{h}^{-1}$ in the methanol existence which acts as a sacrificial agent [77]. In a membrane reactor for POM, oxygen separation membrane prepared by mixed oxide-ion and electron conductor (MIEC) is considered as the key elements of the entire reactor, and its materials are comprehensively studied in research. For some ceramic oxygen permeation membranes, the application of mixed ionic and electronic conductors (MIECs) is considered a suitable contender. In the past decade, several MIEC materials have been developed, and their structure and properties were studied comprehensively. Among the materials studied, the oxygen-deficient perovskite-type oxides are represented as favourable materials for oxygen permeation membrane owing to the high concentration of oxygen vacancy and ionic migrating paths of isotropic oxygen. The A-site cations are generally lanthanides or alkaline earth metal elements such as Ba, Sr, La, Pr etc., and the B-site cations are usually transitioning metal elements such as Co, Fe, Mn, Cu, Cr and Ce [78] [79] [80] [81]. During the oxygen permeation, most of the perovskite-type materials are altered at A- site or B- site.

Among the various perovskite-type oxygen permeable materials, cobalt-based perovskites have gaining increased observation owing to the high permeability of oxygen and tremendous surface oxygen exchange kinetics. The application of cobalt-rich materials is challenging owing to their expensive and toxic nature. Moreover, the phase decomposition of Co-based perovskite membranes, included with reduction of cobalt ions at high temperatures with decreased atmospheric conditions, leads to weakening of membrane structure and deterioration of the oxygen permeability [80] [70] [82]. The instability of cobalt-based perovskite materials prevents their practical applications. So the researchers have modified these materials by replacing cobalt with few high valency anti reduction metal ions such as Mo, Nb, Zr and Ta. Moreover, this method is not able to resolve the structural instability completely [83] [84] [85]. Hence, the cobalt-free materials have gained attention and numerous materials have been studied such as Ba–Ce–Gd–O [86], Y–Ba–Cu–O [87] and La–Sr–Fe–Ga–O [88]. The main demerit of these materials is their limitation to structural stability, large scale production and obtaining homogeneous materials. On contrary, the oxygen separation membrane is composed of few elements and having exceptional structural stability and high oxygen permeability. Cobalt–ferrite, Sr (Co, Fe) O_{3-1} (SCF) transport properties increases at a high temperature around 1000°C , however, the pattern of brown millerite causes structural instability at the temperature around $700\text{-}900^\circ\text{C}$ [14] [89]. To conquer this, the partial replacement of Sr (2+) with various cations, like La (3+) and Ba (2+) is majorly studied under continuous improvement [14][90] [91].

The existence of Lanthanum creates a charge imbalance [90] [91], which is remunerated by the formation of oxygen vacancies; the rhombohedral structure of (La, Sr) (Co, Fe) O_{3-1} (LSCF) compounds at room temperature are converted into the preferred cubic structure at the temperature range $700\text{-}850^\circ\text{C}$. Further, the partial replacement of Sr with Ba cre-

ates cubic (Ba, Sr)(Co, Fe)O₃₋₁ (BSCF) compounds, with enhanced permeation properties. Various permeation study results [55] [92] [93] [94] [95] [96] showed that, among the two mentioned materials, the best compositions identified are La_{0.6}Sr_{0.4}Co_{0.2}Fe_{0.8}O₃₋₁ (LSCF6428) and Ba_{0.5}Sr_{0.5}Co_{0.8}Fe_{0.2}O₃₋₁ (BSCF5582), which have adequate structural stability while heating/cooling among the ambient and operating temperature.

To obtain better ORR activity or ionic conductivity at lower temperatures, a broad range of perovskite-type oxides have been created, which is necessary for enhanced SOFC performance that displays excellent dependability and stability [97]. Both the performance of prospective perovskite materials and the manufacturing techniques for these materials have scope for improvement. Process intensification is one of the benefits that may be derived from the perovskite membrane reactor technology. The membrane's capacity to withstand high temperatures and pressures is the key to its effectiveness [6] [66]. As a new field, the use of Perovskites in oxygen separation, solid oxide fuel cells, and membrane reactors encounter a variety of challenges. Perovskite materials require further study and development in material science and engineering before their application can be widely presented [98].

1.4. Perovskites in SOFC

SOFCs has paramount environmental credits owing to their greater efficiency as a source for the generation of electricity which gains more attention in recent times [99][100]. Substantial research attempts have been made to curtail the working temperature of SOFCs, employing fabricating advanced electrolyte materials, new cathode materials with greater ionic conductivity and catalytic activity to overcome the polarisation losses [101] [102]. In a typical SOFC process, the electrochemical reduction of molecular oxygen occurs over the cathode to oxygen ions, the incorporation of the as-formed oxygen ions into the electrolyte bulk, the diffusion towards the anode at the electrode-electrolyte interface, and the reaction of oxygen ions with fuel over the anode surface ensure to produce electric power and heat. The power yield of SOFCs is evaluated by the electrode polarization resistance and ohmic resistance of the electrolyte. The meagre activity of cathode for the ORR has been the foremost hindrance to acquiring the high-power density of SOFCs at reduced temperatures. The extensive application of SOFCs technology, thus strongly depends on the fabrication of highly efficient electrode materials for ORR and high oxygen reduction reactivity. [6][103] [104].

Perovskite oxides (ABO₃) functions as an energy source that is environmentally active by converting chemical energy into clean and efficient electrical energy. The oxy-fuel combustion using membranes as an electrode or electrolyte in technologies such as the use of oxygen in solid oxide fuel cells (SOFCs), membrane separation and membrane-based reactors are few examples [105] [106]. Lanthanum cobaltite-based perovskites have been extensively studied as possible SOFC cathodes with ceria-doped electrolytes. xSr_xCoO_{3-d} (LSC) perovskites exhibit good oxygen-ionic conductivity and ultrahigh electronic conductivity of about 1000 S cm⁻¹, but poor phase stability [107]. To overcome the stability problem, thermal expansion

and cost of cobalt, a partial substitution of cobalt ion with iron has been found to be effective in terms of phase stability [108] [109] [110].

Significant attempts have been made to alter the phase stability and electrochemical activity of LSC by substituting different rare earth metals for La [111] [112] [113]. Takeda et al. revealed that the substitution of La with Gd, resulting in the production of $\text{Gd}_{1-x}\text{Sr}_x\text{CoO}_{3-d}$ oxides, had a detrimental impact on electrode performance [114]. Doping of various elements has resulted in a variety of properties intended for a particular application. As per experimental pieces of evidence, the iron cation is more resistant in a reducing environment, additionally, Fe with flexible oxidation and the spin state subsidizes to high catalytic activity [115] and $\text{Fe}^{4+}/\text{Fe}^{3+}$ ratio promotes the electrical conductivity [116]. BaFeO_{3-d} (BFO) is one of the most electrochemically active iron-based cathodes. A pure BFO, on the other hand, exists as a combination of phase structures. Different dopants have been introduced to BFO to stabilise the cubic phase at lower temperatures such as Ca, La, Y in the A-site, or Ln, Ce, Zr, Ni, Cu in the B-site [117] [6].

Perovskites are also used in membrane reactors based on oxygen transfer membrane (OTMs). They have drawn a lot of interest since they combine separation and chemical processes in a single unit [6] [118]. A few advantages of using OTMs based perovskites in reactions include (1) no necessity to separate the nitrogen from the air; (2) eradicating certain products through the membrane to increase conversion; and (3) the gradual usage of oxygen reduces contact with partially oxidised products [6] [119] [120]. The foremost purpose of perovskite in OTM includes; refining the selectivity of distributor category membrane reactors and upgrading the conversion in the extractor category of the membrane. The properties which enrich the performance of OTM are high ionic and electronic conductivity with a steady structure [6].

Electrolysis cells of the highest technological level (SOECs) so-called solid oxide fuel cells (SOFCs) use electrodes built of MIEC materials. If mixed properties i.e. ionic and electronic conducting properties are anticipated, this could be accomplished by stimulating metal cation with a lesser valence in A-site and incorporating transition metal ions in the B-site respectively[2]. SOFC produce power by electrochemically oxidising a fuel. Fuel cells are classified depending on their electrolyte material, and SOFCs often use a solid oxide or ceramic electrolyte for characterization [6] [105].

As the perovskite structure (ABO_3) allows for a wide range of compositional changes, there is a lot of potential for generating new useful materials. To improve their suitability as SOFC components and gas separation membranes, perovskite oxide can have its electrochemical and electrical properties adjusted by selecting the appropriate A-site and B-site elements (or element combinations) [18] [19]. Practically the cathode of SOFC must be porous to improve the transport of gas and deliver greater active sites for ORR. Since it is difficult

to explore the properties of porous cathode materials as stated by Chen et al 2012, in such complications thin-film electrodes should be used [7].

A perovskite oxide of an iron-rich electrode membrane, barium ferrite oxide (BaFeO_3) is widely used in SOFCs due to its high electrocatalytic activity and fast surface exchange kinetics. It has a high thermal and chemical stability and is broadly employed in a wide range of applications [121] [122] [123]. Ferrite based perovskites LaFeO_3 , SrFeO_3 and SmFeO_3 are commonly used as anodes in SOFC. But the lack of chemical stability and poor electrical conductivity has made the researchers focus on doping with other metal ions. Thus, metal cations with a higher oxidation state can elevate the stability and the valency of Fe in the perovskites [83] [124]. Newly iron-based perovskite oxides $\text{Ba}_{1-x}\text{LaFeO}_{3-\delta}$ with a minor replacement of Ba^{2+} with La^{3+} stabilizes the oxygen vacancy disordered structure of perovskite and improving its oxygen permeability as well [125] [97] [126]. Significant attention has lately been devoted to the study and to create solid oxide materials capable of conducting oxygen ions into their crystal lattice [127].

MIECs can transport oxygen over a potential gradient when employed as membranes in two separate atmospheres with varying oxygen potentials. The use of perovskite-based oxygen separation membrane technology can be integrated with power-generating cycles that collect carbon dioxide (CO_2) via oxy-fuel combustion [6] [128]. MIEC perovskite exhibits triple phase boundaries (TPBs), the interfacial contact area amongst electrons, oxygen ions and oxygen gases. Hence TPB is the region where the electrode reactions occur, hence larger TPB leads to more active sites and superior performance. This type of perovskite reveals explicit reaction and faster transport properties than the conventional perovskite oxides [134, 135]. The first MIEC cathode material with TPB used was $\text{Sm}_{1-x}\text{Sr}_x\text{CoO}_{3-\delta}$ which has good chemical compatibility as well as higher electronic conductivity leading to greater electrocatalytic activity. Similar to the perovskites phase transition occurs from cubic to tetragonal phase, subsequently decreasing the electrocatalytic activity [111] [112] [129]. Hence certain modifications are required for the MIEC cathode materials to sustain the impeccable electrocatalytic activity [130] [4].

To overcome the issues, owing to the incorporation of Co, Fe as perovskites cations as well as to utilize the merits of these ions in MIEC materials, partial substitution of the perovskites B-site cation with five valence cation was reported [131] [132]. As discussed in the earlier part of the introduction, a tolerance factor greater than one is found to be stable which can be achieved by doping a larger radius cation as a partial substitute for Fe cations [2] [133]. One such cation is Nb^{+5} which can increase the stability of the cubic phase and permeability of oxygen relative to the perovskites that contain exclusively Co or Fe as cations [134]. Nb also plays a crucial role in sensing applications as reported by Akhtar et al 1997. When Nb^{+5} ions were doped in the perovskites containing Fe sites substantial change in the structure of the Fe environment takes place [135].

1.5. B site doping of BaFeO₃

B site defines most of the critical properties of the perovskite materials, and the stability can be enhanced by doping transition elements at the B site [136]. Doping high valency cation at the B site improves the stability of the Perovskites and as well as its structural stability. This also elevates the electrical conducting ability of BaFeO₃ Perovskites. The Fe ions in the B site possessing variable oxidation and spin state develops higher catalytic activity. B site doping with transition metals such as Mn, Fe, Co, Ni, Ca, Mg and Nb have been studied by many researchers. The synchronised occurrence of Co and Fe cations at the B site assist to obtain desirable functional properties [137] [138]. Gao et al reported that doping high valency Nb⁵⁺ ions at the B site improves the structure and properties of the material to a greater extent. It was also reiterated that doping Nb⁵⁺ cations not only enhance the stability of the cathode materials for SOFC applications but also improves its ORR activity[139].

Apart from A site doping, B site doping generates higher oxygen diffusion kinetics than A site. The work by Zhang et al suggested that rare earth element Pr doping at the B site augments the electrochemical property owing to the higher oxygen vacancies [140]. The use of Pr as a dopant is unique as it exhibits 3+ and 4+ oxidation states similar to Fe in the B site of the parent oxide, which bring about fascinating electrical properties [141]. It was reported that B site doping of BeFeO₃ may have a lower electrical conductivity but the oxygen bulk diffusion kinetics is faster which is instigated from its lattice expansion. When the quantity of oxygen vacancies is similar on the A and B sites, the B site dopant is more supportive for overall diffusion kinetics and ORR performance. A site doped BeFeO₃ was found to exhibit higher electrical conductivity than B site doped cathode materials since B site dopants incorporated is redox inactive compared to iron [142]. Consequently, Fe improves the ionic conductivity and phase stability of the cathode active material which increases the power density of SOFC [143]. A single dopant at the A or B site stabilizes the cubic structure with enriched stability. The dopants for the A site are smaller than the parent Ba²⁺ and B site dopant are larger than the parent Fe³⁺ and Fe⁴⁺ ions [144].

In terms of oxygen vacancies, neither of the dopants from the A or B site was found to be beneficial over the other in increasing the oxygen vacancies as illustrated by [145]. After doping A site, lattice size is reduced compared to the parent perovskite material leading to volume shrinkage for transport of ions. This may be considered as the possible reason for faster oxygen diffusion kinetics [143]. The electrical and mechanical properties highly depend upon the microstructural properties. Extreme hardness and boosted ionic conductivity can be achieved for perovskites without any impurity phase [15].

1.6. Mechanical Properties

Elastic constants are used to find out crystal response to external forces described by the elastic modulus, Young's modulus, shear modulus and Poisson's ratio. This has a vital role in assessing various properties such as stability, hardness, stiffness, kind of bonds and material ductility [146] [147]. The mechanical properties allow a practically precise structural analysis of SOFC stacks, which in turn emphasizes the requirement of mechanical characterization. The instrumentation indentation method permits the assessment of the effects of composition and microstructure of LSGM on the hardness at micro- and nanometric length scales. From these results it is inferred, that by defining the LSGM hardness in film/substrate at room temperature, one can conclude the ionic conductivity within the studied temperature range [143].

Young's and Shear modulus mainly depend on the porosity. SOFC ceramic materials strength is not a built-in property that acts as stress concentrators but mainly depends on the manufacturing process defects. Creep occurs if the material is consistently loaded at a temperature near half of its melting point. Based on the mechanism, continuous deformation is categorized into three groups such as diffusion, viscous and dislocation creep. The material creep actions may vary when it undergoes tensile and compressive stress [148]. Creep parameter extraction from bend tests data is considered complex, due to the stress gradient in the sample [149][150]. The elastic modulus of $\text{La}_{0.9}\text{Sr}_{0.1}\text{Ga}_{0.8}\text{Mg}_{0.2}\text{O}_{3-\delta}$ (LSGM1020) and $\text{La}_{0.8}\text{Sr}_{0.2}\text{Ga}_{0.8}\text{Mg}_{0.2}\text{O}_{3-\delta}$ compositions are around 175-195 GPa.

Pathak et al. [2009] evaluated the elastic modulus for the pure and dense (5% porosity) LSGM2020, and attained similar values by two different methods such as resonance technique (175 ± 4 GPa), and 4-point bending test (176 GPa). The shear modulus for LSGM2020 composition was about 70 GPa which is evaluated by torsional resonance frequency [151]. Baskaran et al (1999) estimated hardness and indentation resistance at room temperature for various compositions of lanthanum gallate doped with Ba (LBGM1020), Ca (LCGM1020), Sr (LSGM1020, LSGM2015, LSGM2020), and un-doped. The hardness for LSGM compositions lies between 7-8.2 GPa and the indentation resistance was about around 0.9–1.1 MPa $\sqrt{\text{m}}$ [152]. The perovskite-structured materials permeability is greatly dependent on microstructure, especially grain sizes. It has been reported that the $\text{Ba}_{0.5}\text{Sr}_{0.5}\text{Fe}_{0.8}\text{Zn}_{0.2}\text{O}_{3-\delta}$ membranes permeation rate increases with increasing grain sizes [153]. On the other hand, the permeation rate of $\text{SrCo}_{0.8}\text{Fe}_{0.2}\text{O}_{3-\delta}$ decreases with increasing grain size [154]. In BSCF, it has been observed that the oxygen permeation flux increased with an increase in grain size [155]. While membrane sintering, the oxygen permeation can be improved by an increase of dwell time. The massive variation in grain size distribution among surface and fracture surfaces leads to the sandwich –effect. Here the difference in size should be unbiased, which results in oxygen permeation decline.

Wang et al (2016) investigated the microstructural evolution and mechanical properties

of $\text{Ba}_{0.5}\text{Sr}_{0.5}(\text{Co}_{0.8}\text{Fe}_{0.2})_{1-x}\text{NiXO}_{3-\delta}$ with $X=0, 2, 4, 6, 8, 15, 20,$ and 25 mol%. Hardness and Young's modulus increase with increasing the content of Ni doping from 0 to 8 mol%, because of the lattice distortion strain caused by the solute Ni^{2+} and the precipitation of the secondary-phase NiO. It has been observed that doping also can influence ceramic materials grain aspect ratio. Nonetheless, the grain aspect ratios of BSCF doped with various content of Ni are about 1.8 which is similar to the pure BSCF [156]. Recently, many studies have been focused on substituting rare earth metal ions (e.g. Zr, Bi, La and Gd) to transform the microstructure of BSCF based materials, and to improve the performances [157] [158]. To eradicate the spin transition of the Co^{3+} effect, the focus has been on the partial substitution of B site cations (Fe and Co). Kharton et al (1999) and Wei et al (2010) reported that Ni doping has been established to advance the various properties of perovskite-structured materials such as $\text{LaFeO}_{3-\delta}$ and $\text{GdBaCo}_{0.2}\text{O}_{5+\delta}$ [159] [160].

Yang et al (2012), has studied the establishment of nanoindentation on nanoscale mechanical properties of BKCZY oxides. The results showed that the grain size is closely related to the concentration of K doping. The BKCZY oxides have a hardness between $5.2\pm 0.1 - 9.3\pm 0.2$ GPa and Young's modulus is between $138.5\pm 3.6 - 179.2\pm 2.3$ GPa [157]. Chou et al (2000) examined the mechanical properties of a mixed-conducting perovskite $\text{La}_{1-x}\text{Sr}_x\text{Co}_{0.2}\text{Fe}_{0.8}\text{O}_3$ ($x=0.2-0.8$). Young's and Shear modulus, hardness, nano indentation, fracture toughness, and biaxial flexure strength were determined. The increase in strontium content increases the average grain size from 1.9mm for LSCF-8228 to 21.9 mm for LSCF-2828. It has been observed that Young's and Shear modulus was 152–188 GPa, and 57–75 GPa respectively. Also, the Biaxial flexure strength was about 160 MPa for lesser strontium content (0.2 and 0.4). Moreover, the results indicated that LSCF materials with less strontium content have adequate mechanical properties, which make them capable materials for several applications [161].

One of the most widely used AB_3 perovskite oxides is BaFeO_3 , it exists as a hexagonal structure with lattice parameters $a = 0.568$ and $c = 1.386$ nm respectively [162] [163] [164]. When developed as thin films, BaFeO_3 behaves as a pseudo-cubic perovskite oxide where $a = 0.412$ nm [165] [166]. Depending on the temperature and pressure conditions BaFeO_3 can be oxygen-deficient, which influences its magnetic properties. An increase in the oxygen deficiencies deteriorates its ferromagnetism as reported by Mori 1970 [166]. The reason for the increase is ascertained from the change in the valence state of Fe ions, where Fe^{4+} decreases consequently increasing Fe^{3+} ions. Which is corroborated by an increase in the lattice spacing of the material with decreasing oxygen vacancies [167] [166] [164]. Reports suggest that BaFeO_3 show transition from antiferromagnetic to ferromagnetic around 160 K. Additional transition occurs around 250 K from ferromagnetic to the paramagnetic state [167]. The ferromagnetism behaviour occurs utilizing superexchange energy interaction of $\text{Fe}^{3+}-\text{O}^{2-}-\text{Fe}^{3+}$ linkage [168] [169]. Depending on the preparation method and conditions, $\text{BaFeO}_{3-\delta}$ can exhibit multiple phases such as monoclinic, triclinic, cubic, orthorhombic and hexagonal structures [170] [162] [166] [164]. The doping of various metal ions in the A and

B sites stabilizes the cubic structure of $\text{BaFeO}_{3-\delta}$ [18].

$\text{La}_2\text{NiO}_{4+\delta}$ (LNO) is another widely used promising MIEC electrode material for SOFC but suffers from slow ORR kinetics [65]. To tune the properties necessary for electrode applications, Kolchugin et al in 2016 suggested the doping of Sr^{2+} or Ba^{2+} to produce additional electron holes and hence its conductivity [171]. $\text{La}_{1.8}\text{Sr}_{0.2}\text{NiOO}_{4+\delta}$ (LSNO) and $\text{La}_{1.8}\text{Ba}_{0.2}\text{NiOO}_{4+\delta}$ (LBNO) are prepared by Akbari et al in 2016 and subjected to XRD and mechanical studies [172]. When phase separation of the prepared LSNO and LBNO was observed, the dopant distributions within the material is integrated with the method involved, sintering profile and annealing conditions [169]. Upon doping LNO with Sr^{2+} and Ba^{2+} , the elastic modulus remains unaffected for Sr^{2+} and in the case of Ba^{2+} higher value of elastic modulus was reported. Similarly, the microhardness of LBNO was higher than LNO as well as LSNO at analogous temperature. On the other hand, the fracture toughness of Sr^{2+} doped LNO was higher than Ba^{2+} doped LNO and even the parent LNO [173]. The decrease is owing to the bigger average grain size at elevated temperature which is also reiterated by Chen et al in 2012 [7].

The effect of substitution of Fe in $\text{La}_{0.6}\text{Sr}_{0.4}\text{M}_{0.1}\text{Fe}_{0.9}\text{O}_{3-\delta}$ (LSMF) perovskite nanostructures by doping Co (LSCF), Ni (LSNF) and Cu (LSCuF) at the B site and its mechanical properties were studied by Akbari et al in 2017 [172]. The XRD pattern of the calcined material discloses the mixture of rhombohedral and orthorhombic phases in addition to the presence of a secondary phase (MFe_2O_4). Among the materials synthesized, LSNF shows improved hardness, low fracture toughness and ferroelastic behaviour. LSCF illustrated a higher fracture toughness than the other dopants which may be due to the phase transition from ferroelastic to paraelastic [174].

Ferroelasticity, where the material exhibits a non-linear behaviour and hysteresis in strain curve with perovskite oxides such as LaMO_3 ($\text{M} = \text{Co}, \text{Fe}, \text{Al}$ etc) [175]. Araki et al in 2016 demonstrated that the ferroelastic mechanical characteristics can be evaluated using spherical indentation by experimentally determining indentation stress versus strain curve. The indentation test also known as the impression test provides constant stress and constant load which simplifies the theoretical analysis. Akabari et al in 2018 investigated the mechanical characteristics of LaCaO_3 perovskite using the impression technique. The impression creep which ensues during the loading and unloading at the end of each cycle did not disturb the creeping trend observed [176]. Impression creeps of the prepared LaCaO_3 increase with the varying rate at different applied loads and attains saturation owing to the part affected ferroelastic domains [177]. The coercive stress for the deformation of ferroelastic material can be determined by sensing a deflection on a stress-displacement curve at the time of loading. Hence it can be concluded that the impression method is a feasible alternative to a compression test in unfolding ferroelastic creep [173].

For the perovskite applications in SOFCs, all the components integrated should have the ability to sustain the mechanical stress during the operation of SOFC [178]. Anticipated mechanical properties are vital to avoid failures such as fractures, cracks and delamination.

Most research focuses on the electrical properties, electrochemical properties, different synthesis strategies, structural defects, non-stoichiometry etc [179]. But, mechanical properties also play a vital role in tailoring the appropriate properties of perovskite oxides for SOFC applications. Hence the current work focuses on the development of cathode active material with appropriate mechanical properties its characterization and application in SOFC.

Chapter 2

Literature Review

Solid oxide fuel cells (SOFCs) convert chemical energy directly into electrical energy based on the electrochemical principles and are considered as a growing technology for static power production with minimal impacts on the environment. The three active components in SOFC are the anode, cathode and the electrolyte. One of the major drawbacks in SOFCs is that the conventional LSM cathodes operates at high temperature and the cell assembly also requires higher temperature [180]. At lower temperature degradation of the electrochemical cell occurs, which declines the electrochemical performance and overall efficiency of the fuel cells. This could be overcome by developing new materials which could operate at reduced temperature without compromising its efficiency [181].

Multivalent B site dopants are selected based on their capability for a better redox reactions during the operation of SOFCs. This feature leads to the formation of disorder which augments the hopping mechanism, where the lower charged cations transform to higher positively charged cations. This process continues until variable oxidation state material exists in ABO_3 perovskites [182] [183]. In the search for hybrid material with versatile properties and flexibility, ABO_3 type perovskites come into play. Since, different dopants can be synergized in the A and B site which has the possibility to develop several electrode materials for its use in SOFC with wide range of properties tunable for differing applications [6].

This chapter will focus on the electrode materials developed based on ABO_3 perovskite oxide for SOFCs application, their merits, demerits and characteristics of the developed material in enhancing the SOFCs performance.

2.1. $BaFeO_{3-\delta}$ based cathode for SOFCs

One of the most outstanding electrochemically active iron based perovskites oxide cathode material is $BaFeO_{3-\delta}$ (BFO) [184]. BFO shows chemical and thermal stability along with enhanced electrocatalytic activity, fast surface exchange kinetics, owing to the presence of Fe ions which can exhibit multiple valency demonstrating stronger resistance [16] [79]. When $BaFeO_{3-\delta}$ was used as a single cell cathode power density of 870 mWcm^{-2} obtained at 7000

°C, indicating its high catalytic activity [184]. But $\text{BaFeO}_{3-\delta}$ exists as a multiphase oxide because of the mismatch in the ionic radius of Ba and Fe. It is known that the cubic lattice structure leads to better performance for the designated applications of perovskite type oxides [6]. To obtain the cubic lattice structure various cations like La, Sm, Zr, Nb, Sn etc are doped into the $\text{BaFeO}_{3-\delta}$. Dong et. al in 2016 prepared Sn doped $\text{BaFe}_{0.95}\text{Sn}_{0.05}\text{O}_{3-\delta}$ as a cathode material for intermediate SOFCs. The developed material has superior ORR kinetics, electrocatalytic activity and good stability [185].

For instance, Liu et al in 2018 fabricated SOFC cathode material $\text{BaM}_{0.05}\text{Fe}_{0.95}\text{O}_{3-\delta}$ ($M = \text{Ti, Zr, Ce}$) to operate at intermediate temperature. When Ti was used as dopant, the material has complex phase which varies with temperature. Zr as dopant shows cubic phase above 400°C whereas, Ce displays the cubic perovskite structure up to 10000°C. The three dopants used in this case has the same valence state of 4+, Ce^{4+} forms the stable cubic structure due to the smaller length between Ce-O and Ba-O bonds. The power density for $\text{BaCe}_{0.05}\text{Fe}_{0.95}\text{O}_{3-\delta}$ was 482 mWcm^{-2} at 750°C and has conductivity of $5\text{-}9 \text{ S cm}^{-1}$ [186].

A systematic investigation on dopants on A and B site of the parent $\text{BaFeO}_{3-\delta}$ was evaluated as a cathode material for SOFCs. For A-site, dopants like La^{3+} , Sm^{3+} , Gd^{3+} and for B-site dopants such as Zr^{4+} and Ce^{4+} were chosen as partial substituents respectively. Substitution of 5 mol % was selected for this study since, substitution less than 5 % can't stabilize the cubic phase. On the other hand, substitution higher than 5 % reduces the oxygen vacancy with decrease in the lattice energy of the material. When electrical conductivity was compared among the dopants at A and B site, BFO with A-site doping elucidate increased conductivity than the dopants in B-site [187].

Oxygen vacancies can be generated by doping aliovalent cations resulting in elevated oxygen ion conductivity of the materials. An electrochemical reaction for the absorbed oxygen molecules should be converted into anions and allowed to permit through the electrolyte material and the cathode [Ranlov 1995] [188]. $\text{Ba}_{0.95}\text{La}_{0.05}\text{FeO}_{3-\delta}$ and $\text{BaFe}_{0.95}\text{Zr}_{0.05}\text{FeO}_{3-\delta}$ with higher oxygen vacancies performs better in comparison to the other dopants used. When considering the oxygen vacancy as well as the mobility of oxygen ions, B-site doping is more supportive for the ORR operation as well as for the diffusion kinetics [145]. Ba doped $\text{La}_{1-x}\text{Ba}_x\text{Co}_{0.2}\text{Fe}_{0.8}\text{O}_{3-\delta}$ investigated by Gedziorowski et al stated that with increase in the amount of Ba, oxygen non-stoichiometry increases with declined distortion in the perovskite structure. The high conductivity observed in the prepared material with $x = 0.4$ is still not adequate for SOFC application. In conclusion, the electrode material with Ba as dopant have low conductivity than Sr doped materials [189].

A symmetrical arrangement of SOFC with cathode and anode being the same material has been put forward and inspected by several researchers [190]. Symmetrical SOFCs is beneficial over the conventional SOFC since, the former excludes formation of coke and sulphur poisoning and also its cost effective. Many perovskites oxides of the type ABO_3 have been used for symmetrical cell fabrication like $\text{La}_{0.75}\text{Sr}_{0.25}\text{Cr}_{0.5}\text{Mn}_{0.5}\text{O}_{3-\delta}$, $\text{La}_{0.5}\text{Sr}_{0.5}\text{Cr}_{0.5}\text{Ti}_{0.5}\text{O}_{3-\delta}$ [191], $\text{La}_{0.4}\text{Sr}_{0.6}\text{Cr}_{0.2}\text{Fe}_{0.7}\text{Nb}_{0.1}\text{O}_{3-\delta}$ [192] and so on. Double perovskite oxide $\text{LaSrMnCoO}_{5+\delta}$

with cubic structure shows an average CTE value of $15.8 \times 10^{-6} \text{ K}^{-1}$ in the temperature range of 30-1000°C and electrical conductivity of $111\text{-}140 \text{ Scm}^{-1}$ [193]. The coefficient of thermal expansion (CTE) value reported is higher compared to the standard electrolytes such as yttria stabilized zirconia (YSZ), $\text{Sm}_{0.2}\text{Ce}_{0.8}\text{O}_{1.9}$ (SDC), $\text{La}_{0.9}\text{Sr}_{0.1}\text{Ga}_{0.8}\text{Mg}_{0.2}\text{O}_{2.85}$ (LSGM) [194] [195] [196].

A symmetrical cell with $\text{BaFe}_{0.9}\text{Zr}_{0.1}\text{O}_{3-\delta}$ (BFZ) was synthesized, fabricated along with LSGM supported symmetrical SOFC and its performance was analysed. A highest power density of 1097 mWcm^{-2} was achieved at 800°C which is due to the low polarisation resistance of $0.105 \text{ } \Omega \text{ cm}^2$. Any electrode material developed should be operating in redox environment and redox stability plays a pivot role in determining its characteristics. The developed BFZ has a remarkable redox stability [197]. Interestingly, Gou et al in 2021 fabricated a cathode material for SOFC application by doping Pr at the B-site of $\text{BaFeO}_{3-\delta}$ perovskite oxide [198]. This novel cathode material developed could overcome the CO_2 poisoning that affects the robustness of SOFCs and also satisfies the demand for good electrochemical activity [199] [200]. This was also reaffirmed by Zhang et al 2020 and Chen et al 2017, that Pr doping improves the cubic phase stability and ORR kinetics which augments the electrochemical property [140] [200]. $\text{BaFe}_{0.95}\text{Pr}_{0.05}\text{O}_{3-\delta}$ was used as a cathode in SOFC which revealed a lower impedance of $0.061 \text{ } \Omega \text{ cm}^2$ and power density of 798.7 mW cm^{-2} at 7500°C. The thermo gravimetric analysis (TGA) performed on the prepared cathode material signposts the existence of oxygen vacancies at high temperatures. The CTE value for Pr^{3+} based materials are near similar with La based materials owing to the similar electronegativity value of Pr^{3+} and La^{3+} [201].

Tin doped $\text{PrBaFe}_2\text{O}_{5+\delta}$ was developed as an anode material for SOFCs by [202]. Double perovskites of the type $\text{AA}'\text{BB}_2\text{O}_{5+\delta}$ has been employed as cathode materials in SOFCs with A site containing element in lanthanide series and Ba or Sr as A'site with first row transition element as the B-site cation [17] [203]. Karen in 2004 developed double perovskites of the type $\text{LnBaFe}_2\text{O}_{5+\delta}$ as anode material which was stable chemically and thermally at temperature around 1000°C. This was further developed by Dong et al (2017) to improve the catalytic activity and conductivity [202]. $\text{PrBaFe}_{2-x}\text{O}_{5+\delta}$ was synthesized by combustion method and used as an anode for SOFC applications. The XRD analysis suggested that the as synthesized $\text{PrBaFe}_{2-x}\text{O}_{5+\delta}$ anode material shows change of phase from tetragonal to cubic phase upon heating. The electrochemical activity of the developed material was comparatively better than the ceramic anodes used so far [202].

Reversible solid oxide cells (RSOC) are gaining attention in recent times and considered as a promising energy conversion device. RSOC has dual behaviour which can utilize fuel from electricity and electricity from fuel. In the development of high performance air electrode for RSOCs, the commonly used LSM is not employed, instead highly conductive MIEC electrode materials were used [204]. Dong in 2020 reported a next generation air electrode for RSOC application by doping Nd to the conventional $\text{BF}_{0.1}\text{Ba}_{0.95}\text{Nd}_{0.03}\text{FeO}_{3-\delta}$ was prepared and in-situ X-ray diffraction analysis was performed to analyse the effect of partial substitution of

Nd³⁺ into BFO matrix. High electrical conductivity of about 24.31 Scm⁻¹ was obtained for Ba_{0.97}Nd_{0.03}FeO_{3- δ} oxide as air electrode which also demonstrates largest oxygen deficiency enhancing the electrocatalytic activity.

A bifunctional catalyst for unitized regenerative fuel cells (URFCs) and SOFCs was investigated for alkaline earth metals doped bismuth iron oxides. Based on the simplification of system design, integration of two operations into a single device as in this case URFCs along with SOFCs are under consideration [205] [206]. Among the alkaline earth metals used for doping into the A-site, Bi_{0.6}Ca_{0.4}FeO_{3- δ} (BCFO) shows superior OER and ORR activity. The BET surface area of BCFO electrode material was determined to be 9.4 m²g⁻¹ with an exchange current density of 5.17 x 10⁻⁸ mA cm⁻² respectively. Bi³⁺ (1.17 Å) and Ca²⁺ (1.14 Å) with a very small difference in the ionic radii tends to decline the crystallite size which is found to upgrade ORR and OER activities. The fabricated BCFO electrode material shows a fast electron transport property which was also reaffirmed from electrochemical impedance spectroscopy (EIS) [207].

2.2. Lanthanum doping of BaFeO_{3- δ}

Traditional electrode material used for high-temperature SOFCs is La_{0.8}Sr_{0.2}MnO₃(LSM), which has a lattice structure similar to perovskite-type and deliver pure electronic conductivity in the range of 150–250 S cm⁻¹ [208]. LSM meritoriously increases the electron-hole concentration as well as the electronic conductivity of the material. The use of LSM is limited owing to its insignificant ORR which occurs at TPBs, to overcome this, use of MIEC oxides were suggested. Chou et al 2000 investigated the effect of Sr doping on the mechanical properties of La_{1-x}Sr_xCo_{0.2}Fe_{0.8}O₃ (LSCF) where (x = 0.2 – 0.8). The material with lower content of Sr i.e., x = 0.2 exhibits a higher toughness of 1.5 MPa(m)^{1/2} and microhardness was found to decline slightly by increasing the Sr content [161]. However, the problem in accordance with the use of LSCF is the degradation of its performance by segregation of Sr species from the perovskites [209] [210] [201]. Segregation also takes place in Sr containing LSM based cathode materials used for high temperature SOFC applications [211] [212] [213]. This occurs due to the larger difference in radius between the dopant Sr²⁺ in comparison to La³⁺ [214].

Chen et al in 2020 developed La_{0.6}Sr_{0.4}Co_{0.2}Fe_{0.8}O_{3- δ} (LSCF) perovskite cathode material for advanced SOFCs operating at low temperature. Making use of the ionic conductivity and electrocatalytic activity, new functional materials can be developed [215]. LSCF has never been employed as an electrolyte due to its high electronic conductivity of 300 Scm⁻¹ at 750°C. Based on these observations Chen et al developed the novel and first application of LSFC material as functional electrolyte combining with sodium carbonate. The cell fabricated based on LSCF with Na₂CO₃ electrolyte can have desired performance for intermediate or low temperature SOFCs. The composite electrolyte LSCF/Na₂CO₃ delivers ionic transport pathways to improve ionic conductivity, the so called composite effect [216] [217]. The cell

was operated for 1.5 h at 550°C at current density of 64 mAcm⁻², the cell delivered a steady voltage of 0.73 V representing its durability. This study provides a novel perspective for the design of potential electrolytes for advanced low temperature solid oxide fuel cell applications [215].

Many iron based oxides were developed as an electrode material for SOFC applications such as La_{1-x}Sr_xFeO_{3-δ} [218], Ba_{1-x}Sr_xZn_{1-y}Fe_yO_{3-δ} [155], Bi_{1-x}Sr_xFeO_{3-δ} [219] [219] as an alternative to Co based electrode materials. Misra et al 2017 worked on the oxygen sensing ability of SrZr_{1-x}Fe_xO_{3-δ} material which discloses semiconducting behaviour at higher temperatures. The electrical conductivity of the synthesized material was in the range of 10^{-9.5} to 10^{-8.0} Scm⁻¹. The substitution of Fe in the place of Zr from SrZrO₃ is desirable due to the similar ionic radii of Fe (0.645 Å) and Zr (0.72 Å) respectively. Increasing iron concentration leads to lattice parameters reduction which increases the conductivity values. But these iron based electrodes for SOFC applications reveal lower performance at intermediate temperature. Recently, Ba_{0.95}La_{0.05}FeO_{3-δ} (BLF) was employed as a proton conducting electrode in SOFCs revealing a good performance [220].

Dong et al in 2012 synthesized Co free Ba_{0.95}La_{0.05}FeO_{3-δ} by sol gel process and its electrochemical performance was evaluated [54]. It was inferred that doping of La³⁺ into the perovskite structure changes the spin and oxidation state of Fe ions in the B-site. Hence the size of B-site cation equals with Ba²⁺ of the perovskites in the A-site. The high temperature in situ XRD analysis revealed that the developed BLF perovskites retained its lattice structure indicative of its thermodynamic stability. One essential criteria for a fuel cell cathode material is to have operational stability [221], the BLF electrode shows stability for around 1200 h of time period with a minor fluctuation. But, no phase transition and performance degradation [222] was observed, when it is investigated using symmetric cell test. In conclusion, the exceptional electrocatalytic activity and high stability of the developed BLF makes it a promising material as cathode for intermediate SOFC applications.

Mixed ionic electronic perovskite cathode LaNi_{1-x}Co_xO_{3-δ} for intermediate SOFC was synthesized as cathode material by Irshad et al. LiNiO_{3-δ} although was one of the widely used cathode material, its instability at higher temperature lead to the partial substitution of the Ni ions with Co at the B-site [223] [224]. The effect of cobalt doping was evaluated based on their properties such as size, morphology, electrical conductivity etc. Cobalt based materials are also used in double perovskite oxides as a cathode since, they exhibit high electrocatalytic activity along with suitable electronic and ionic conductivity. Based on the studies it was also inferred that cobalt based materials have higher conductivity than cobalt free materials [225]. Lim et al 2019 also studied the impact of Co doping to LiNiO_{3-δ} cathodes and observed an increase in catalytic activity, electronic and ionic conductivity [226]. The substitution of Co ions at the B site in perovskite oxide changes the symmetry of perovskites which is substantiated from XRD studies. Increasing the concentration of Co increases the oxygen vacancies and Co concentration of 0.6 was found to be optimum which reveals a maximum conductivity of 1.2 x 10³ Scm⁻¹. It can be concluded that LaNi_{1-x}Co_xO_{3-δ} with

$x=0.6$ has power density of 0.45 Wcm^{-2} compared to the other concentration ($x = 0.4, 0.8$) [227].

La doped SrTiO_3 was developed as a sensing agent for hydrogen sensing in SOFCs to measure in the temperature range of $600\text{-}800^\circ\text{C}$. La is doped on the A-site of the cubic SrTiO_3 perovskites oxide and undoped SrTiO_3 was examined in this study. 30 % of La was found to show better sensing ability at higher temperature of 700°C , high doping of La uplifts the creation of free carriers in the material [228]. Oxygen vacancies are created at high temperature by means of exchange of oxygen with the atmosphere which improves the free carriers in the material, ideal for sensing applications [229]. Kim et al in 2014 developed a stable cathode material $\text{La}_{0.5}\text{Ba}_{0.5}\text{Sr}_{0.5}\text{Co}_{0.8}\text{Fe}_{0.2}\text{O}_{3-\delta}$ (LBSCF) for intermediate SOFCs [230]. MIECs are used in SOFC to overcome the electrocatalytic disputes and cathode materials were developed with excellent ORR activity. The undoped BSCF has structural instabilities which leads to phase transition from cubic phase to a mixture of cubic and hexagonal perovskites phase [80] [231].

La doping can reduce the tolerance factor (tf) in BSCF and also develops a stable cubic perovskite phase [232]. The tolerance factor of LBSCF was calculated based on the substitution of La^{3+} ions into the A-site and was within the range of 1.014-1.033 indicating minimal distortion in the cubic phase symmetry than the undoped BSCF [230]. Apart from oxygen vacancies, ionic conductivity also depends upon geometric factors, where highly symmetrical perovskites have better ionic conductivity [188]. Jung and Edward in 2011 pointed out that on operating for long term, the structure of BSFC changes from the cubic phase to hexagonal phase. The electrical conductivity and power density for LBSCF is 900 Scm^{-1} and 0.81 W cm^{-2} respectively for 100 h reiterating good electrochemical activity and stability upon doping with La^{3+} ions [230].

2.3. Niobium doping of $\text{BaFeO}_{3-\delta}$

Highly charged cations such as Nb^{5+} and Ta^{5+} being ferroactive cations [233] when doped into the perovskite oxides was observed to enhance the chemical stability, suppresses the phase transition along with increase in the oxygen conductivity [234]. When compared to the $\text{Fe}^{4+/3+}$ ions, it is difficult to reduce Nb^{5+} ions [235]. Apart from the generation of oxygen vacancies by Nb^{5+} ions in the lattice, the smaller electronegativity of Nb^{5+} improves the whole conductivity, hence improving its electrochemical performance [165]. Researchers have employed these type of cations for the fabrication of oxygen permeable membranes, but its application in the field of electrodes is limited [236] [237].

Belenkaya et al (2015) developed $\text{SrCo}_{0.8-x}\text{Fe}_{0.2}\text{M}_x\text{O}_{3-\delta}$ ($M = \text{Nb}, \text{Ta}$) by partial isomorphic substitution of Co with the ferroactive cations. The phase transformation and the partial isomorphous substitution of Co was carried out by in situ XRD studies in isostoichiometric mode to exclude any modification in oxygen stoichiometry upon increase in temperature. The authors stated for the first time that the phase transition implicates the establishment of brownmillerite-tetragonal phase as an intermediate. The size depends on the concentration

Table 2.1: Electronic conductivity, Ionic conductivity and CTE values of La based perovskite materials

Cathode Material	Electronic conductivity (S cm ⁻¹)	Ionic conductivity (S cm ⁻¹)	Temper- -ature (°C)	CTE (10 ⁻⁶ K ⁻¹)	Reference
La _{0.8} Sr _{0.2} MnO _{3-δ}	150 - 250		1000 - 800		[36, 37]
La _{0.72} Sr _{0.18} MnO ₃	34-56		800		[69]
La _{0.7} Sr _{0.3} MnO ₃	240		800	11.7	[70, 71]
LaSrMnCoO _{5+δ}	111-140		1000	15.8	[17]
La _{1-x} Sr _x CoO _{3-δ}	1867		800	18-20	[72]
La _{0.8} Sr _{0.2} FeO ₃	90		700	12.2	[73]
La _{0.6} Sr _{0.4} FeO ₃	129	5.6 x 10 ⁻³	800	16.3	[71]
La _{0.6} Sr _{0.4} CoO ₃	1600	0.22	800	20.5	[74, 75]
La _{1-x} Sr _x CoFeO ₃	87-1050	0.058-8 x 10 ⁻³		14.8-21.4	[76]
La _{0.6} Sr _{0.4} Co _{0.2} Fe _{0.8} O ₃	302	8 x 10 ⁻³	800		[74]
La _{0.6} Sr _{0.4} Co _{0.2} Fe _{0.8} O _{3-δ}	302	8 x 10 ⁻³	800		[77]
Pr _{0.8} Sr _{0.2} Co _{0.2} Fe _{0.8} O ₃	76 - 950	1.5-4.4 x 10 ⁻⁵	800	12.8-21.3	[74]
La _{0.6} Sr _{0.4} Co _{0.2} Fe _{0.8} O _{3-δ}	300	0.02-0.2 (for 10 %)	750		[47]

of the dopant and textural change from lamellar to tweed [238].

Cascos et al in 2014 [239] developed Nb doped SrCo_{1-x}Nb_xO_{3-δ} as a cathode material for SOFC applications at high temperature. The incorporation of Nb⁵⁺ was studied from neutron powder diffraction data, since neutrons are profound to the presence of oxygen vacancies. The thermal expansion of the developed perovskite oxide measurement between the temperature range of 400 to 850°C was 26.8 x 10⁻⁶K⁻¹ under air atmosphere. This is significantly higher than the conventional SOFC electrolyte used in combination with LSGM as electrode (12.5 x 10⁻⁶K⁻¹). The electrical conductivity increases to 50 S cm⁻¹ at 850°C which is higher compared to the other derivatives such as Ba_{0.5}SrCo_{0.8}Fe_{0.2}O_{3-δ} [4] [240] and SrCo_{0.8}Fe_{0.2}O_{3-δ} [197]. The incorporation of Nb⁵⁺ at Co position circumvents the formation of competent hexagonal phase in the perovskites.

SrMn_{0.875}Nb_{0.125}O_{3-δ}(SMN) and SrCo_{0.875}Nb (SCN) materials are prepared as a novel oxygen intercalated electrode materials for supercapacitor application. The formation of high pressure novel 6H phase was obtained for the Nb substituted SMN for the first time. SCN gives a specific capacitance of 894 mF cm⁻² in an aqueous electrolyte, higher than the SMN electrode material. The capacity retention of SMN and SCN material in combination with activated carbon electrode after 10000 cycles is 46.81 and 82.33 μWh cm⁻² respectively. The dominating performance of SCN electrode material is owing to its porosity, shorter B-O bond length and increased oxygen content [241] [89]. Porosity affects the mechanical properties as it offers mechanical support to the electrolyte layer. In the case of SOFCs cathodes around 30-40 % porosity is required, since porosity can lower the mechanical as well as electrical properties [198] [200].

Yao et al in 2019 prepared Nb and W co-doped $\text{SrFeO}_{3-\delta}$ for intermediate temperature SOFC electrode. The co-doping resulted in an electrode material $\text{SrNb}_{0.1}\text{W}_{0.1}\text{Fe}_{0.8}\text{O}_{3-\delta}$ with a superior oxygen vacancy leading to an improved electrochemical performance and raised thermal expansion coefficient. Based on the thermogravimetric analysis, higher weight loss occurs in the synthesized electrode material than the individually doped electrodes. This illustrates the formation of more oxygen vacancies, advantageous as a cathode material for SOFC applications [242].

Partial substitution of Fe from $\text{SrFeO}_{3-\delta}$ perovskite oxide with Nb to form $\text{SrNb}_{0.05}\text{Fe}_x\text{O}_{0.095}$ which is used as cathode for SOFCs[243]. Iron based perovskite oxides are gaining interest among the researchers owing to the redox behaviour and low price of iron [244]. Mossbauer spectral analysis revealed the higher amount of Fe^{3+} and lower amount of Fe^{4+} with increasing Nb^{5+} , this substantiates the lattice volume expansion. Further to explore the ORR activity of the fabricated cathode material, electrochemical impedance spectroscopy (EIS) was employed. It is correlated from EIS that superior non-stoichiometry leads to exceptional ORR activity. The electrical conductivity studies shown that by increasing doping of Nb^{5+} , the conductivity declined owing to the blocking effect of Nb^{5+} . It can be concluded that optimization of electrical conductivity is required for further enhancement of the fuel cells [243]. Cobalt free cathode material was prepared by doping 10 mol% of Nb^{5+} to obtain $\text{BaFe}_{0.9}\text{Nb}_{0.1}\text{O}_{3-\delta}$ (BFNb) operating at intermediate temperature for SOFC application by Wang et al 2021. When the sintering temperature was elevated, the cubic phase was decreased which may be due to the existence of impurity (BaFe_2O_4) at 1100°C . The doped material exhibits several pathways for the transport of oxygen ion which arises because of the disordered oxygen vacancies [245] [246]. The long term stability of the developed BFNb was tested by operating single cell at 700°C for 30 h time, which showed no downturn of the current density. It was also indicated by the authors that the developed $\text{BaFe}_{0.9}\text{Nb}_{0.1}\text{O}_{3-\delta}$ although with its low conductivity, it still accomplishes the demand for conductivity as an electrode in SOFC applications [247].

Nb and Pd co-doped $\text{La}_{0.57}\text{Sr}_{0.38}\text{Co}_{0.19}\text{Fe}_{0.665}\text{Nb}_{0.095}\text{Pd}_{0.05}\text{O}_{3-\delta}$ was developed as a stable cathode material along with YSZ electrolyte for SOFC application. The purpose of Nb doping is to improve the chemical stability and Pd leads to an enhanced electrochemical activity. From XRD analysis pure perovskite phase was obtained and 31.8 % of Sr content was doped in the developed material as affirmed by XPS analysis. The co-doping of Nb and Pd promotes the chemical compatibility between the electrode and the electrolyte. The cell with $\text{La}_{0.57}\text{Sr}_{0.38}\text{Co}_{0.19}\text{Fe}_{0.665}\text{Nb}_{0.095}\text{Pd}_{0.05}\text{O}_{3-\delta}$ as cathode demonstrates excellent stability for 175 h under the study conditions[248]. The suppression of Sr^{2+} segregation can be elucidated based on the lattice expansion and loss of oxygen vacancies due to the doping of Nb^{5+} [249] [250]. The addition of Nb^{5+} ions provide more space for the larger Sr^{2+} ion which decreases the surface segregation of Sr and reduces the valence state of B site cation [225] [251].

2.4. Mechanical Properties of perovskites based oxides

Rached et al (2017) [252] focused on the stability of magnetic phase, mechanical, electrical and optical properties of double perovskite oxides Pb_2FeMO_6 by applying the ab-initio plane-wave technique. They evaluated elastic constants and relevant mechanical properties such as bulk modulus, shear and Young's modulus, Poisson's ratio and Debye temperature. The results indicated that the observed compounds are constant at high temperature. LaFeO_3 contains orthorhombic crystal structure having three valent iron and anti-ferromagnetic insulator at room temperature [253] [254]. Sr replacement instead of LA enhances the electronic and oxygen ionic conductivity. Hence $\text{La}_{1-x}\text{Sr}_x\text{FeO}_{3-\delta}$ compound is widely used in gas sensors, electrodes, oxygen permeable membrane, oxidation catalysts and solid oxide fuel cells [255] [256]. In high temperature electrochemical devices, ceramic components mechanical properties are considered as significant parameter to estimate the steadfastness. The variation in component thermal expansion coefficients or component chemical expansion in an oxygen gradient initiate the tensile stresses which leads to device malfunction. [257] [258]. The orthorhombic perovskites at room temperature have four-point bending strength in the range of 100–140 MPa [259] [260], while the fracture toughness is in the range 2.0–2.8 MPa $\text{m}^{1/2}$ [261] [262]. Moreover, the bend strength and fracture toughness remains constant or increase with temperature. For rhombohedral and cubic perovskites, the four-point bending strength was observed in the range 100–160 MPa [118,119] at room temperature. The fracture toughness of rhombohedral and cubic perovskites remains lesser at room temperature when compared to the orthorhombic compounds and usually decline or tends to be constant with rising temperature [261][262][263].

While applying stress, monolithic ceramics shows elastic behaviour and generally it is fragile in nature. Few ceramics have non-elastic behaviour called ferroelastic by equivalence with the stress–strain relationship with polarization of a ferroelectric material in an electric field and the magnetization of a ferromagnetic material in magnetic fields [264]. The both rhombohedral and orthorhombic perovskites have exhibited Ferroelastic behaviour. Fossdal et al (2015)[265] have investigated the LaFeO_3 mechanical properties as a function of temperature, and related these properties with structural properties. The mechanical properties in this paper are described based on the ferroelasticity. The results showed that the highest fracture toughness attained is about $3.1 \pm 0.3 \text{ MPa m}^{1/2}$, at 800 °C temperature. At the room temperature obtained fracture strength rises from $202 \pm 18 \text{ MPa}$ to $235 \pm 38 \text{ MPa}$ at 800 °C owing to the fracture toughness raise among these temperatures. The potential mechanical properties of LaFeO_3 are considered as a suitable material in devices with high temperature.

Okamura et al. [266] described the elastic modulus showed inconsistent behaviour at the temperature range from 473 to 1173K. Initially, it decreased hastily in the temperature from 473 to 873K, subsequently increased in the temperature from 873 to 1173K, and decreased over again. The shear modulus showed similar deeds like elastic modulus, however the Pois-

son's ratio, showed notable changes in the temperature 873K. These changes are ascribed to the LSGM bulk structural changes in the transitional temperature range. Moreover, high internal friction values were examined in the temperature from 473K to 773K.

Baskaran et al [1999] [152] and Stevenson et al [1998] [267] measured the LSGM1020 fracture toughness between the densities 95 and 98% by using notched beam analysis, and they obtained $\sim 2.0\text{--}2.2$ MPa $\sqrt{\text{m}}$ at room temperature, and declining to ~ 1.0 MPa $\sqrt{\text{m}}$ at 1000°C. The authors also assessed the indentation resistance by using Vickers indentation method, and attained the value around 0.9–1.1 MPa $\sqrt{\text{m}}$ at room temperature. The indentation resistance for other LSGM materials with different chemical composition, are 1.63 MPa $\sqrt{\text{m}}$ for $(\text{La}_{0.9}\text{Sr}_{0.1})_{0.9}\text{Ga}_{0.8}\text{Mg}_{0.2}\text{O}_{3-\delta}$ and 1.28 MPa $\sqrt{\text{m}}$ for $(\text{La}_{0.9}\text{Sr}_{0.1})_{0.9}\text{Ga}_{0.8}\text{Mg}_{0.2}\text{O}_{3-\delta}$ [268]. Khandy et al 2018 [269] investigated the electronic structure, mechanical stability, magnetic and thermal properties of BaCfO₃ perovskite by density functional theory calculations, using full potential linearized augmented plane wave method. The mechanical stability of the material has been determined by calculating elastic constants, in addition to the anticipated mechanical properties such as Young modulus (Y), Bulk modulus (B), the Shear modulus (G) and the Poisson ratio (ν). The B/G experimental data and Cauchy pressure for the current material reveals its elastic nature. The experimental values of B and G are 114.00 GPa and 50.28 GPa at ambient conditions and the poison's ratio was $0 < \nu < 0.5$. This lower poison ratio value implies a superior plastic performance which suggests that material is elastic in nature [269].

Huang et al (2011) [270] assessed the elastic and fracture toughness of $\text{La}_2\text{NiO}_{4+\delta}$ by using 4-points bending tests as a function of temperature (from room temperature (RT) up to 900°C). Both parameters are increased to some extent when the temperature rises from RT to 700°C. Moreover, at higher temperature, the elastic modulus decreases whereas the fracture stress increases. In addition to this, resonance method is used to assess elastic modulus and dense specimen's internal friction. The sturdy change of both parameters between the room temperature and 100°C are considered for an orthorhombic tetragonal phase transition. The orthorhombic-tetragonal transition takes place between RT and 150°C, and the tetragonal structure is maintained from 150 to 800°C [129]. There is no phase transition at higher temperature. It has been observed that the coefficient of thermal expansion values is stable from RT to 1000°C.

Chen et al (2015) [178] reported the mechanical properties of dense $\text{La}_2\text{NiO}_{4+\delta}$ membranes. They have focused more on grain size and the anisotropic nature of $\text{La}_2\text{NiO}_{4+\delta}$ crystal structure, which directs to the intensification of residual stresses or micro-cracking. The bi-axial fracture strength of the sintered materials increased from ~ 108 to ~ 155 MPa which decline the average grain size of the membranes from 9.6 to 4.2 μm . The hardness and fracture toughness, calculated by using Vickers indentation method, also declined with increasing grain size. The maximum hardness was around ~ 958 MPa which was observed before the decrease in hardness with increasing grain size. The predicted fracture toughness, reached a maximum of 3.2 ± 0.4 MPa $\text{m}^{0.5}$, which also decrease with increasing grain size. The crystallographic anisotropy developed in the ceramics during cooling gives rise to residual stresses, which is

proposed as the main reason for the detected decrease in hardness, fracture strength and fracture toughness with increasing grain size.

Orlovskaya et al [271], studied the thermal and mechanical properties of LaCoO_3 and $\text{La}_{0.8}\text{Ca}_{0.2}\text{CoO}_3$ perovskites and crack growth of $\text{La}_{0.8}\text{Ca}_{0.2}\text{CoO}_3$. The mechanical performance of two cobaltites have been assessed based on the ferroelastic hysteresis properties such as non-symmetry in bending of both stress and strain distributions, non-linear deformation upon applied load from the arbitrary low stresses, and ferroelastic toughening. Values of Young's moduli of LaCoO_3 and $\text{La}_{0.8}\text{Ca}_{0.2}\text{CoO}_3$ analysed by impulse excitation technique as well as a secant modulus in 0–9 MPa stress range examined from stress–strain deformation curves in bending and uniaxial compression depicts similarity. It is observed that LaCoO_3 and $\text{La}_{0.8}\text{Ca}_{0.2}\text{CoO}_3$ have E modulus in the range 70–76 GPa and 114–141 GPa respectively at room temperature. The storage modulus (dynamic young modulus) showed considerable softening in the temperature range 150–400°C for both cobaltite's.

Lipinska et al. [272] have investigated the mechanical properties of porous $\text{Ba}_{0.5}\text{Sr}_{0.5}\text{Co}_{0.8}\text{Fe}_{0.2}\text{O}_{3-\delta}$ using depth-sensitive micro-indentation and ring-on-ring biaxial bending tests. Indentation tests have been carried out to assess the hardness and fracture toughness. The fracture toughness of dense and porous $\text{Ba}_{0.5}\text{Sr}_{0.5}\text{Co}_{0.8}\text{Fe}_{0.2}\text{O}_{3-\delta}$ materials is observed to be the same. The hardness with a load of 10 N is around 0.87 ± 0.03 GPa at room temperature, which is less than the value reported by Wang et al [273] owing to the upper indentation load. Chou et al [161] have evaluated the effect of Sr-doping on the mechanical properties of $\text{La}_{1-x}\text{Sr}_x\text{Co}_{0.2}\text{Fe}_{0.8}\text{O}_3$ ($x=0.2-0.8$) and the materials has been synthesized by combustion synthesis technique. The material with lesser Sr content ($x=2$) have lower toughness around $1.0-1.1 \text{ MPa(m)}^{1/2}$. Moreover, the microhardness also identified with an indentation load 2kg and rise in Sr composition declines the microhardness slightly. Sammes et al. investigated the mechanical properties of $\text{La}_{0.8}\text{Sr}_{0.2}\text{Ga}_{1-x}\text{Mg}_x\text{O}_{3-\delta}$ ($x=0.1-0.2$) and their results suggested that synthesis technique have an effect on strength and fracture toughness of the material. The Mg content increase cause reduction in the fracture toughness. Hassan et al [274] studied the high temperature SOFC compounds in order to verify their mechanical and thermal properties. Ba, Ca niobate as an electrolyte is used, SrCeO_3 and SrZrO_3 stabilised with 5% Yb used as the cathode materials and a cermet of 50:50 wt% Ba, Ca niobate and Ni as the anode respectively. The Vickers hardness fracture toughness of the cathode materials (SrZrO_3 stabilised with 5% Yb) is 4.6 GPa and $1.54 \text{ MPa(m)}^{1/2}$, respectively. The results concluded that all the studied materials can be a potential cathode material for its use in SOFCs.

2.5. Perovskite Applications in Membrane

In the oxygen separation membrane scenario, the mixed ionic-electronic conducting (MIEC) perovskite has been used as ionic transport membrane to produce oxygen, which is compet-

Table 2.2: Fracture toughness and hardness of different perovskite oxides

Material	Fracture toughness	Hardness	References
	(MPa (m) ^{1/2})	(GPa)	
Ba _{0.5} Sr _{0.5} Co _{0.8} Fe _{0.2} O _{3-δ}	-	0.87±0.03	[132]
La _{0.58} Sr _{0.4} Co _{0.2} Fe _{0.8} O _{3-δ} Ce _{0.8} Gd _{0.2} O ₂	1.2-1.8	8.1-9.8	[137]
La _{0.8} Sr _{0.2} Co _{0.2} Fe _{0.8} O ₃	1.5	6.8	[136]
La _{0.6} Sr _{0.4} Co _{0.2} Fe _{0.8} O _{3-δ}	0.54-0.99	0.69-5.76	[138]
Pb ₂ FeMoO ₆	-	4.83	[100]
Pb ₂ FeReO ₆	-	5.13	[100]
Pb ₂ FeWO ₆	-	2.96	[100]
La _{0.9} Ba _{0.1} Ga _{0.8} Mg _{0.2} O _{3-δ}	0.76 ± 0.07	8.4 ± 0.2	[117]
La _{0.9} Ca _{0.1} Ga _{0.8} Mg _{0.2} O _{3-δ}	0.68 ± 0.14	8.6 ± 0.2	[117]
La _{0.8} Sr _{0.2} Ga _{0.9} Mg _{0.1} O _{3-δ}	1.00 ± 0.06	8.2 ± 0.2	[117]
La _{0.8} Sr _{0.2} Ga _{0.85} Mg _{0.15} O _{3-δ}	1.11 ± 0.10	7.8 ± 0.4	[117]
La _{0.8} Sr _{0.2} Ga _{0.8} Mg _{0.1} O _{3-δ}	1.22 ± 0.06	-	[139]
SrCeO ₃ +5% Yb	2.08	-	[136]
SrZrO ₃ +5% Yb	1.54	4.6	[136]

itive in the means of energy and capital consumption when compared to the conventional cryogenic distillation [140]. Perovskite oxides which contain transition metal cations in the B-sites shows mixed ionic-electronic conductivity and consequently, high oxygen reduction activity. This property facilitates the formation of better triple phase boundaries (the interfaces between oxygen ion, oxygen gas and electron), where the oxygen reduction reaction takes place at the pure ionic/ electronic conductor. As membrane within the membrane reactor, perovskite permits both separation and catalytic processes in single step [141]. The perovskite-based oxygen separation membrane technology proposes advantages for integration in power generation cycles with carbon dioxide (CO₂) capture by oxy-fuel combustion [275].

Teraoka et al [276] described the high electrical conductivity and oxygen permeability of La_{1-x}Sr_xCo_{1-y}Fe_yO_{3-δ} series MIEC perovskite oxides, which gained increasing interests from the scientific communities. The other work reported the substitution of A and B site ions in La_{1-x}Sr_xCo_{1-y}Fe_yO_{3-δ} in mixed conducting oxide [144] and concluded that the oxygen permeation performance is enhanced in the order of <Sr< Ca < Ba (with Sr in A site replaced by Na, Ca, and Ba) and La <Pr<Nd< Sm <Gd (with La in A site substituted by Pr, Nd, Sm, and Gd). However, Fe, Cr, and Mn doping into B-site has negative outcome on oxygen permeation flux. This result entails that the fractional substitution of A and B site cations can drastically influence the performance of oxygen permeation owing to their composition and phase structure change.

Perovskite kind SrCo_{0.8}Fe_{0.2}O_{3-δ} exhibited tremendous oxygen permeability [145-147], the fluxes has attained 2.82 mL cm⁻² min⁻¹ at 850°C under the air/helium environment [277].

On the other hand, the cubic structure of $\text{SrCo}_{0.8}\text{Fe}_{0.2}\text{O}_{3-\delta}$ oxide has been sustained at high temperature ($>790^\circ\text{C}$) and high oxygen partial pressure ($>0.1\text{ atm}$). The temperature reduced below 790°C encourages the phase transformation owing to the formation of mixed oxygen vacancy disordering and ordering. The limited stability of $\text{SrCo}_{0.8}\text{Fe}_{0.2}\text{O}_{3-\delta}$ used for membrane reactors was also stated. Pei et al [146] determined the long term stability of $\text{SrCo}_{0.8}\text{Fe}_{0.2}\text{O}_{3-\delta}$ membrane in the tubular membrane reactor, and observed that there are two factors which cause the membrane stability degradation and membrane cracking. They are the surface tension force from the gradient difference across the two sides of the membrane and the thermal expansion coefficient disparity owing to the membrane material decomposition in which one side is opened to the reducing atmosphere.

The fractional substitution of other metal ions into $\text{SrCo}_{0.8}\text{Fe}_{0.2}\text{O}_{3-\delta}$ membrane, causes the enhancement of material stability. Prado et al [278] studied the doping effect of La^{3+} on the phase structure of $\text{La}_{1-x}\text{Sr}_x\text{Co}_{0.8}\text{Fe}_{0.2}\text{O}_{3-\delta}$ membrane and established that the compound could sustain consistent perovskite structure under pure nitrogen atmosphere with the La^{3+} doping amount at 0.4 mol fraction. Moreover, shao et al [279] has developed mixed conducting $\text{Ba}_{0.5}\text{Sr}_{0.5}\text{Co}_{0.8}\text{Fe}_{0.2}\text{O}_{3-\delta}$ (BSCF) perovskite oxide with better oxygen permeability and structure stability by utilizing Ba^{2+} to partially replace Sr^{2+} in the A-site. It has exhibited that the doping of Ba^{2+} into A-site restricted the B-site ions oxidation at high temperature and reducing atmosphere. Other method engages the metal ion utilization with fixed valence state such as Ga^{3+} , Ti^{4+} , and Zr^{4+} to replace cobalt ions at B-site to enhance the material stability at the intensive operating conditions.

Tong et al [280] synthesized perovskite type $\text{BaZr}_{0.2}\text{Co}_{0.4}\text{Fe}_{0.4}\text{O}_{3-\delta}$ which exhibited the consistent oxygen permeation fluxes over the long time about 2200 h at 850°C . The results entailed that amalgamation of tetravalent metal ions and oxygen ions has enhanced the stability of the material, however, the doping of tetravalent metal ions (Ti^{4+} and Zr^{4+}) into B-site leads to decline in the performance of oxygen permeation. Kharton et al [281][151] recognized this decline to the coulombic force among B-site ions and oxygen ions which also elucidates that the $\text{A}^{3+}\text{B}^{3+}\text{O}^3$ has enhanced ion conductivity than $\text{A}^{2+}\text{B}^{4+}\text{O}^3$.

Zhu et al [282] synthesized novel cobalt-free $\text{BaCe}_{1-y}\text{Fe}_y\text{O}_{3-\delta}$ based on BaCeO_3 oxide by using Fe to partly replace Ce into the B-site. The doping of Ba^{2+} with large ionic radius at A-site decreases the energy of metal-oxygen bond and enhances the crystal lattice free volume. In addition, it carries the tolerance factor closer to 1. In the ionic radius size view, the perfect structure of $\text{La}(\text{Sr})\text{Ga}(\text{Mg})\text{O}_3$ solid oxide leads to constructive oxygen ion conductivity of 0.08 S cm^{-1} at 800°C . The fractional doping of transition metal elements such as Fe and Ni on the B-site of $\text{La}(\text{Sr})\text{Ga}(\text{Mg})\text{O}_3$ enhanced the material electronic conductivity. Mg to substitute Fe in $\text{La}_{1-x}\text{Sr}_x\text{Ga}_{1-y}\text{Fe}_y\text{O}_3$ which improves the oxygen permeation fluxes significantly. The study results suggested that Mg doping plays a crucial role in decrease the bond energy between metal ions and oxygen ions towards increasing the oxygen vacancy concentration.

Kharton et al. [281] developed a dual-phase membrane which consists of fluorite-type ionic

conducting (IC) oxide (i.e., $\text{Ce}_{0.8}\text{Gd}_{0.2}\text{O}_{2-\delta}$ (GDC)) for oxygen ionic transport and perovskite-type electronic conducting (EC) oxide (i.e., $\text{La}_{0.7}\text{Sr}_{0.3}\text{MnO}_{3-\delta}$ (LSM)) for electronic transport. The oxygen surface-exchange reaction is usually projected to be restricted at the triple phase boundary (TPB). Thus, the performance of oxygen permeation has been enhanced by substitution of pure EC oxide with a perovskite-type MIEC oxide (LCSF) for oxygen ionic and electronic transport. The prologue of ionic transport to the EC phase enlarges the oxygen surface-exchange reaction ahead of TPBs and preferably more in MIEC surface. [283].

Fang et al [284] synthesized a dual-phase membrane, by means of ionic conducting fluorite-type MIEC oxide (i.e., $\text{Ce}_{0.85}\text{Gd}_{0.1}\text{Cu}_{0.02}\text{O}_{2-\delta}$ (CGCO)) and an electronic conducting perovskite-type MIEC oxide (i.e., $\text{La}_{0.6}\text{Ca}_{0.4}\text{FeO}_{3-\delta}$ (LCF)). This approach causes concurrent oxygen ionic and electronic transport in MIEC phases, which broaden the oxygen surface exchange reaction to the overall dual-phase membrane surface, the surface-exchange reaction rate increases as well as bulk diffusion for oxygen permeation. The maximum oxygen permeation flux was around $0.70 \text{ mL cm}^{-2} \text{ min}^{-1}$ which is attained with a 0.5 mm thick membrane at 950°C by using pure CO_2 as the sweep gas. In addition, the membrane has outstanding stability in CO_2 presence at lesser temperature level for longer duration.

Lu et al [2016] [285] developed Fe-based perovskite MIEC with $\text{BaFe}_{1-x}\text{Gd}_x\text{O}_{3-\delta}$ ($0.025 \leq x \leq 0.20$) compositions to apply for oxygen permeation membrane. Trivial Gd doping ($x=0.025$) stabilize the cubic structure of $\text{BaFe}_{1-x}\text{Gd}_x\text{O}_{3-\delta}$ perovskite. The Gd replacement of $\text{BaFe}_{1-x}\text{Gd}_x\text{O}_{3-\delta}$ perovskite enhances the structural and chemical permanence in atmosphere containing CO_2 and H_2O and decreases the thermal expansion coefficient. The $\text{BaFe}_{0.975}\text{Gd}_{0.025}\text{O}_{3-\delta}$ membrane shows quick oxygen surface exchange kinetics and high bulk diffusion coefficient. This attains a high oxygen permeation flux of $1.37 \text{ mL cm}^{-2} \text{ min}^{-1}$ for 1 mm thick membrane at 950°C under Air/He oxygen gradient, maintained consistent at 900°C for 100 h. The findings of this study are anticipated to present guidelines for the high performance MIEC material design.

2.6. Miscellaneous applications

Single perovskites are considered as a group of cost-effective catalysts with high activity [286] [142] and are greatly tunable in their chemical compositions. This permits the perovskites in wide variety of energy and environment-oriented catalytic applications such as high and low temperature electrochemical redox reactions, photo(electro) chemical conversions, and advanced oxidation process. Though single perovskites continue to succeed, it has been identified that it shows inadequate activity and unsatisfactory stability. At the same time, double perovskites are established to express as a promising alternative, which exhibits comparable and higher catalytic performance. The double perovskite structure can have many imperative benefits to the physicochemical properties, affecting activity, stability, and efficiency in related applications.

Sengodan et al [287] found the use of A-site layered double perovskite $\text{PrBaMn}_2\text{O}_{5+\delta}$ (PBMO), which has been grown in situ from the single perovskite $\text{Pr}_{0.5}\text{Ba}_{0.5}\text{Mn}_2\text{O}_{5+\delta}$ in fuel conditions,

as an anode for SOFCs. The layered structure of PBMO encourages the valency of Mn cations ($\text{Mn}^{4+}/\text{Mn}^{3+}/\text{Mn}^{2+}$), which facilitate superior electrical conductivity, greater oxygen vacancy level, and better fuel oxidation activity compared with LSCM. PBMO is chemically stable while operation because of its A-site ordering configuration.

The layered double perovskite $\text{LnBaCo}_2\text{O}_{5+\delta}$ series ($\text{Ln} = \text{lanthanides or Y}$) have been studied as high-performance oxygen electrodes for SOFCs before it is being used as fuel electrodes [288]. Even though single perovskite $\text{Ba}_{0.5}\text{Sr}_{0.5}\text{Co}_{0.8}\text{Fe}_{0.2}\text{O}_{3-\delta}$ (BSCF) exhibits notable ORR activity with low area-specific resistance (ASR) of 0.05–0.07 $\Omega \text{ cm}^2$ at 600°C [162], it is not considered for commercial use owing to its unsteady structure at typical operating temperature and unsuited thermal expansion with other cell components [240]. Particularly, $\text{PrBaCo}_2\text{O}_{5+\delta}$ (PBC) shows an ASR of 0.15–0.40 $\Omega \text{ cm}^2$ at 600°C [289] [290], which is comparable to BSCF. B-site cation ordering in double perovskites have been considered as cathode materials for SOFCs [77][291]. For instance, $\text{Ba}_2\text{Bi}_{0.1}\text{Sc}_{0.2}\text{Co}_{1.7}\text{O}_{6-\delta}$ (BBSC) also possesses a same ASR of 0.22 $\Omega \text{ cm}^2$ at 600°C [292]. A number of double perovskites (ex: $\text{Sr}_2\text{Fe}_{1.5}\text{Mo}_{0.5}\text{O}_{6-\delta}$ (SFM)) maintain high conductivity and stability under reducing and oxidizing atmosphere, hence it is used as cathode catalyst in symmetric SOFCs. Recently, double perovskites such as SFM and PBMO is considered to serve as cathode and/or anode to catalyse the electrolysis of water and/or carbon dioxide in high-temperature solid oxide electrolysis cells (SOECs) [293] [294].

BaBiO_3 has been applied for a variety of photochemical processes such as volatile organic compound decomposition, dye contaminant degradation and carbon dioxide conversion [295] [31] due to its appropriate band-edge positions. Replacement of Nb for Bi leads to the pattern of a phase-pure $\text{Ba}_2\text{Bi}_{1.4}\text{Nb}_{0.6}\text{O}_6$ double perovskite with low bandgap around 1.6 eV. Recent studies have exposed its prospective as both photoanode and photocathode in photo electrochemical (PEC) water splitting, which shows analogous photocurrent density of 0.2 mA cm^{-2} at 1.23 and 0 V versus the reversible hydrogen electrode when used in a PEC device individually [296] [297].

Perovskite oxides are considered as capable catalysts in a variety of catalytic reactions, owing to their low cost, high electrochemical stability, high electronic/ionic conductivity, and the outstanding structured capability to control a broad variety of doping and substituting elements. Moreover, Perovskite oxides exhibits better electron and ion conductivity, which gives some oxygen vacancies to augment the oxygen ion transfer [298]. In addition, these have been applied as bifunctional catalysts owing to its notable specific catalytic activity towards ORR and OER in alkaline solutions [299]. Example: LaMnO_3 shows high catalytic activity because of defective cation-deficient lattice and the presence of manganese in two oxidation states ($\text{Mn}^{3+}/\text{Mn}^{4+}$), that leads to moderately stable and constant oxygen excess [300]. Employing graphene for perovskite sample, improves the electrochemical performance of the perovskite catalyst.

Jung et al described that perovskites based on Co/Fe shows outstanding ORR and OER activity [301]. Also some studies stated that the thermal stability of perovskites with Co^{3+}

in the B-site is lesser compared with Mn^{3+} [184]. The alteration of B-site atom (ex: Mn and Co) tunes the oxygen adsorption energy on the catalysts surface, and consequently change the catalytic activity. Zhao et al 2018 [302] synthesized Co doped $\text{La}_{0.4}\text{Sr}_{0.6}\text{MnO}_3$ nanoparticles by sol-gel method and investigated their catalysis effect. These composites exhibit better catalytic activity and lower potential gap when it is tested in rechargeable lithium-air batteries. When these samples are tested as catalysts for Li-air batteries at a current density of 100 mA g^{-1} , the discharge capacities for $\text{La}_{0.4}\text{Sr}_{0.6}\text{Co}_x\text{Mn}_{1-x}\text{O}_3$ ($x= 0.4$) catalysts was 7227 mAh g^{-1} , respectively. In addition, the cell using $\text{La}_{0.4}\text{Sr}_{0.6}\text{Co}_{0.4}\text{Mn}_{0.6}\text{O}_3$ as catalyst with capacity limitation of 1000 mAh g^{-1} shows good cycling stability up to 46 cycles. The upgraded electrochemical performance recommends that suitable doping of Co in place of Mn site of $\text{La}_{0.4}\text{Sr}_{0.6}\text{MnO}_3$ could be a promising path to advance the catalytic activity.

Chapter 3

Methodology

3.1. Materials

The study involves fabrication of three different sample listed in Table 3 and characterising their properties involves to analyse how the doping had an impact over the material. As discussed in the literature study, the methods and techniques to fabricate the sample material by sol-gel, sintering and densification are elaborated here. Then it followed by the discussion of testing methods and settings for the test that would be followed during the test are discussed.

Table 3.1: Materials components and their terminology

Sample	Material
BFO	BaFeO_{3-d}
BLFO	$\text{Ba}_{0.95}\text{La}_{0.05}\text{FeO}_{3-d}$
BFNbO	$\text{BaFe}_{0.9}\text{Nb}_{0.1}\text{O}_{3-d}$

3.2. Sol-Gel Method

Sol-gel is a wet chemical method to produce a solid compound from small molecules through chemical reactions in a liquid phase. It is commonly used to fabricate metal oxides. Sol is the particles in a liquid phase and gel is the three dimensional continuous network contains a liquid phase.

3.2.1. Principle

The sol-gel method involves chemical process, initially the raw materials will be dispersed in a solvent, and hydrolysis reaction performed to create an active monomer. Then sol is formed by polymerizing the active monomer, and a gel contains a spatial structure network is formed. After ageing, drying, heat treatment, sintering and densification of the particles, the final structure is produced in required form. By using sol-gel method, the samples for the

material shown in Table 3.1 would be fabricated. And the fabrication is to produce powdered form of the sample and perform calcination to produce the material in solid disc form.

3.2.2. Fabrication of BFO

The table 4 shows the amount of precursor that would be added to the sol for BFO. At first, precise amount of metal nitrates using balance and two 50 ml beakers, are taken and added magnet bar to each beaker. Then, 30 ml distilled water would be added to each beaker. Using a magnetic stirrer, the metal nitrates are dissolved in distilled water. The, Mixing dissolved metal nitrates in one 100ml baker and removing small magnets and added a bigger magnet to the 100 ml baker. Now, citric acid is added to the solution. At last, Ethylene glycol will be added in drops using syringe to the solution. Raising magnetic stirrer to 80°C and keep it for gel formation.

Table 3.2: List of Precursor and Quantity for BFO

Precursor	Molar ratio	mw(g/mol)	Quantity used (g)
Ba(NO ₃) ₂	1	261.33	4.3555
Fe(NO ₃) ₃ .9H ₂ O	1	404.00	6.7333
Citric acid (C ₆ H ₈ O ₇)	1.39	192.12	3.2021
Ethylene Glycol (C ₂ H ₆ O ₂)		62.0678	1.601029167

3.2.3. Fabrication of La-doped-BFO

The table 5 shows the amount of precursor that would be added to the sol for BLFO. Initially, the same steps were followed for the BLFO sample preparation. But prior to the addition of citric solution to the mixture, measured quantity of lanthanum nitrate will be added to the mixture. Then the addition of citric acid and ethylene glycol were followed. Also, the magnetic stirrer temperature would be raised to 80°C and keep it for gel formation.

Table 3.3: List of Precursor and Quantity for BLFO

Precursor	Molar ratio	mw(g/mol)	Quantity used (g)
Ba(NO ₃) ₂	0.95	261.33	4.9653
Fe(NO ₃) ₃ .9H ₂ O	1	404.00	8.0799
La(NO ₃) ₃ .6H ₂ O	0.05	433.01	0.4330
Citric acid (C ₆ H ₈ O ₇)	1.4	192.12	5.4440
Ethylene Glycol (C ₂ H ₆ O ₂)		62.0678	1.921235

3.2.4. Fabrication of Nb-doped-BFO

The table 6 shows the amount of precursor that would be added to the sol for BLFO. Initially, the same steps were followed for the BFNbO sample preparation. But prior to the addition

of citric solution to the mixture, measured quantity of Niobium ammonium oxalate will be added to the mixture. Then the addition of citric acid and ethylene glycol were followed. Also, the magnetic stirrer temperature would be raised to 80°C and keep it for gel formation.

Table 3.4: List of Precursor and Quantity for BFNbO

Precursor	Molar ratio	mw(g/mol)	Quantity used (g)
Ba(NO ₃) ₂	1	261.33	3.7333
Fe(NO ₃) ₃ .9H ₂ O	0.9	404.00	5.1942
C ₄ H ₄ NNbO ₉ .xH ₂ O	0.1	302.98	0.4328
Citric acid (C ₆ H ₈ O ₇)	1.3	192.12	3.5575
Ethylene Glycol (C ₂ H ₆ O ₂)		62.0678	1.7787



Figure 3.1: (a) Dissolving metal nitrites in distilled water and (b) Dried gel

The liquid phase removal through a drying process, which is usually associated with shrinkage and densification. The distribution of porosity in the gel affects the solvent removal rate. The figure (a) (b) shows the dissolving nitrites in distilled water and dried gel. Afterwards, a thermal treatment, is often required in order to support the polycondensation and therefore it could improve the mechanical properties and structural stability of the component through sintering and densification.

3.3. Calcination and Sintering

The heat treatment for the three samples are scheduled for different calcination and sintering temperature and formulated in the table 3.5. For all three different samples, obtained dried gel is grinded and placed in an oven (fig. 3.2(a)) for drying at 300°C which is same for all three samples. Then the powder is placed in a furnace for calcination (fig. 3.2(b)) and

Table 3.5: A heat treatment plan for calcination and sintering

	Drying Temp	Drying time	Calcination Temp	Calcination holding time	Powder Code	Sintering Temp.	Sint. Hold Time	Disc code
	(°C)	(h)	(°C)	(h)		(°C)	(h)	
P1-BFO	300	24	600	2	BFO-600C-1300-2h	1300	15	BFO-600-2-1300-15
P1-BFO	300	24	700	5	BFO-700C-1300-5h	1300	10	BFO-700-5-1300-24
						1300	24	BFO-700-5-1300-24
P2-BFO	300	24	800	5	BFO-800C-1300-5h	1300	5	BFO-800-5-1300-5
			900	5	BFO-900C-1300-5h	1300	24	BFO-900-5-1300-24
			1000	5	BFO-1000C-5h	1300	24	BFO-1000-5-24
P3-BLFO	300	24	700	5	BFO-700C-5h	1300	15	BFO-700-5-15
			900	5	BLFO-900C-5h	1300	24	BLFO-900-5-24
P4-BFNbO	300	24	1000	5	BFNbO-1000C-5h	-	-	-

the temperature for calcination is depends on the sample mixture. After the completion of calcination, the calcined powder (fig. 3.2(c)) are cooled under 30°C and collected in capsules. The final sintered disc shape material is produced as shown in (fig. 3.2(d)).



3.4. XRD (X-RAY DIFFRACTION)

X-Ray diffraction is a non-destructive technique to examine the crystallographic structure of given material. It can also be used to view the chemical composition, crystalline size, orientation. XRD is commonly used to examine the crystalline materials but non-crystalline material also have been examined in several studies.

3.4.1. Principle

When the given material is subjected to a fine beam of X-rays, based on the atomic structure of the material, the ray gets diffracted at specific angles with altered intensity and producing diffracted patterns. The observed intensity and the diffracted pattern then used to analyse



Figure 3.2: (a) Drying in oven, (b) Calcination in heat treatment furnace, (c) Calcined powder and (d) Disc shaped Sintered sample

the material.

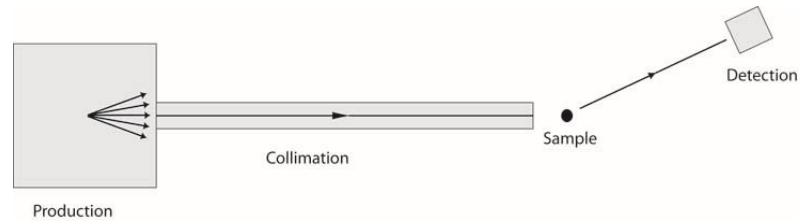


Figure 3.3: Stages of XRD

The above figure 4 described the stages of XRD. The working of XRD comprises of three stages namely, Production, Collimation and Detection. In production stage, there will be X-ray produced by a given source. There are different sources available to produce X-rays such as Synchrotron, X-ray tube. The second stage Collimation involves mechanisms to produce thin beam of X-rays. Detecting the given sample will be the final stage in XRD. There will be a detector placed to measure the diffraction angles of give sample. Using the interpretation of the diffraction pattern and Brigg's law, various properties and characteristics of materials can be analysed, such as comparing the observed the diffracted pattern and intensity of x-ray with pre-recorded database consists of diffraction pattern and intensity of x-ray for different materials, to find the arrangement of atoms in a crystalline structure using the peak position and intensity information is To determine crystallite size and strain, the diffracted peaks widths is used.

3.4.2. XRD experiments

Crystalline nature and phase purity were examined using powder X-ray diffraction (XRD) technique using Bruker D8 X-ray diffractometer with Cu $K\alpha$. For the fabricated samples, the 2θ step size was 0.02° with the integration time of 1s per step, over the scan range 2θ from 20° to 80° . Then, by Scherrer's equation (1) crystallite sizes are calculated,

$$\tau = \frac{K\lambda}{\beta \cos\theta}$$

Where,

τ = crystalline size.

K = dimensionless shape factor.

λ = wavelength of X-ray.

β = the line broadening at half the maximum intensity and denoted as 2θ in some cases.

θ = Bragg's angle.

3.5. Thermogravimetric Analysis / Differential Thermal Analysis

The combination of thermogravimetric analysis/ differential thermal analysis is a common method to efficiently measure and analyse the given sample for thermal properties in a single apparatus. Thermogravimetry is used to measure the mass change in given sample and to detect factors that affects the mass change in given sample such as decomposition, oxidation, evaporation and the effects arises due to change in temperature. The Differential thermal analysis is used to determine the melting, sublimation, glass transitions, and crystallization by interpreting the resultant DTA graph for the given sample.

3.6. Scanning Electron Microscope (SEM)

The scanning electron microscope is an electron microscope that commonly used to examine a specimen which might be organic or inorganic by scanning it. The light microscopes have wavelength limitation which paved the way to develop SEM.

3.6.1. Principle

The scanning electron microscope uses electron gun to project a beam of electrons which triggers the emission of primary and secondary scattered electrons. Electrons at higher energy level are primarily scattered electron and electrons scattered at lower energy level are secondary scattered electrons. These secondary scattered electrons emitted from the specimen produce signals that gives information about the specimen. The Fig 5 shows the schematic diagram of SEM, gives us the working nature of SEM. An electron used to produce beam of electrons moves at high speed and on hitting the specimen, the electrons are divided into primary and secondary scattered electrons, the secondary scattered electrons which are at low energy level is them able to produce signals which contains information about surface of the specimen. The secondary electrons enters a detector and strikes a scintillator. Then, a signal is sent to cathode ray tube in the form of electric current converted by photomultiplier by using the light flashes emitted by the electrons. The produced image by the CRT can be viewed and recorded.

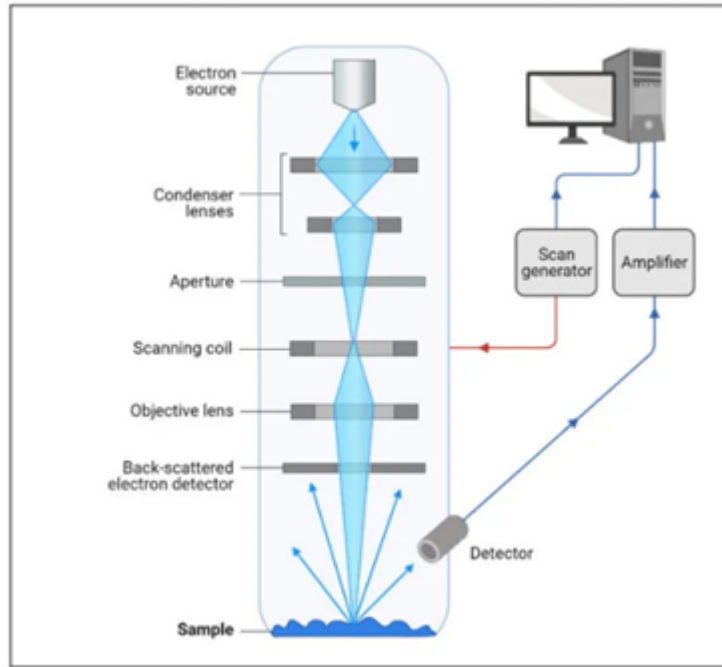


Figure 3.4: Schematic diagram of SEM

3.6.2. Applications

The scanning electron microscope is commonly used to examine the sample collected from living beings such as leaf, human blood and inorganic materials surface and provide details that are complex for light microscope. For the fabricated sample, SEM is used to analyse the morphology, particle size and distribution. The results would be recorded as image for further discussion.

3.7. Mechanical Testing

3.7.1. Sample Preparation

In order to perform mechanical tests, the samples were produced in the form of bars and discs by uniaxial pressing at 90MPa and sintering. The powders were mixed with 5wt% PVA binder and uniaxially pressed. The organic additives in the samples were burnt by heating the sample at a rate of 60°C/h and held at different temperature range (1250 to 1400°C), and soaked 5 times for 15 hr to determine the suitable condition for densification.

3.7.2. Uniaxial Compression Test

For compression test, the sample is grinded and polished for the bar shape at the dimension of 10 x 5 x 5 mm. In machine setup, the polished sample bar was placed between two alumina

rods with 10 mm diameter and the load was gradually increased from 5 N to a 300 N, 600 N and 900 N cyclic loads. Fig 3.5 shows the uniaxial compression test setup for the samples.

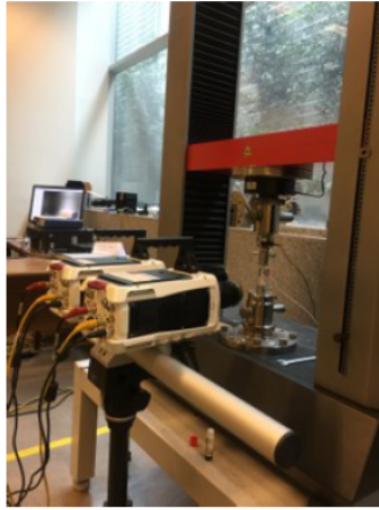


Figure 3.5: Experimental setup for compression test

Digital image correlation (DIC) technique is an optical method that employs image registration techniques which measures the changes in images, which can be used to calculate strains, and full-field displacements. A speckle pattern of high contrast would be applied on the sample surface and recorded by cameras continuously from initial load to final fracture. The software in DIC would identify the characteristic features appear on the pattern and tracks it from initial load to final fracture. The Fig. 6 shows, the specimen was applied with speckle pattern by matte paint. A facet size of 25 pixels was selected with an experimental resolution of the acquired images of 54 pixels per millimetre.



Figure 3.6: (a) Sample specimen before applying speckle pattern



Figure 3.7: (b) Specimen with speckle pattern by matte paint

3.7.3. Micro hardness test

Micro hardness test is testing of hardness for given material by applying small loads. Vickers hardness test method was used here to measure the hardness of the sample which would be in disc form. For any material subjected to micro hardness test, it is evident to follow these:

- At diagonal and low lengths hardness increases significantly for all types of loads.
- When the load is less, the pronounced effect can be more.
- In a vertical position, large hardness differences seen in small measurements.

For Vickers hardness test, the indent size is obtained by measuring the two square indent diagonals. About 15 indentations for 15 seconds dwelling time per load were performed. The indented surface is measured under SEM for the direct measurements of crack and indentation fracture toughness (K_{IC}) was calculated.

Chapter 4

Results And Discussion

4.1. Structural Characterisation

This chapter discuss the results from XRD, SEM, compression and hardness tests conducted on the fabricated BFO, BLFO and BFNbO samples. XRD tests were conducted to determine the crystal structure of the materials, SEM is to examine the porosity, morphological and topography on the surface of the samples and indentation marks and possible cracks for micro hardness and fracture toughness measurements. The compression tests are to evaluate the mechanical properties of the materials, and Hardness test is conducted for measuring the hardness of the samples.

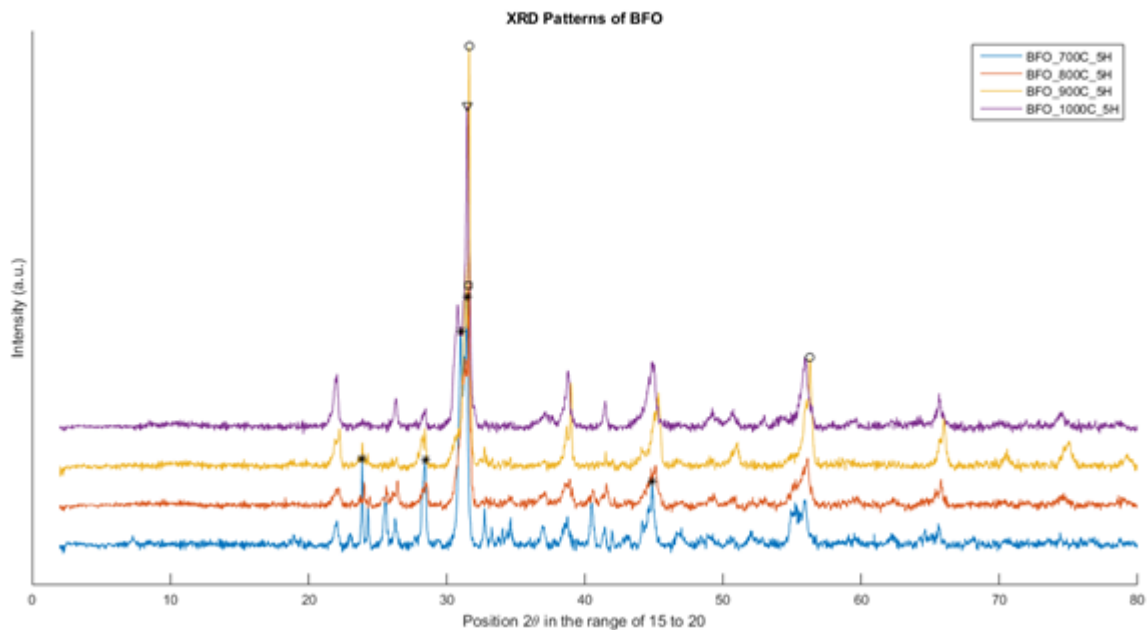
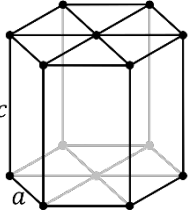


Figure 4.1: XRD Patterns of BFO powders calcined at Various Temperatures for 5 hours.

From the figure 9, it can be observed, with increasing calcination temperature the extra peaks that are belong to the impurities and the secondary phases are reduced, the structure

of powder calcined at 1000°C has hexagonal crystal structure as shown in the table 8.

Table 4.1: Crystal structure of BFO

BaFeO_{2.75}		
Crystal system	Hexagonal	
Space group	P63/mmc	
Space group number	194	

It can be observed that there are peak formation to BFO at different temperatures. The peak position of BFO was invariant but only the intensity of peak due to increase in the The XRD analysis of the 700°C , 800°C , 900°C and 1000°C calcined powders reveals the complete transformation of BFO.

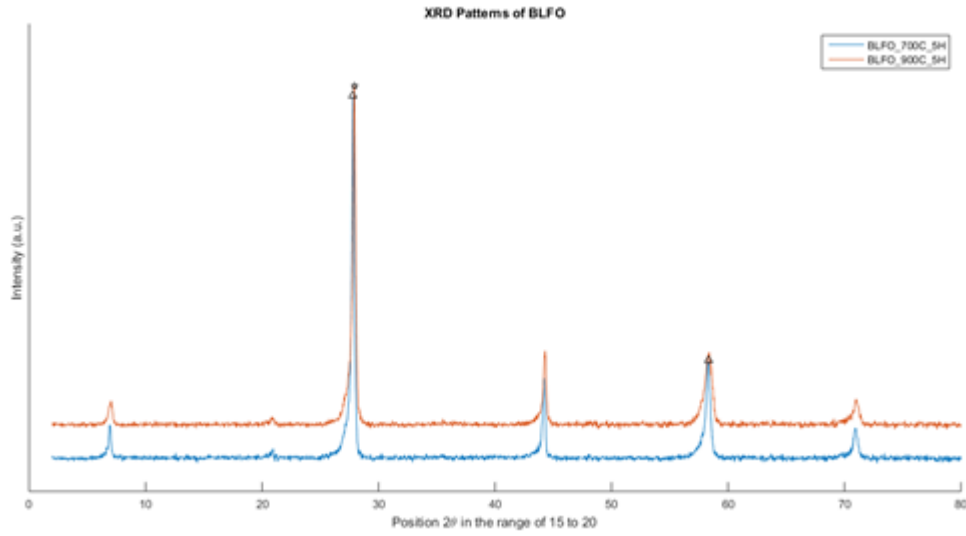
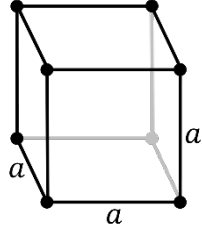


Figure 4.2: XRD Patterns of BLFO powders calcined at Various Temperature for 5 hours.

Figure 10 shows the XRD patterns of BLFO powders calcined at 900 and 1000°C for 5 hours. The structure of BLFO is cubic with details represented in table 9, which means that doping BFO with La stabilized cubic structure of BFO to room temperature.

Table 4.2: Crystal structure of BLFO

$\text{Ba}_{0.95}\text{La}_{0.05}\text{FeO}_3$		
Crystal system	Cubic	
Space group	Pm-3m	
Space group number	221	

The X-ray diffraction patterns of the BFNbO powders calcined at 1000°C temperature are shown in the figure 11. From the different patterns of XRD. The structure of BFNbO is more close to Tetragonal with details represented in table 10.

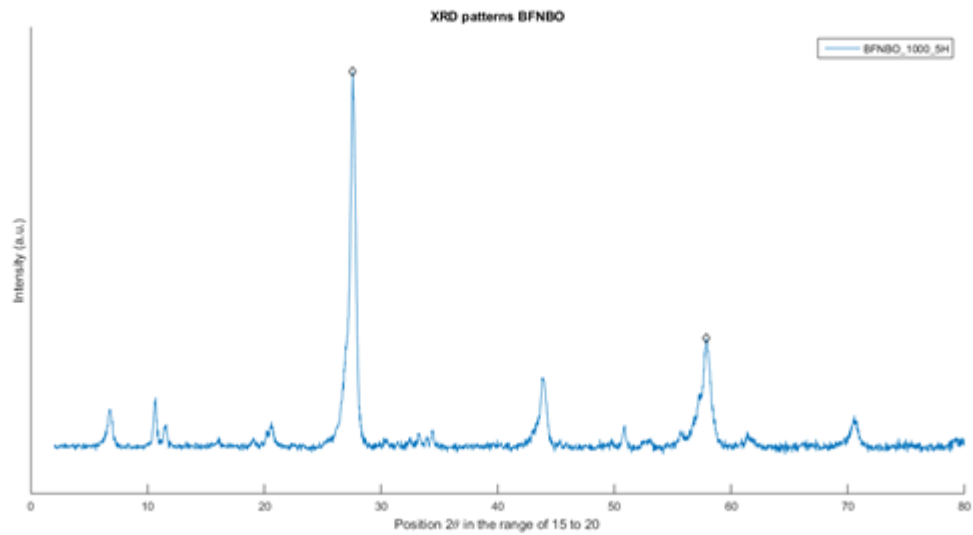
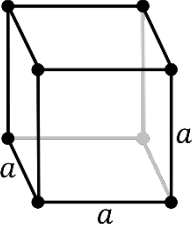


Figure 4.3: XRD Patterns of BFNbO powders calcined at Various 1000°C for 5 hours.

Table 4.3: Crystal structure of BFNbO

$\text{BaFe}_{0.95}\text{Nb}_{0.1}\text{O}_3$		
Crystal system	Tetragonal	
Space group	P4bm	
Space group number	100	

4.2. SEM Results

4.2.1. SEM results for BFO

The fractured surface of fabricated bar samples of BFO is examined under SEM and several images were taken at different scales. The images were captured at 15kV accelerating voltage. Fig 12 shows the SEM results for the sample at 330x and 980x.

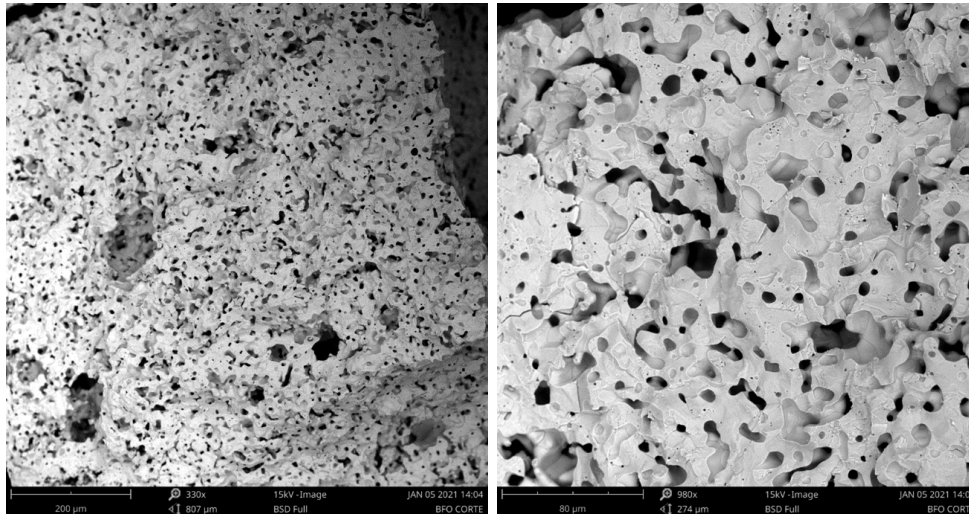


Figure 4.4: SEM images of BFO captured at (a) 330x at 200 μm (b) 980x at 80 μm by BSD

As it can be seen the porosity is visible for the BFO. The size of the captured images were scaled at 200 μm for fig 12 (a) and 80 μm fig 12 (b). At this scale, the surface of the sample are seen for morphology and other information. In order to understand more the next set of images were taken at (a) 680x at 100 μm and (b) 2900x at 20 μm . The images produced from Back scattered Detector at different resolutions shows information about the surface of the given BFO fabricated sample yet in order to understand the topographical information on the surface of the sample SED based images were also taken.

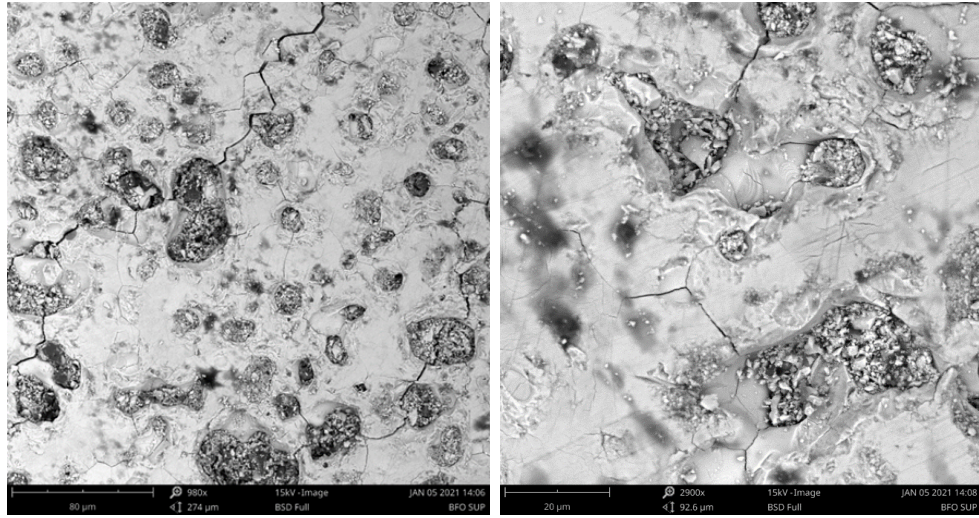


Figure 4.5: SEM images of BFO captured at (a) 680x at 100 μm (b) 2900x at 20 μm by BSD

A set of images were taken at fig 13 (a) 680x at 100 μm and fig 13 (b) 2900x at 20 μm at an accelerated voltage of 15kV. The dwells on the surface can be clearly seen in image captured by SED. There are some cracks observed for the sintered sample at the surface of the material. Also, samples shows high amount of porosity which shows its poor densification.

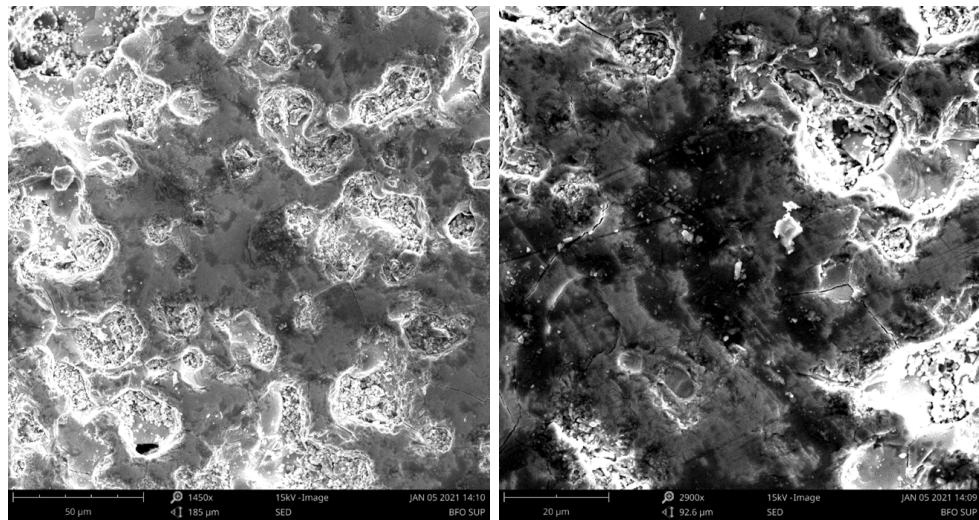


Figure 4.6: SEM images of BFO captured at (a) 1450x μm at 50 (b) 2900x at 92.6 μm by SED

The topological features like dwells, rises on the surface of the material can be seen clearly on the surface from the captured images fig 14 (a)(b).

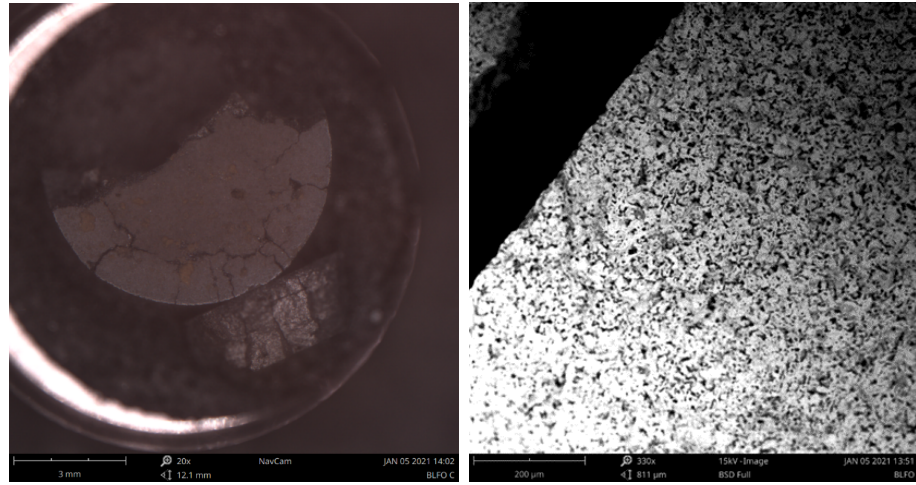


Figure 4.7: SEM images of BLFO captured at (a) 20x μm at 12.1mm (b) 330x at 811 μm by SED

A set of images were taken at fig 15 (a) sample that was scanned and fig 15 (b) 330x at 811 μm at an accelerated voltage of 15kV. The dwells on the surface can be clearly seen in image captured by SED.

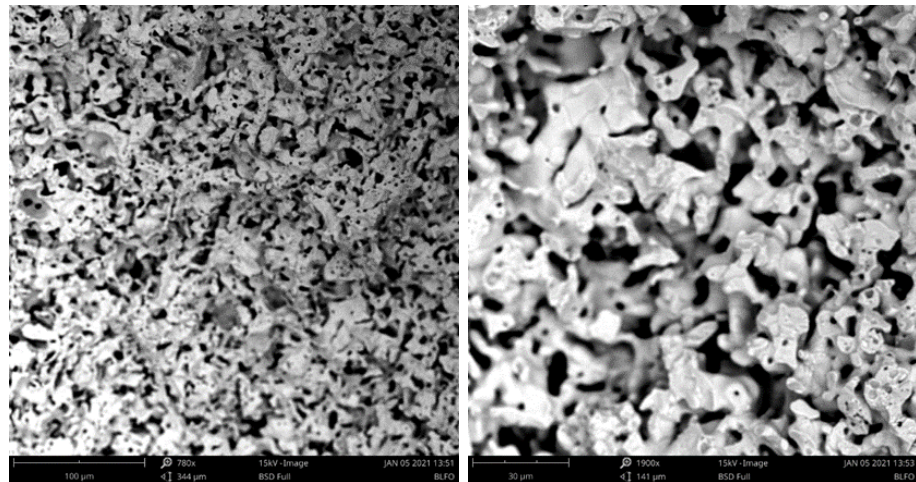


Figure 4.8: SEM images of BLFO captured at (a) 780x at 344 μm (b) 1900x at 141 μm by BSD

The SEM images for BLFO sample is shown in fig 16 (a) 780x at 344 μm and Fig 16 (b) 1900x at 141 μm by BSD at an accelerated voltage of 15kV.

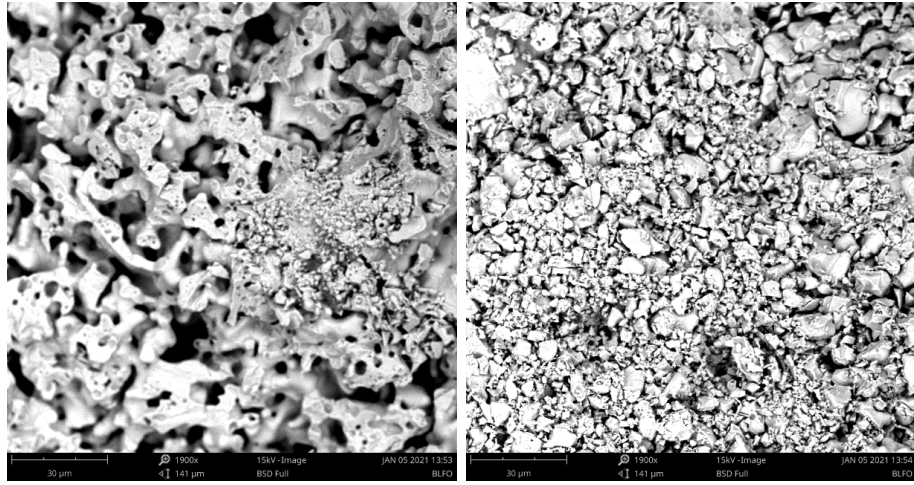


Figure 4.9: SEM images of BLFO captured at (a) 1900x at 141 μm (b) 1900x at 141 μm by BSD

The Fig. 17 (a) (b) shows the porous nature on the surface of the examined BLFO sample, which means that doping with La did not help BFO densification.

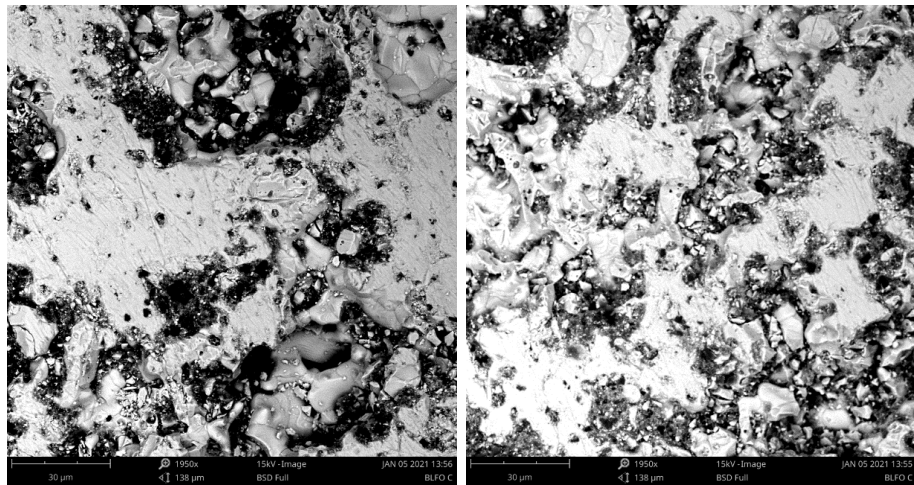


Figure 4.10: SEM images of BLFO captured at (a) 1950x at 138 μm (b) 1950x at 138 μm by BSD

The Fig. 18(a) (b) shows the surface of the examined BLFO sample.

4.2.2. SEM results for BFNbO:

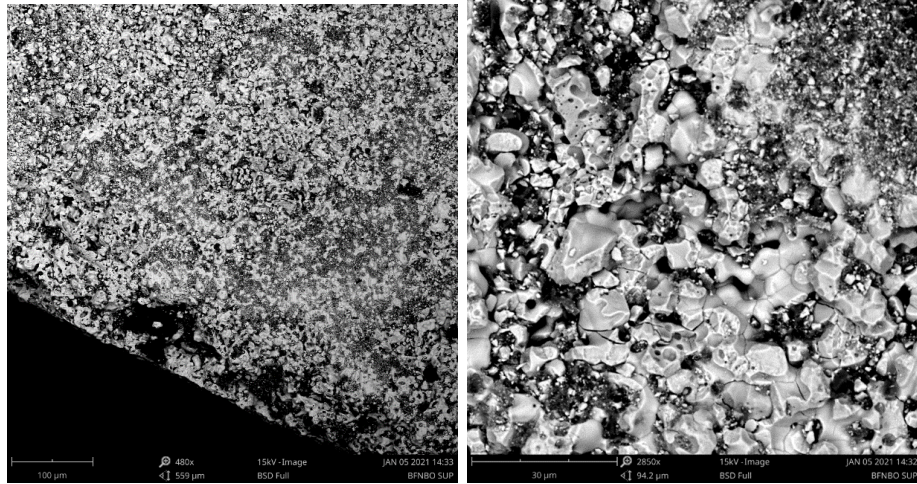


Figure 4.11: SEM images of BFNbO captured at (a) 1450x μm at 50 (b) 2900x at 92.6 μm by SED

The SEM images for BFNbO sample is shown in fig 19 (a) 1450x μm at 50 and (b) 2900x at 92.6 μm by SED at an accelerated voltage of 15kV. The Fig. 19 (a) (b) shows the porous nature on the surface of the examined BFNbO sample. The sintering and the densification reduced the porosity nature of the material as the structure was rigidly constructed. The relative density of BFO, BLFO and BFNbO samples are comparable around 70 percent of theoretical density of BFO.

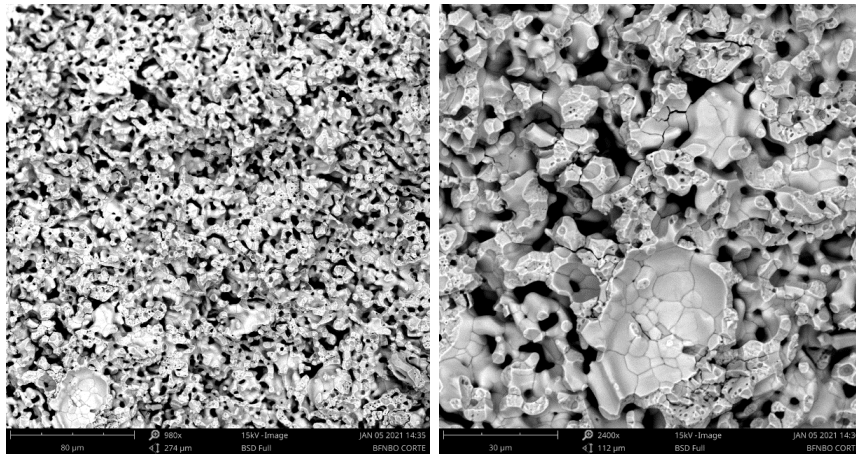


Figure 4.12: SEM images of BFNbO captured at (a) 1450x μm at 50 (b) 2900x at 92.6 μm by SED

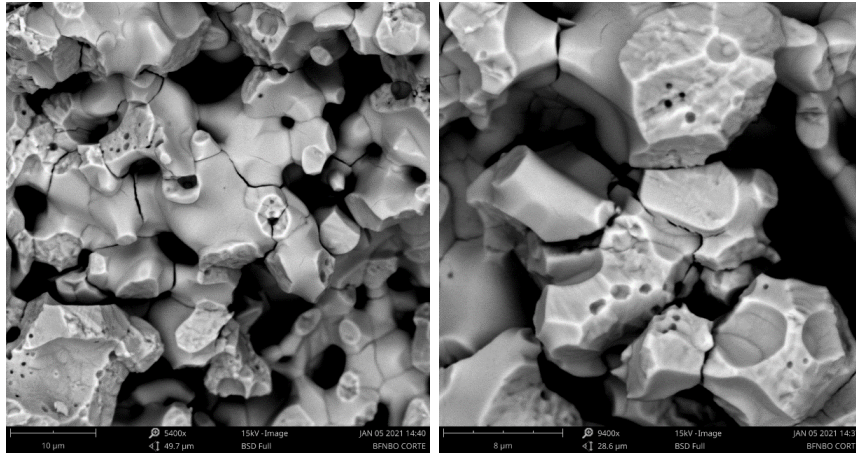


Figure 4.13: SEM images of BFNbO captured at (a) 1450x μm at 50 (b) 2900x at 92.6 μm by SED

The Fig. 21 (a) (b) shows the porous nature on the surface of the examined BFNbO sample.

4.3. Compression Tests

The BFO bar samples were loaded in three cycles, and the corresponding deformations were captured by DIC technique using Istra software. The Fig 4.12. to 4.16 shows the load-deformation curves for BFO, BLFO and BFNbO bar samples are recorded by universal test machine just as reference.

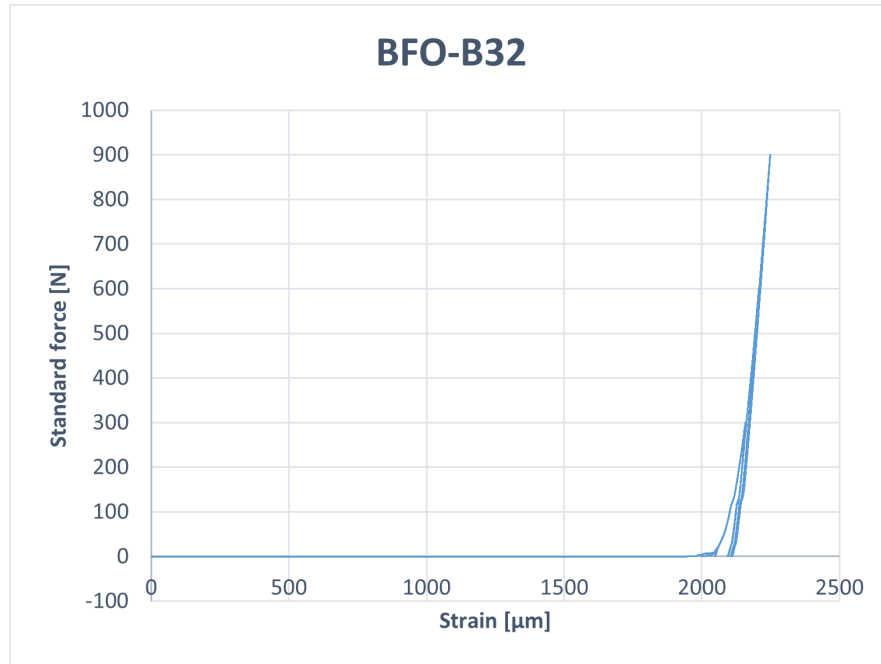


Figure 4.14: Strain vs Force for BFO

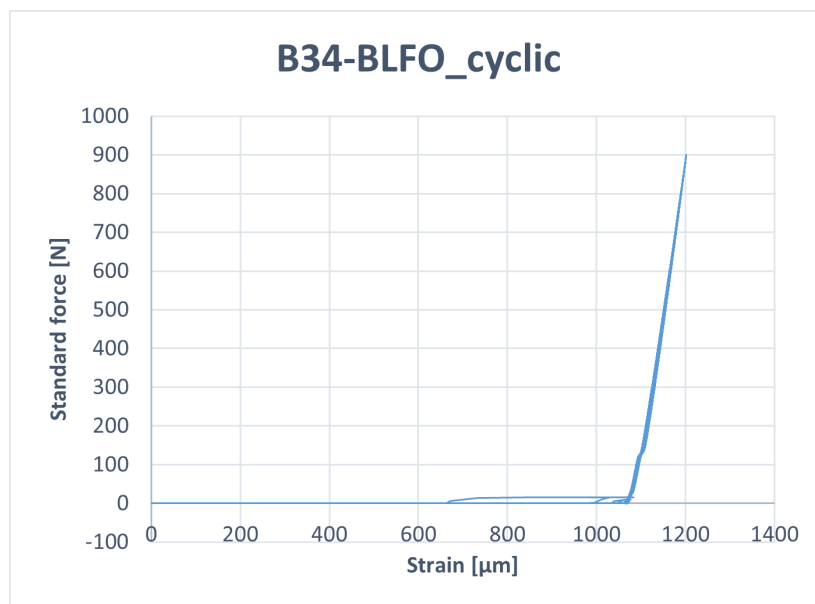


Figure 4.15: Strain vs Force for BFO

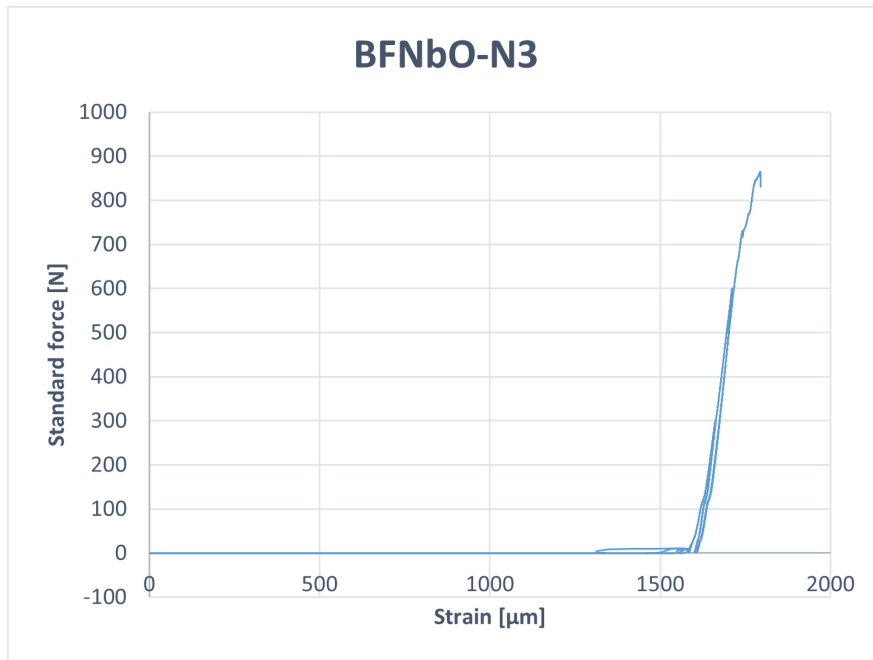


Figure 4.16: Strain vs Force for BFO

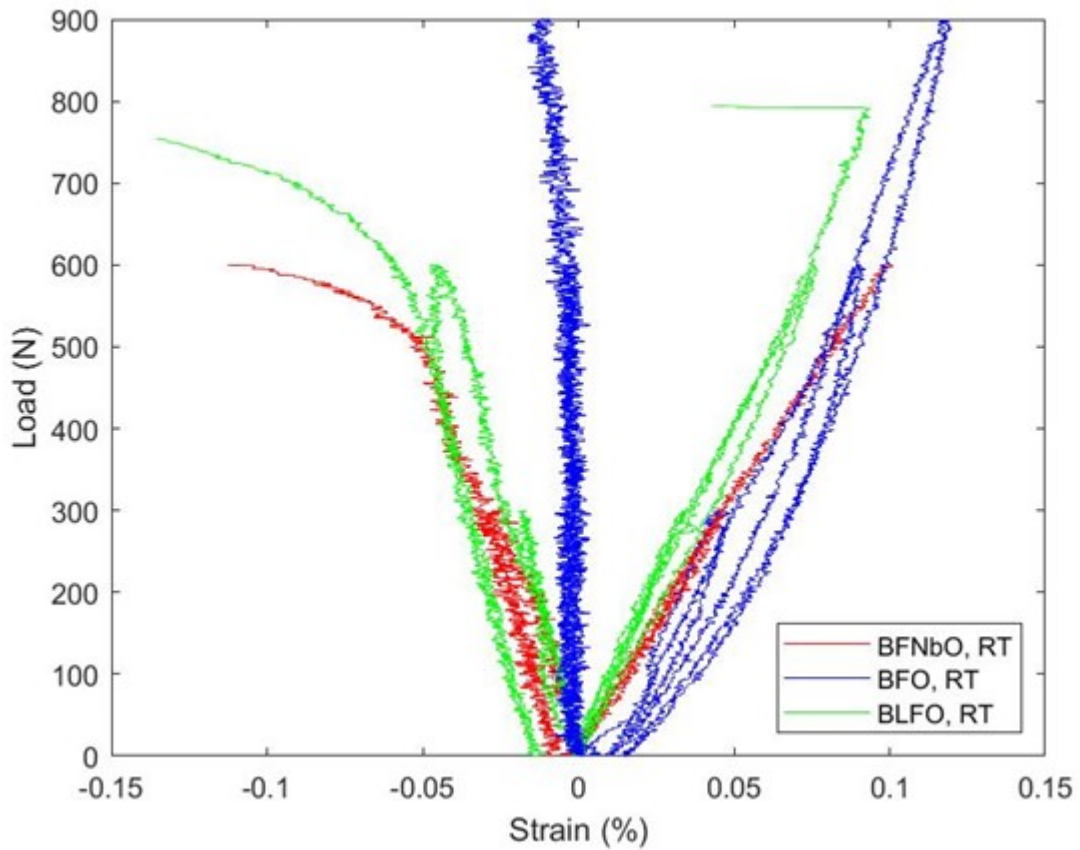


Figure 4.17: Comparison of axial and lateral stress-strain curves of BFO, BLFO, BFNbO samples tested at room temperature.

As it can be observed from the Fig. 25, BFO samples show non-linear elastic behaviour as its structure is hexagonal and not symmetric. However, by being doped with La or Nb its structure maintained its symmetry to room temperature, so its elastic behaviour is closer to linear behaviour. Also, it can be seen that samples doped with La and Nb are fractured at lower loads that may be attributed to lower strength, which need more investigation.

The mechanical properties of the proposed perovskite oxide are expected to be achieved by stabilizing the cubic lattice structure by B-site doping with ferro active metal elements like Niobium (Nb) and Lanthanum (La) The effect of B-site doping on the morphological, physicochemical and mechanical properties was analysed Mechanical and from the fig 25 it can be observed that the doped materials could not able to perform as the non-doped materials however, they could reflect the original properties closely. This shows that the mechanical properties are not affected much in the doped materials.

4.3.1. Microhardness Test

4.3.1.1. Effect of La and Nb doping on Micro Hardness and fracture toughness of BFO

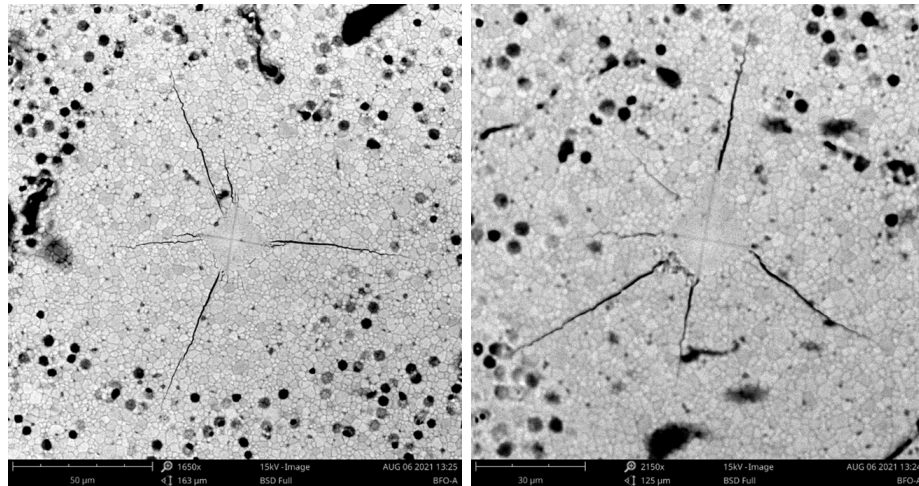


Figure 4.18: SEM images of indented BFO captured at (a) 1650x at 163 μm (b) 2150x at 125 μm by BSD

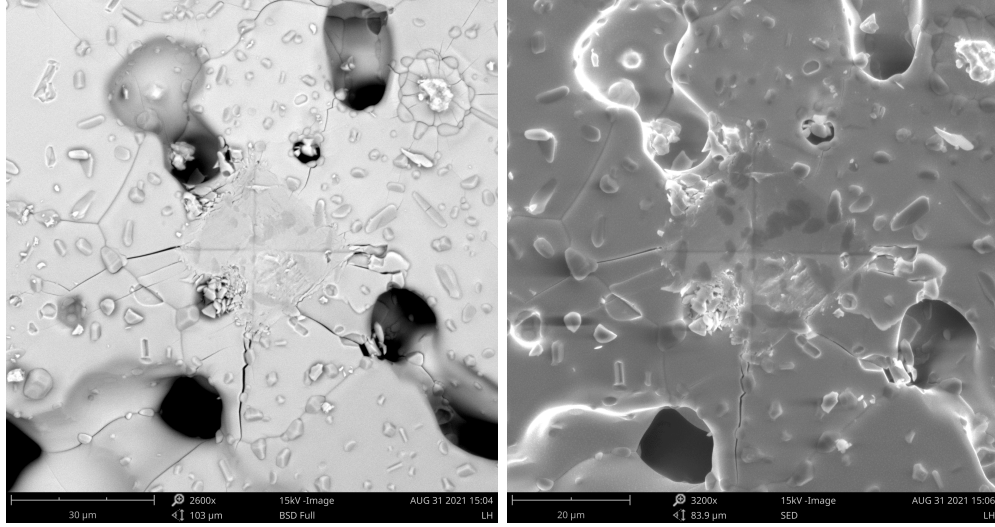


Figure 4.19: SEM images of indented BLFO captured at (a) 1650x at 163 μm (b) 2150x at 30 μm by BSD

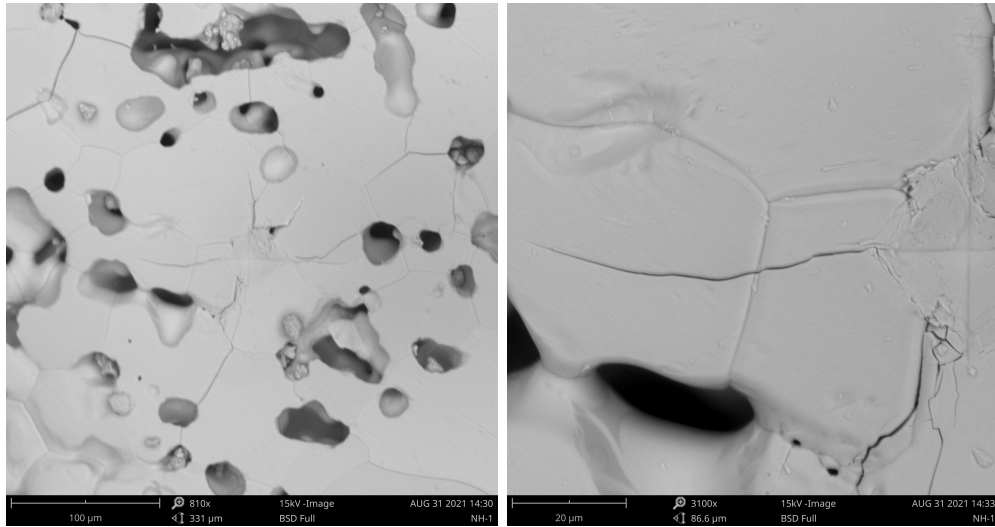


Figure 4.20: SEM images of indented BFNbO captured at (a) 1650x at 163 μm (b) 2150x at 30 μm by BSD

Figs. 26-28 show the indentation marks observed on the BFO, BLFO and BFNbO samples, respectively. It is observed that, cracks have been observed near the indentation marks and inter-granularly transmit through neighbouring grains, which can be used to determine the fracture toughness. Many equations with some conditions and limitations have been proposed for measuring indentation fracture toughness as reviewed by Ponton and Rawlings [188] [303]

$$K_{IC} = 0.0089 \left(\frac{E}{0.927 H_v} \right)^{2/5} \frac{P}{a\sqrt{l}} c = a + l \quad (4.1)$$

Where, P is the applied load, H_v is the Vickers hardness, E is the elastic modulus of the material measured by bending test, a and c are diagonal and crack length generated by the indentation. In order to compare, the equation (2) proposed by was used to analyse the

fracture.

$$K_{IC} = 0.0089 \left(\frac{E}{0.927H_v} \right)^{1/2} \frac{P}{c^{3/2}} \quad (4.2)$$

The Micro hardness indentation done by the Vickers hardness machine and the produced dwells and falls are inspected under SEM for hardness measurements. The figures shows different indentation points recorded on the surface to test the hardness.

Table 4.4: Micro-hardness measurements for BFO, BLFO and BFNbO

Applied load (N)	Hardness (GPa)	KIC(MPa.m ^{0.5})	KIC (MPa.m ^{0.5})
		Niihara 's eq.	Anistis 's eq.
BFO	7.45±1.4	0.64±0.14	0.3±0.13
BLFO	26.44±13.9	1.34±0.74	0.83±0.65
BFNbO	16.6±8.8	0.26±0.12	0.69±0.03

From the table 11, the hardness and fracture toughness of sintered BFO, BLFO and BFNbO samples were calculated using the Niihara and Anistis method based on the equation (1) and (2).

As it can be seen, the hardness and fracture toughness of thee materials which are compared based on the Niihara and Anistis's methods and there is a significant difference can be seen for the hardness between the three materials. Although, the individual doping showed lower strength than the undoped material. However, standard deviation of microhardness obtained for BLFO and BFNbO samples arwe high which can be due to using few indentations and it needs more investigation. As it can be seen in SEM micrographs and by calculated fracture toughness, it seems that doping BFO with La can improve its fracture toughness.

In summary, The XRD tests showed the crytal structure of the fabricated samples. And the SEM results showed how the porosity changed for the doping material. The hardness of the doped and non doped material showed some difference based on the Niihara and Anistis method. However, the stress stain analysis showed the linear behaviour of the materials. Depending on the application, the suitable material should be analysed, and the doping variance could affect further. Thus, the morphological and material characteristics were obtained from XRD, SEM, and mechanical tests. [304] [305].

In summary, The XRD tests showed the crytal structure of the fabricated samples. And the SEM results showed how the porosity changed for the doping material. The hardness of the doped and non doped material showed some difference based on the Niihara and Anistis

method. However, the stress strain analysis showed the linear behaviour of the materials. Depending on the application, the suitable material should be analysed, and the doping varaience could affect further. Thus, the morphological and meaterial characteristics were obtained from XRD, SEM, and mechanical tests.

Chapter 5

Conclusion

The study focused on characterizing the synthesized BFO, BLFO, and BFNbO and analyzed it by several techniques. Answering research question one, the mechanical characteristics and structure of doped BaFeO was analyzed using the XRD, Compression and hardness tests, and for research question 2, the effect of La and Nb doping was observed in the SEM and Hardness tests. Initially, the samples were fabricated using sol-gel and later sintered at different temperatures appropriately, and samples were prepared for testing. At first, characterize the cubic structure and porosity nature of the material. The samples are observed using XRD and SEM techniques. From XRD results, it came to know that BFO_{2.73} has a hexagonal crystal system and the XRD patterns showed the presence of impurities through the peaks. And observing BLFO powder, the XRD patterns showed the presence of impurities through the peaks and had a cubic crystal system. For the BFNbO powder, the XRD patterns showed the presence of impurities through the peaks and had a tetragonal crystal system. The SEM results showed the variations of porosity nature among the BFO, BLFO and BFNbO. The doping on the material impacted the porosity nature of the material.

The fabricated materials showed a non-linear elastic behaviour by the stress-strain relationship developed to form the compression test. The Lanthanum (La) and Niobium (Nb) doping on the material have less significant effects on the mechanical property of the doped materials than the original material. However, the doped materials are fractures at lower loads due to the lower strength, which might need further investigation. For the hardness test, the fabricated materials are subjected to Vicker's hardness test. The material is observed under SEM for measurements and analyzed using Niihara and Anitis method. These two methods are followed to evaluate the measured hardness, and comparing among the fabricated materials at different loads showed us the hardness varied to the different loads.

Bibliography

- [1] Pena, M. y Fierro, J., “Chemical structures and performance of perovskite oxides,” *Chemical reviews*, vol. 101, no. 7, pp. 1981–2018, 2001.
- [2] Sunarso, J., Baumann, S., Serra, J., Meulenbergh, W., Liu, S., Lin, Y., y Da Costa, J. D., “Mixed ionic–electronic conducting (miec) ceramic-based membranes for oxygen separation,” *Journal of membrane science*, vol. 320, no. 1-2, pp. 13–41, 2008.
- [3] Fabbri, E., D’Epifanio, A., Di Bartolomeo, E., Licocchia, S., y Traversa, E., “Tailoring the chemical stability of $\text{Ba}_{1-x}\text{Zr}_x\text{O}_{3-\delta}$ protonic conductors for intermediate temperature solid oxide fuel cells (it-sofcs),” *Solid State Ionics*, vol. 179, no. 15-16, pp. 558–564, 2008.
- [4] Shao, Z., Haile, S. M., Ahn, J., Ronney, P. D., Zhan, Z., y Barnett, S. A., “A thermally self-sustained micro solid-oxide fuel-cell stack with high power density,” *Nature*, vol. 435, no. 7043, pp. 795–798, 2005.
- [5] Fergus, J. W., “Perovskite oxides for semiconductor-based gas sensors,” *Sensors and Actuators B: Chemical*, vol. 123, no. 2, pp. 1169–1179, 2007.
- [6] Sunarso, J., Hashim, S. S., Zhu, N., y Zhou, W., “Perovskite oxides applications in high temperature oxygen separation, solid oxide fuel cell and membrane reactor: a review,” *Progress in Energy and Combustion Science*, vol. 61, pp. 57–77, 2017.
- [7] Chen, H.-C., Huang, C.-W., Wu, J. C., y Lin, S.-T., “Theoretical investigation of the metal-doped SrTiO_3 photocatalysts for water splitting,” *The Journal of Physical Chemistry C*, vol. 116, no. 14, pp. 7897–7903, 2012.
- [8] Royer, S., Duprez, D., Can, F., Courtois, X., Batiot-Dupeyrat, C., Laassiri, S., y Alamdari, H., “Perovskites as substitutes of noble metals for heterogeneous catalysis: dream or reality,” *Chemical reviews*, vol. 114, no. 20, pp. 10292–10368, 2014.
- [9] Arul, N. S. y Nithya, V. D., *Revolution of Perovskite*. Springer, 2020.
- [10] Kanhere, P. y Chen, Z., “A review on visible light active perovskite-based photocatalysts,” *Molecules*, vol. 19, no. 12, pp. 19995–20022, 2014.
- [11] Bhalla, A., Guo, R., y Roy, R., “The perovskite structure—a review of its role in ceramic science and technology,” *Materials research innovations*, vol. 4, no. 1, pp. 3–26, 2000.
- [12] Anderson, M. T., Greenwood, K. B., Taylor, G. A., y Poepfelmeier, K. R., “B-cation

- arrangements in double perovskites,” *Progress in solid state chemistry*, vol. 22, no. 3, pp. 197–233, 1993.
- [13] Yoshiya, M., Fisher, C., Iwamoto, Y., Asanuma, M., Ishii, J., y Yabuta, K., “Phase stability of $\text{BaCo}_{1-x}\text{Fe}_x\text{O}_{3-\delta}$ by first principles calculations,” *Solid State Ionics*, vol. 172, no. 1-4, pp. 159–163, 2004.
- [14] Zhang, K., Sunarso, J., Shao, Z., Zhou, W., Sun, C., Wang, S., y Liu, S., “Research progress and materials selection guidelines on mixed conducting perovskite-type ceramic membranes for oxygen production,” *RSC advances*, vol. 1, no. 9, pp. 1661–1676, 2011.
- [15] Liang, F., Partovi, K., Jiang, H., Luo, H., y Caro, J., “B-site La -doped $\text{BaFe}_{0.95-x}\text{La}_x\text{Zr}_{0.05}\text{O}_{3-\delta}$ perovskite-type membranes for oxygen separation,” *Journal of Materials Chemistry A*, vol. 1, no. 3, pp. 746–751, 2013.
- [16] Baiyee, Z. M., Chen, C., y Ciucci, F., “A *dft+u* study of a-site and b-site substitution in $\text{BaFe}_{0.3}\text{O}_{3-\delta}$,” *Physical Chemistry Chemical Physics*, vol. 17, no. 36, pp. 23511–23520, 2015.
- [17] Liu, X., Zhao, H., Yang, J., Li, Y., Chen, T., Lu, X., Ding, W., y Li, F., “Lattice characteristics, structure stability and oxygen permeability of $\text{BaFe}_{1-x}\text{Y}_x\text{O}_{3-\delta}$ ceramic membranes,” *Journal of membrane science*, vol. 383, no. 1-2, pp. 235–240, 2011.
- [18] Dong, F., Chen, Y., Ran, R., Chen, D., Tadé, M. O., Liu, S., y Shao, Z., “ $\text{Ba}_{0.05}\text{Fe}_{0.95}\text{O}_{3-\delta}$ as a new oxygen reduction electrocatalyst for intermediate temperature solid oxide fuel cells,” *Journal of Materials Chemistry A*, vol. 1, no. 34, pp. 9781–9791, 2013.
- [19] Lu, Y., Zhao, H., Cheng, X., Jia, Y., Du, X., Fang, M., Du, Z., Zheng, K., y Świerczek, K., “Investigation of In -doped $\text{BaFe}_{0.3}\text{O}_{3-\delta}$ perovskite-type oxygen permeable membranes,” *Journal of Materials Chemistry A*, vol. 3, no. 11, pp. 6202–6214, 2015.
- [20] Sanjulián, J. F., Chennabasappa, M., García-Martín, S., Nénert, G., Wattiaux, A., Gaudin, E., y Toulemonde, O., “Oxygen vacancy ordering in $\text{Sr}_{0.25}\text{Co}_{0.75}\text{O}_{2.63}$ perovskite material,” *Dalton Transactions*, vol. 46, no. 5, pp. 1624–1633, 2017.
- [21] Watanabe, K., Yuasa, M., Kida, T., Teraoka, Y., Yamazoe, N., y Shimano, K., “High-performance oxygen-permeable membranes with an asymmetric structure using $\text{Ba}_{0.95}\text{La}_{0.05}\text{FeO}_{3-\delta}$ perovskite-type oxide,” *Advanced Materials*, vol. 22, no. 21, pp. 2367–2370, 2010.
- [22] Lisi, L., Bagnasco, G., Ciambelli, P., De Rossi, S., Porta, P., Russo, G., y Turco, M., “Perovskite-type oxides: II. redox properties of $\text{LaMn}_{1-x}\text{Ce}_x\text{O}_3$ and $\text{LaCo}_{1-x}\text{Ce}_x\text{O}_3$ and methane catalytic combustion,” *Journal of Solid State Chemistry*, vol. 146, no. 1, pp. 176–183, 1999.
- [23] Voorhoeve, R., Remeika, J., y Trimble, L., “Defect chemistry and catalysis in oxidation and reduction over perovskite-type oxides,” *Annals of the New York Academy of*

Sciences, vol. 272, no. 1, pp. 3–21, 1976.

- [24] Ishihara, T., “Oxide ion conductivity in perovskite oxide for solid electrolyte,” en *Perovskite oxide for solid oxide fuel cells*, pp. 65–93, Springer, 2009.
- [25] Thirumal, M., Jain, P., y Ganguli, A., “Molten salt synthesis of complex perovskite-related dielectric oxides,” *Materials chemistry and physics*, vol. 70, no. 1, pp. 7–11, 2001.
- [26] Jiráček, Z., Hirschner, J., Kaman, O., Knížek, K., Levinský, P., Maryško, M., y Hejtmánek, J., “Structure and transport properties of $\text{La}_{1-x}\text{Sr}_x\text{MnO}_3$ granular ceramics,” *Journal of Physics D: Applied Physics*, vol. 50, no. 7, p. 075001, 2017.
- [27] Xia, W., Li, L., Wu, H., Xue, P., y Zhu, X., “Molten salt route of $\text{La}_{1-x}\text{Ca}_x\text{MnO}_3$ nanoparticles: microstructural characterization, magnetic and electrical transport properties,” *Materials Characterization*, vol. 131, pp. 128–134, 2017.
- [28] McCormick, P. G., Tsuzuki, T., Robinson, J. S., y Ding, J., “Nanopowders synthesized by mechanochemical processing,” *Advanced materials*, vol. 13, no. 12-13, pp. 1008–1010, 2001.
- [29] Kong, L. B., Zhang, T., Ma, J., y Boey, F., “Progress in synthesis of ferroelectric ceramic materials via high-energy mechanochemical technique,” *Progress in Materials Science*, vol. 53, no. 2, pp. 207–322, 2008.
- [30] Zouari, S., Ellouze, M., Nasri, A., Cherif, W., Hlil, E., y Elhalouani, F., “Morphology, structural, magnetic, and magnetocaloric properties of $\text{Pr}_{0.7}\text{Ca}_{0.3}\text{MnO}_3$ nanopowder prepared by mechanical ball milling method,” *Journal of Superconductivity and Novel Magnetism*, vol. 27, no. 2, pp. 555–563, 2014.
- [31] Khamman, O., Wongmaneerung, R., Chaisan, W., Yimnirun, R., y Ananta, S., “Preparation of perovskite nanopowders by vibro-milling technique,” *Journal of alloys and compounds*, vol. 456, no. 1-2, pp. 492–497, 2008.
- [32] Brinker, C., Hurd, A., Schunk, P., Frye, G., y Ashley, C., “Review of sol-gel thin film formation,” *Journal of Non-Crystalline Solids*, vol. 147, pp. 424–436, 1992.
- [33] Yoshimura, M. y Byrappa, K., “Hydrothermal processing of materials: past, present and future,” *Journal of Materials Science*, vol. 43, no. 7, pp. 2085–2103, 2008.
- [34] Zhu, X. y Hang, Q., “Microscopical and physical characterization of microwave and microwave-hydrothermal synthesis products,” *Micron*, vol. 44, pp. 21–44, 2013.
- [35] Ganguli, A. K., Ganguly, A., y Vaidya, S., “Microemulsion-based synthesis of nanocrystalline materials,” *Chemical Society Reviews*, vol. 39, no. 2, pp. 474–485, 2010.
- [36] Chandler, C. D., Roger, C., y Hampden-Smith, M. J., “Chemical aspects of solution routes to perovskite-phase mixed-metal oxides from metal-organic precursors,” *Chemical reviews*, vol. 93, no. 3, pp. 1205–1241, 1993.
- [37] Hench, L. L. y West, J. K., “The sol-gel process,” *Chemical reviews*, vol. 90, no. 1,

pp. 33–72, 1990.

- [38] Brutchey, R. L. y Morse, D. E., “Template-free, low-temperature synthesis of crystalline barium titanate nanoparticles under bio-inspired conditions,” *Angewandte Chemie*, vol. 118, no. 39, pp. 6714–6716, 2006.
- [39] Kamiya, H., Gomi, K., Iida, Y., Tanaka, K., Yoshiyasu, T., y Kakiuchi, T., “Preparation of highly dispersed ultrafine barium titanate powder by using microbial-derived surfactant,” *Journal of the American Ceramic Society*, vol. 86, no. 12, pp. 2011–2018, 2003.
- [40] Pechini, M. P., “Method of preparing lead and alkaline earth titanates and niobates and coating method using the same to form a capacitor,” 1967. US Patent 3,330,697.
- [41] Han, J.-M., Joung, M.-R., Kim, J.-S., Lee, Y.-S., Nahm, S., Choi, Y.-K., y Paik, J.-H., “Hydrothermal synthesis of BaTiO₃ nanopowders using TiO₂ nanoparticles,” *Journal of the American Ceramic Society*, vol. 97, no. 2, pp. 346–349, 2013, doi:10.1111/jace.12755.
- [42] Hayashi, H., Noguchi, T., Islam, N. M., Hakuta, Y., Imai, Y., y Ueno, N., “Hydrothermal synthesis of batio₃ nanoparticles using a supercritical continuous flow reaction system,” *Journal of Crystal Growth*, vol. 312, no. 12-13, pp. 1968–1972, 2010.
- [43] Papadas, I. T., Ioakeimidis, A., Armatas, G. S., y Choulis, S. A., “Low-temperature combustion synthesis of a spinel NiCo₂ o₄ hole transport layer for perovskite photo-voltaics,” *Advanced Science*, vol. 5, no. 5, p. 1701029, 2018, doi:10.1002/advs.201701029.
- [44] Varma, A., Mukasyan, A. S., Rogachev, A. S., y Manukyan, K. V., “Solution combustion synthesis of nanoscale materials,” *Chemical Reviews*, vol. 116, no. 23, pp. 14493–14586, 2016, doi:10.1021/acs.chemrev.6b00279.
- [45] Kingsley, J. y Patil, K., “A novel combustion process for the synthesis of fine particle -alumina and related oxide materials,” *Materials Letters*, vol. 6, no. 11-12, pp. 427–432, 1988, doi:10.1016/0167-577x(88)90045-6.
- [46] Toniolo, J., Takimi, A., y Bergmann, C., “Nanostructured cobalt oxides (co₃o₄ and CoO) and metallic co powders synthesized by the solution combustion method,” *Materials Research Bulletin*, vol. 45, no. 6, pp. 672–676, 2010, doi:10.1016/j.materresbull.2010.03.001.
- [47] Qi, X., Zhou, J., Yue, Z., Gui, Z., y Li, L., “Auto-combustion synthesis of nanocrystalline LaFeO₃,” *Materials Chemistry and Physics*, vol. 78, no. 1, pp. 25–29, 2003, doi:10.1016/s0254-0584(02)00341-3.
- [48] Assirey, E. A. R., “Perovskite synthesis, properties and their related biochemical and industrial application,” *Saudi Pharmaceutical Journal*, vol. 27, no. 6, pp. 817–829, 2019, doi:10.1016/j.jsps.2019.05.003.

- [49] Gawande, M. B., Shelke, S. N., Zboril, R., y Varma, R. S., “Microwave-assisted chemistry: Synthetic applications for rapid assembly of nanomaterials and organics,” *Accounts of Chemical Research*, vol. 47, no. 4, pp. 1338–1348, 2014, doi: [10.1021/ar400309b](https://doi.org/10.1021/ar400309b).
- [50] Leadbeater, N. E., “Review of aqueous microwave assisted chemistry: Synthesis and catalysis,” *Journal of the American Chemical Society*, vol. 133, no. 6, pp. 2011–2011, 2011, doi: [10.1021/ja111493p](https://doi.org/10.1021/ja111493p).
- [51] Li, L., Song, J., Lu, Q., y Tan, X., “Synthesis of nano-crystalline $\text{sm}_{0.5}\text{sr}_{0.5}\text{co}(\text{fe})\text{o}_3$ -perovskite oxides by a microwave-assisted sol–gel combustion process,” *Ceramics International*, vol. 40, no. 1, pp. 1189–1194, 2014, doi: [10.1016/j.ceramint.2013.07.004](https://doi.org/10.1016/j.ceramint.2013.07.004).
- [52] Dimesso, L., “Pechini processes: An alternate approach of the sol–gel method, preparation, properties, and applications,” en *Handbook of Sol-Gel Science and Technology*, pp. 1–22, Springer International Publishing, 2016, doi: [10.1007/978-3-319-19454-7_123-1](https://doi.org/10.1007/978-3-319-19454-7_123-1).
- [53] Lin, Y.-J., Chang, Y.-H., Yang, W.-D., y Tsai, B.-S., “Synthesis and characterization of ilmenite NiTiO_3 and CoTiO_3 prepared by a modified pechini method,” *Journal of Non-Crystalline Solids*, vol. 352, no. 8, pp. 789–794, 2006, doi: [10.1016/j.jnoncrysol.2006.02.001](https://doi.org/10.1016/j.jnoncrysol.2006.02.001).
- [54] Dong, F., Chen, D., Chen, Y., Zhao, Q., y Shao, Z., “La-doped $\text{bafeo}_{3-\delta}$ perovskite as a cobalt-free oxygen reduction electrode for solid oxide fuel cells with oxygen-ion conducting electrolyte,” *Journal of Materials Chemistry*, vol. 22, no. 30, pp. 15071–15079, 2012.
- [55] Shao, Z., Yang, W., Cong, Y., Dong, H., Tong, J., y Xiong, G., “Investigation of the permeation behavior and stability of a $\text{ba}_{0.5}\text{sr}_{0.5}\text{co}_{0.8}\text{fe}_{0.2}\text{o}_{3-\delta}$ oxygen membrane,” *Journal of Membrane Science*, vol. 172, no. 1-2, pp. 177–188, 2000.
- [56] Hou, S.-e., Alonso, J. A., y Goodenough, J. B., “Co-free, iron perovskites as cathode materials for intermediate-temperature solid oxide fuel cells,” *Journal of Power Sources*, vol. 195, no. 1, pp. 280–284, 2010.
- [57] Wachsman, E. D., Marlowe, C. A., y Lee, K. T., “Role of solid oxide fuel cells in a balanced energy strategy,” *Energy & Environmental Science*, vol. 5, no. 2, pp. 5498–5509, 2012.
- [58] Xian, H., Li, F.-L., Li, X.-G., Zhang, X.-W., Meng, M., Zhang, T.-Y., y Tsubaki, N., “Influence of preparation conditions to structure property, nox and so2 sorption behavior of the bafeo_{3-x} perovskite catalyst,” *Fuel processing technology*, vol. 92, no. 9, pp. 1718–1724, 2011.
- [59] Chakraborty, A., Basu, R. N., y Maiti, H. S., “Low temperature sintering of $\text{la}(\text{ca})\text{cro}_3$ prepared by an autoignition process,” *Materials Letters*, vol. 45, no. 3-4, pp. 162–166, 2000.

- [60] Rivas-Vázquez, L., Rendón-Angeles, J., Rodríguez-Galicia, J., Gutierrez-Chavarria, C., Zhu, K., y Yanagisawa, K., “Preparation of calcium doped $\text{LaCoO}_{3-\delta}$ fine powders by hydrothermal method and its sintering,” *Journal of the European Ceramic Society*, vol. 26, no. 1-2, pp. 81–88, 2006.
- [61] Onuma, S., Miyoshi, S., Yashiro, K., Kaimai, A., Kawamura, K., Nigara, Y., Kawada, T., Mizusaki, J., Sakai, N., y Yokokawa, H., “Phase stability of $\text{La}_{1-x}\text{Ca}_x\text{Co}_{3-\delta}$ in oxidizing atmosphere,” *Journal of Solid State Chemistry*, vol. 170, no. 1, pp. 68–74, 2003.
- [62] Oishi, M., Yashiro, K., Hong, J.-O., Nigara, Y., Kawada, T., y Mizusaki, J., “Oxygen nonstoichiometry of b-site doped $\text{LaCoO}_{3-\delta}$,” *Solid State Ionics*, vol. 178, no. 3-4, pp. 307–312, 2007.
- [63] Wang, H., Tablet, C., Feldhoff, A., y Caro, J., “A cobalt-free oxygen-permeable membrane based on the perovskite-type oxide $\text{Ba}_{0.5}\text{Sr}_{0.5}\text{Zn}_{0.2}\text{Fe}_{0.8}\text{O}_{3-\delta}$,” *Advanced Materials*, vol. 17, no. 14, pp. 1785–1788, 2005.
- [64] Verbraeken, M. C., Ramos, T., Agersted, K., Ma, Q., Savaniu, C. D., Sudireddy, B. R., Irvine, J. T. S., Holtappels, P., y Tietz, F., “Modified strontium titanates: from defect chemistry to sofc anodes,” *Rsc Advances*, vol. 5, no. 2, pp. 1168–1180, 2015.
- [65] Shen, Q., Zheng, Y., Luo, C., y Zheng, C., “Development and characterization of $\text{Ba}_{1-x}\text{Sr}_x\text{Co}_{0.8}\text{Fe}_{0.2}\text{O}_{3-\delta}$ perovskite for oxygen production in oxyfuel combustion system,” *Chemical Engineering Journal*, vol. 255, pp. 462–470, 2014.
- [66] Zeng, Y., Lin, Y., y Swartz, S., “Perovskite-type ceramic membrane: synthesis, oxygen permeation and membrane reactor performance for oxidative coupling of methane,” *Journal of membrane science*, vol. 150, no. 1, pp. 87–98, 1998.
- [67] Lv, M., Sun, X., Wei, S., Shen, C., Mi, Y., y Xu, X., “Ultrathin lanthanum tantalate perovskite nanosheets modified by nitrogen doping for efficient photocatalytic water splitting,” *ACS nano*, vol. 11, no. 11, pp. 11441–11448, 2017.
- [68] Fu, Q., He, T., Li, J., y Yang, G., “Band-engineered SrTiO_3 nanowires for visible light photocatalysis,” *Journal of Applied Physics*, vol. 112, no. 10, p. 104322, 2012.
- [69] Zhou, C., Shi, R., Waterhouse, G. I., y Zhang, T., “Recent advances in niobium-based semiconductors for solar hydrogen production,” *Coordination Chemistry Reviews*, vol. 419, p. 213399, 2020.
- [70] Liu, Y., Zhu, X., Li, M., O’Hayre, R. P., y Yang, W., “Nanoparticles at grain boundaries inhibit the phase transformation of perovskite membrane,” *Nano letters*, vol. 15, no. 11, pp. 7678–7683, 2015.
- [71] Wu, J., Zhou, C., Zhao, Y., Shang, L., Bian, T., Shao, L., Shi, F., Wu, L.-Z., Tung, C.-H., y Zhang, T., “One-pot hydrothermal synthesis and photocatalytic hydrogen evolution of pyrochlore type $\text{K}_2\text{Nb}_2\text{O}_6$,” *Chinese Journal of Chemistry*, vol. 32, no. 6, pp. 485–490, 2014.

- [72] Kato, H., Kobayashi, H., y Kudo, A., “Role of ag^+ in the band structures and photocatalytic properties of $agmo_3$ (m : Ta and nb) with the perovskite structure,” *The Journal of Physical Chemistry B*, vol. 106, no. 48, pp. 12441–12447, 2002.
- [73] Qu, Z., Wang, J., Tang, J., Shu, X., Liu, X., Zhang, Z., y Wang, J., “Carbon quantum dots/ $knbo_3$ hybrid composites with enhanced visible-light driven photocatalytic activity toward dye waste-water degradation and hydrogen production,” *Molecular Catalysis*, vol. 445, pp. 1–11, 2018.
- [74] Feng, J., Wang, Z., Wang, J., Wan, L., Yan, S., Li, Z., y Zou, Z., “Nearly monodispersed $linbo_3$ nanocrystals synthesized by a nonaqueous sol–gel process and their photocatalytic h_2 evolution activities,” *European Journal of Inorganic Chemistry*, vol. 2013, no. 24, pp. 4142–4145, 2013.
- [75] Shi, H., Li, X., Wang, D., Yuan, Y., Zou, Z., y Ye, J., “ $Nanbo_3$ nanostructures: facile synthesis, characterization, and their photocatalytic properties,” *Catalysis letters*, vol. 132, no. 1, pp. 205–212, 2009.
- [76] Li, G., Kako, T., Wang, D., Zou, Z., y Ye, J., “Synthesis and enhanced photocatalytic activity of $nanbo_3$ prepared by hydrothermal and polymerized complex methods,” *Journal of Physics and Chemistry of Solids*, vol. 69, no. 10, pp. 2487–2491, 2008.
- [77] Zhou, C., Chen, G., y Wang, Q., “High photocatalytic activity of porous $k4nb6o17$ microsphere with large surface area prepared by homogeneous precipitation using urea,” *Journal of Molecular Catalysis A: Chemical*, vol. 339, no. 1-2, pp. 37–42, 2011.
- [78] Zhang, Z., Chen, Y., Tade, M. O., Hao, Y., Liu, S., y Shao, Z., “Tin-doped perovskite mixed conducting membrane for efficient air separation,” *Journal of Materials Chemistry A*, vol. 2, no. 25, pp. 9666–9674, 2014.
- [79] Teraoka, Y., Shimokawa, H., Kang, C. Y., Kusaba, H., y Sasaki, K., “Fe-based perovskite-type oxides as excellent oxygen-permeable and reduction-tolerant materials,” *Solid State Ionics*, vol. 177, no. 26-32, pp. 2245–2248, 2006.
- [80] Efimov, K., Xu, Q., y Feldhoff, A., “Transmission electron microscopy study of $ba_{0.5}sr_{0.5}co_{0.8}fe_{0.2}o_{3-\delta}$ perovskite decomposition at intermediate temperatures,” *Chemistry of Materials*, vol. 22, no. 21, pp. 5866–5875, 2010.
- [81] Gupta, S., Zhong, Y., Mahapatra, M., y Singh, P., “Processing and electrochemical performance of manganese-doped lanthanum-strontium chromite in oxidizing and reducing atmospheres,” *international journal of hydrogen energy*, vol. 40, no. 39, pp. 13479–13489, 2015.
- [82] Liang, F., Jiang, H., Luo, H., Caro, J., y Feldhoff, A., “Phase stability and permeation behavior of a dead-end $ba_{0.5}sr_{0.5}co_{0.8}fe_{0.2}o_{3-\delta}$ tube membrane in high-purity oxygen production,” *Chemistry of Materials*, vol. 23, no. 21, pp. 4765–4772, 2011.
- [83] Cheng, Y., Zhao, H., Teng, D., Li, F., Lu, X., y Ding, W., “Investigation of ba fully

- occupied a-site baco_{0.7}fe_{0.3}-xnbx_{0.3}- δ perovskite stabilized by low concentration of nb for oxygen permeation membrane,” *Journal of Membrane Science*, vol. 322, no. 2, pp. 484–490, 2008.
- [84] Gasparyan, H., Claridge, J., y Rosseinsky, M., “Oxygen permeation and stability of mo-substituted bscf membranes,” *Journal of Materials Chemistry A*, vol. 3, no. 35, pp. 18265–18272, 2015.
- [85] Cheng, H., Yao, W., Lu, X., Zhou, Z., Li, C., y Liu, J., “Structural stability and oxygen permeability of baco_{0.7}fe_{0.2}m_{0.1}o₃- δ (m= ta, nb, zr) ceramic membranes for producing hydrogen from coke oven gas,” *Fuel Processing Technology*, vol. 131, pp. 36–44, 2015.
- [86] Lu, Y., Dixon, A. G., Moser, W. R., Ma, Y. H., y Balachandran, U., “Oxygen-permeable dense membrane reactor for the oxidative coupling of methane,” *Journal of Membrane Science*, vol. 170, no. 1, pp. 27–34, 2000.
- [87] Yang, D., Lu, H., Song, H., Mo, J., Li, G., Chen, C., Guo, Y., y Hu, X., “Experimental study of oxygen diffusion and permeation through yba₂cu₃o_{7-x} membranes,” *Journal of membrane science*, vol. 233, no. 1-2, pp. 45–50, 2004.
- [88] Geffroy, P.-M., Bassat, J.-M., Vivet, A., Fourcade, S., Chartier, T., Del Gallo, P., y Richet, N., “Oxygen semi-permeation, oxygen diffusion and surface exchange coefficient of la (1-x)sr_xfe (1-y)gayo₃- δ perovskite membranes,” *Journal of Membrane Science*, vol. 354, no. 1-2, pp. 6–13, 2010.
- [89] Kruidhof, H., Bouwmeester, H. J., Doorn, R. v., y Burggraaf, A., “Influence of order-disorder transitions on oxygen permeability through selected nonstoichiometric perovskite-type oxides,” *Solid State Ionics*, vol. 63, pp. 816–822, 1993.
- [90] Li, S., Lü, Z., Huang, X., Wei, B., y Su, W., “Thermal, electrical, and electrochemical properties of lanthanum-doped ba_{0.5}sr_{0.5}co_{0.8}fe_{0.2}o₃-,” *Journal of Physics and Chemistry of Solids*, vol. 68, no. 9, pp. 1707–1712, 2007, [doi:10.1016/j.jpcs.2007.04.014](https://doi.org/10.1016/j.jpcs.2007.04.014).
- [91] LEIN, H., WIJK, K., y GRANDE, T., “Thermal and chemical expansion of mixed conducting la_{0.5}sr_{0.5}fe_{1-x}Co_xO₃- materials,” *Solid State Ionics*, vol. 177, no. 19-25, pp. 1795–1798, 2006, [doi:10.1016/j.ssi.2006.02.033](https://doi.org/10.1016/j.ssi.2006.02.033).
- [92] Engels, S., Markus, T., Modigell, M., y Singheiser, L., “Oxygen permeation and stability investigations on MIEC membrane materials under operating conditions for power plant processes,” *Journal of Membrane Science*, vol. 370, no. 1-2, pp. 58–69, 2011, [doi:10.1016/j.memsci.2010.12.021](https://doi.org/10.1016/j.memsci.2010.12.021).
- [93] Lakshminarayanan, N., Choi, H., Kuhn, J. N., y Ozkan, U. S., “Effect of additional b-site transition metal doping on oxygen transport and activation characteristics in la_{0.6}sr_{0.4}(co_{0.18}fe_{0.72}x_{0.1})o₃- (where x=zn, ni or cu) perovskite oxides,” *Applied Catalysis B: Environmental*, vol. 103, no. 3-4, pp. 318–325, 2011, [doi:10.1016/j.apcatb.2011.01.038](https://doi.org/10.1016/j.apcatb.2011.01.038).

- [94] Ovenstone, J., Jung, J.-I., White, J. S., Edwards, D. D., y Misture, S. T., “Phase stability of BSCF in low oxygen partial pressures,” *Journal of Solid State Chemistry*, vol. 181, no. 3, pp. 576–586, 2008, [doi:10.1016/j.jssc.2008.01.010](https://doi.org/10.1016/j.jssc.2008.01.010).
- [95] Tan, X., Wang, Z., Meng, B., Meng, X., y Li, K., “Pilot-scale production of oxygen from air using perovskite hollow fibre membranes,” *Journal of Membrane Science*, vol. 352, no. 1-2, pp. 189–196, 2010, [doi:10.1016/j.memsci.2010.02.015](https://doi.org/10.1016/j.memsci.2010.02.015).
- [96] Tan, X., Liu, N., Meng, B., Sunarso, J., Zhang, K., y Liu, S., “Oxygen permeation behavior of $\text{La}_{0.6}\text{Sr}_{0.4}\text{Co}_{0.8}\text{Fe}_{0.2}\text{O}_{3-\delta}$ hollow fibre membranes with highly concentrated CO_2 exposure,” *Journal of Membrane Science*, vol. 389, pp. 216–222, 2012.
- [97] Watanabe, K., Ninomiya, S., Yuasa, M., Kida, T., Yamazoe, N., Haneda, H., y Shimano, K., “Microstructure effect on the oxygen permeation through $\text{Ba}_{0.95}\text{La}_{0.05}\text{FeO}_3$ -membranes fabricated by different methods,” *Journal of the American Ceramic Society*, pp. no–no, 2010, [doi:10.1111/j.1551-2916.2010.03700.x](https://doi.org/10.1111/j.1551-2916.2010.03700.x).
- [98] Shellaiyah, M. y Sun, K. W., “Review on sensing applications of perovskite nanomaterials,” *Chemosensors*, vol. 8, no. 3, p. 55, 2020.
- [99] Stambouli, A. B. y Traversa, E., “Solid oxide fuel cells (sofcs): a review of an environmentally clean and efficient source of energy,” *Renewable and sustainable energy reviews*, vol. 6, no. 5, pp. 433–455, 2002.
- [100] Steele, B. C. y Heinzl, A., “Materials for fuel-cell technologies,” en *Materials for sustainable energy: a collection of peer-reviewed research and review articles from nature publishing group*, pp. 224–231, World Scientific, 2011.
- [101] Pergolesi, D., Fabbri, E., D’Epifanio, A., Di Bartolomeo, E., Tebano, A., Sanna, S., Licocchia, S., Balestrino, G., y Traversa, E., “High proton conduction in grain-boundary-free yttrium-doped barium zirconate films grown by pulsed laser deposition,” *Nature materials*, vol. 9, no. 10, pp. 846–852, 2010.
- [102] Vohs, J. M. y Gorte, R. J., “High-performance sofc cathodes prepared by infiltration,” *Advanced Materials*, vol. 21, no. 9, pp. 943–956, 2009.
- [103] Zhou, W., Sunarso, J., Zhao, M., Liang, F., Klandt, T., y Feldhoff, A., “A highly active perovskite electrode for the oxygen reduction reaction below 600 c,” *Angewandte Chemie International Edition*, vol. 52, no. 52, pp. 14036–14040, 2013.
- [104] Yang, W., Hong, T., Li, S., Ma, Z., Sun, C., Xia, C., y Chen, L., “Perovskite $\text{Sr}_{1-x}\text{Ce}_x\text{CoO}_{3-\delta}$ ($0.05 \leq x \leq 0.15$) as superior cathodes for intermediate temperature solid oxide fuel cells,” *ACS applied materials & interfaces*, vol. 5, no. 3, pp. 1143–1148, 2013.
- [105] Brinkman, K. y Huang, K., “Solid oxide fuel cells and membranes,” *Chem. Eng. Prog.*, vol. 112, pp. 44–9, 2016.
- [106] Choudhury, A., Chandra, H., y Arora, A., “Application of solid oxide fuel cell technology for power generation—a review,” *Renewable and Sustainable Energy Reviews*,

vol. 20, pp. 430–442, 2013.

- [107] Skinner, S. J., “Recent advances in perovskite-type materials for solid oxide fuel cell cathodes,” *International Journal of Inorganic Materials*, vol. 3, no. 2, pp. 113–121, 2001.
- [108] Kostogloudis, G. C. y Ftikos, C., “Properties of a-site-deficient $\text{La}_{0.6}\text{Sr}_{0.4}\text{Co}_{0.2}\text{Fe}_{0.8}\text{O}_{3-\delta}$ -based perovskite oxides,” *Solid State Ionics*, vol. 126, no. 1-2, pp. 143–151, 1999.
- [109] Waller, D., Lane, J., Kilner, J., y Steele, B., “The structure of and reaction of a-site deficient $\text{La}_{0.6}\text{Sr}_{0.4-x}\text{Co}_{0.2}\text{Fe}_{0.8}\text{O}_3$ - perovskites,” *Materials Letters*, vol. 27, no. 4-5, pp. 225–228, 1996, doi:10.1016/0167-577x(95)00289-8.
- [110] Tu, H., “ $\text{Ln}_{0.4}\text{Sr}_{0.6}\text{Co}_{0.8}\text{Fe}_{0.2}\text{O}_3$ - (Ln=La, Pr, Nd, Sm, Gd) for the electrode in solid oxide fuel cells,” *Solid State Ionics*, vol. 117, no. 3-4, pp. 277–281, 1999, doi:10.1016/S0167-2738(98)00428-7.
- [111] Hibino, T., “A low-operating-temperature solid oxide fuel cell in hydrocarbon-air mixtures,” *Science*, vol. 288, no. 5473, pp. 2031–2033, 2000, doi:10.1126/science.288.5473.2031.
- [112] Ishihara, T., Honda, M., Shibayama, T., Minami, H., Nishiguchi, H., y Takita, Y., “Intermediate temperature solid oxide fuel cells using a new LaGaO_3 based oxide ion conductor: I. doped as a new cathode material,” *Journal of The Electrochemical Society*, vol. 145, no. 9, pp. 3177–3183, 1998, doi:10.1149/1.1838783.
- [113] Koyama, M., ju Wen, C., Masuyama, T., Otomo, J., Fukunaga, H., Yamada, K., Eguchi, K., y Takahashi, H., “The mechanism of porous $\text{Sm}_{0.5}\text{Sr}_{0.5}\text{CoO}_3$ cathodes used in solid oxide fuel cells,” *Journal of The Electrochemical Society*, vol. 148, no. 7, p. A795, 2001, doi:10.1149/1.1378290.
- [114] TAKEDA, Y., “ $\text{Gd}_{1-x}\text{Sr}_x\text{CoO}_3$ for the electrode of solid oxide fuel cells,” *Solid State Ionics*, vol. 86-88, pp. 1187–1190, 1996, doi:10.1016/0167-2738(96)00285-8.
- [115] Song, X., Le, S., Zhu, X., Qin, L., Luo, Y., Li, Y., Sun, K., y Chen, Y., “High performance $\text{BaFe}_{1-x}\text{Bi}_x\text{O}_3$ - as cobalt-free cathodes for intermediate temperature solid oxide fuel cells,” *International Journal of Hydrogen Energy*, vol. 42, no. 24, pp. 15808–15817, 2017, doi:10.1016/j.ijhydene.2017.05.061.
- [116] Kharton, V., Yaremchenko, A., Patrakeev, M., Naumovich, E., y Marques, F., “Thermal and chemical induced expansion of $\text{La}_{0.3}\text{Sr}_{0.7}(\text{Fe}, \text{Ga})\text{O}_3$ - ceramics,” *Journal of the European Ceramic Society*, vol. 23, no. 9, pp. 1417–1426, 2003, doi:10.1016/S0955-2219(02)00308-4.
- [117] Papargyriou, D. y Irvine, J., “Nickel nanocatalyst exsolution from $(\text{La}, \text{Sr})(\text{Cr}, \text{Mn}, \text{Ni})\text{O}_3$ (m Mn, Fe) perovskites for the fuel oxidation layer of oxygen transport membranes,” *Solid State Ionics*, vol. 288, pp. 120–123, 2016, doi:10.1016/j.ssi.2015.11.007.
- [118] Falkenstein-Smith, R. L., *Oxygen Transport Membrane Reactors for Oxy-Fuel Com-*

bustion and Carbon Capture Purposes. PhD thesis, Syracuse University, 2017.

- [119] Yaremchenko, A. A., Kharton, V. V., Valente, A. A., Veniaminov, S. A., Belyaev, V. D., Sobyenin, V. A., y Marques, F. M. B., “Methane oxidation over mixed-conducting $\text{SrFe}(\text{al})\text{o}_3\text{--SrAl}_2\text{o}_4$ composite,” *Phys. Chem. Chem. Phys.*, vol. 9, no. 21, pp. 2744–2752, 2007, [doi:10.1039/b617409b](https://doi.org/10.1039/b617409b).
- [120] Shen, Z., Lu, P., Hu, J., y Hu, X., “Performance of $\text{ba}_{0.5}\text{sr}_{0.5}\text{co}_{0.8}\text{fe}_{0.2}\text{o}_3$ membrane after laser ablation for methane conversion,” *Catalysis Communications*, vol. 11, no. 10, pp. 892–895, 2010, [doi:10.1016/j.catcom.2010.03.016](https://doi.org/10.1016/j.catcom.2010.03.016).
- [121] Gibb, T. C., “Magnetic exchange interactions in perovskite solid solutions. part 5. the unusual defect structure of SrFeO_{3-y} ,” *J. Chem. Soc., Dalton Trans.*, no. 7, pp. 1455–1470, 1985, [doi:10.1039/dt9850001455](https://doi.org/10.1039/dt9850001455).
- [122] Wattiaux, A., Fournès, L., Demourgues, A., Bernaben, N., Grenier, J., y Pouchard, M., “A novel preparation method of the SrFeO_3 cubic perovskite by electrochemical means,” *Solid State Communications*, vol. 77, no. 7, pp. 489–493, 1991, [doi:10.1016/0038-1098\(91\)90726-c](https://doi.org/10.1016/0038-1098(91)90726-c).
- [123] MORI, S., “Phase transformation in barium orthoferrate, BaFeO_{3-x} ,” *Journal of the American Ceramic Society*, vol. 49, no. 11, pp. 600–605, 1966, [doi:10.1111/j.1151-2916.1966.tb13176.x](https://doi.org/10.1111/j.1151-2916.1966.tb13176.x).
- [124] Shu, L., Sunarso, J., Hashim, S. S., Mao, J., Zhou, W., y Liang, F., “Advanced perovskite anodes for solid oxide fuel cells: A review,” *International Journal of Hydrogen Energy*, vol. 44, no. 59, pp. 31275–31304, 2019, [doi:10.1016/j.ijhydene.2019.09.220](https://doi.org/10.1016/j.ijhydene.2019.09.220).
- [125] Kida, T., Ninomiya, S., Watanabe, K., Yamazoe, N., y Shimano, K., “High oxygen permeation in $\text{ba}_{0.95}\text{la}_{0.05}\text{fe}_3$ - membranes with surface modification,” *ACS Applied Materials & Interfaces*, vol. 2, no. 10, pp. 2849–2853, 2010, [doi:10.1021/am100524k](https://doi.org/10.1021/am100524k).
- [126] Kida, T., Takauchi, D., Watanabe, K., Yuasa, M., Shimano, K., Teraoka, Y., y Yamazoe, N., “Oxygen permeation properties of partially a-site substituted BaFeO_{3-} perovskites,” *Journal of The Electrochemical Society*, vol. 156, no. 12, p. E187, 2009, [doi:10.1149/1.3231690](https://doi.org/10.1149/1.3231690).
- [127] Hashim, S., Mohamed, A., y Bhatia, S., “Oxygen separation from air using ceramic-based membrane technology for sustainable fuel production and power generation,” *Renewable and Sustainable Energy Reviews*, vol. 15, no. 2, pp. 1284–1293, 2011, [doi:10.1016/j.rser.2010.10.002](https://doi.org/10.1016/j.rser.2010.10.002).
- [128] Fang, W., Zhang, C., Steinbach, F., y Feldhoff, A., “Stabilizing perovskite structure by interdiffusional tailoring and its application in composite mixed oxygen-ionic and electronic conductors,” *Angewandte Chemie*, vol. 129, no. 26, pp. 7692–7696, 2017, [doi:10.1002/ange.201702786](https://doi.org/10.1002/ange.201702786).
- [129] Xia, C., “ $\text{Sm}_{0.5}\text{sr}_{0.5}\text{co}_3$ cathodes for low-temperature SOFCs,” *Solid State Ionics*, vol. 149, no. 1-2, pp. 11–19, 2002, [doi:10.1016/s0167-2738\(02\)00131-5](https://doi.org/10.1016/s0167-2738(02)00131-5).

- [130] Zhu, Y., Zhou, W., Ran, R., Chen, Y., Shao, Z., y Liu, M., “Promotion of oxygen reduction by exsolved silver nanoparticles on a perovskite scaffold for low-temperature solid oxide fuel cells,” *Nano Letters*, vol. 16, no. 1, pp. 512–518, 2015, doi:10.1021/acs.nanolett.5b04160.
- [131] Aguadero, A., de la Calle, C., Alonso, J. A., Escudero, M. J., Fernández-Díaz, M. T., y Daza, L., “Structural and electrical characterization of the novel SrCo_{0.9sb0.1o3}-perovskite: Evaluation as a solid oxide fuel cell cathode material,” *Chemistry of Materials*, vol. 19, no. 26, pp. 6437–6444, 2007, doi:10.1021/cm071837x.
- [132] NAGAI, T., ITO, W., y SAKON, T., “Relationship between cation substitution and stability of perovskite structure in SrCoO₃-based mixed conductors,” *Solid State Ionics*, vol. 177, no. 39-40, pp. 3433–3444, 2007, doi:10.1016/j.ssi.2006.10.022.
- [133] Liang, F., Partovi, K., Jiang, H., Luo, H., y Caro, J., “B-site la-doped BaFe_{0.95-xLaxZr0.05o3}-perovskite-type membranes for oxygen separation,” *J. Mater. Chem. A*, vol. 1, no. 3, pp. 746–751, 2013, doi:10.1039/c2ta00377e.
- [134] Li, F., Xu, Y., Xia, S., Liu, J., Yan, Y., Cheng, F., Jiang, L., y Huang, Y., “LaSrCoO_{4±@la0.5sr0.5coo3}- core-shell hybrid as the cathode materials for solid oxide fuel cells,” *Journal of Alloys and Compounds*, vol. 819, p. 152996, 2020, doi:10.1016/j.jallcom.2019.152996.
- [135] Akhtar, M., Akhtar, Z., Dragun, J., y Catlow, C., “Electrical conductivity and extended x-ray absorption fine structure studies of SrFe_{1-xNbxO3} and BaFe_{1-xNbxO3} systems,” *Solid State Ionics*, vol. 104, no. 1-2, pp. 147–158, 1997, doi:10.1016/s0167-2738(97)00351-2.
- [136] Wang, D., Xia, Y., Lv, H., Miao, L., Bi, L., y Liu, W., “PrBaCo_{2-xTaxO5}based composite materials as cathodes for proton-conducting solid oxide fuel cells with high CO₂ resistance,” *International Journal of Hydrogen Energy*, vol. 45, no. 55, pp. 31017–31026, 2020, doi:10.1016/j.ijhydene.2020.08.094.
- [137] Volkova, N., Mychinko, M. Y., Golovachev, I., Makarova, A., Bazueva, M., Zyaikin, E., Gavrilova, L. Y., y Cherepanov, V., “Structure and properties of layered perovskites ba_{1-ln} fe_{1-co} o₃- (ln = pr, sm, gd),” *Journal of Alloys and Compounds*, vol. 784, pp. 1297–1302, 2019, doi:10.1016/j.jallcom.2018.12.391.
- [138] Cherepanov, V., Aksenova, T., Gavrilova, L., y Mikhaleva, K., “Structure, nonstoichiometry and thermal expansion of the NdBa_{(co, fe)2o5}layered perovskite,” *Solid State Ionics*, vol. 188, no. 1, pp. 53–57, 2011, doi:10.1016/j.ssi.2010.10.021.
- [139] Gao, L., Li, Q., Sun, L., Zhang, X., Huo, L., Zhao, H., y Grenier, J.-C., “A novel family of nb-doped bi_{0.5sr0.5feo3}- perovskite as cathode material for intermediate-temperature solid oxide fuel cells,” *Journal of Power Sources*, vol. 371, pp. 86–95, 2017, doi:10.1016/j.jpowsour.2017.10.036.
- [140] Zhang, W., Zhang, L., Guan, K., Zhang, X., Meng, J., Wang, H., Liu, X., y Meng,

- J., “Effective promotion of oxygen reduction activity by rare earth doping in simple perovskite cathodes for intermediate-temperature solid oxide fuel cells,” *Journal of Power Sources*, vol. 446, p. 227360, 2020, [doi:10.1016/j.jpowsour.2019.227360](https://doi.org/10.1016/j.jpowsour.2019.227360).
- [141] Ortiz-Vitoriano, N., de Larramendi, I. R., de Muro, I. G., Larrañaga, A., de Larramendi, J. I. R., y Rojo, T., “A novel one step synthesized co-free perovskite/brownmillerite nanocomposite for solid oxide fuel cells,” *Journal of Materials Chemistry*, vol. 21, no. 26, p. 9682, 2011, [doi:10.1039/c1jm10911a](https://doi.org/10.1039/c1jm10911a).
- [142] Wang, J., Saccoccio, M., Chen, D., Gao, Y., Chen, C., y Ciucci, F., “The effect of a-site and b-site substitution on bafeo3- δ : an investigation as a cathode material for intermediate-temperature solid oxide fuel cells,” *Journal of Power Sources*, vol. 297, pp. 511–518, 2015.
- [143] Morales, M., Roa, J., Tartaj, J., y Segarra, M., “A review of doped lanthanum gallates as electrolytes for intermediate temperature solid oxides fuel cells: From materials processing to electrical and thermo-mechanical properties,” *Journal of the European Ceramic Society*, vol. 36, no. 1, pp. 1–16, 2016, [doi:10.1016/j.jeurceramsoc.2015.09.025](https://doi.org/10.1016/j.jeurceramsoc.2015.09.025).
- [144] Shannon, R. D. y Prewitt, C. T., “Effective ionic radii in oxides and fluorides,” *Acta Crystallographica Section B Structural Crystallography and Crystal Chemistry*, vol. 25, no. 5, p. 925–946, 1969, [doi:10.1107/s0567740869003220](https://doi.org/10.1107/s0567740869003220).
- [145] Wang, W., Tadé, M. O., y Shao, Z., “Research progress of perovskite materials in photocatalysis-and photovoltaics-related energy conversion and environmental treatment,” *Chemical Society Reviews*, vol. 44, no. 15, pp. 5371–5408, 2015.
- [146] Jamal, M., Sarvestani, N. K., Yazdani, A., y Reshak, A. H., “Mechanical and thermodynamical properties of hexagonal compounds at optimized lattice parameters from two-dimensional search of the equation of state,” *RSC Adv.*, vol. 4, no. 101, pp. 57903–57915, 2014, [doi:10.1039/c4ra09358e](https://doi.org/10.1039/c4ra09358e).
- [147] Reshak, A. y Jamal, M., “Dft calculation for elastic constants of tetragonal structure of crystalline solids with wien2k code: A new package (tetra-elastic),” *Int. J. Electrochem. Sci.*, vol. 8, pp. 12252–12263, 2013.
- [148] Wereszczak, A. A., Ferber, M. K., Kirkland, T. P., Barnes, A. S., Frome, E. L., y Menon, M. N., “Asymmetric tensile and compressive creep deformation of hot-isostatically-pressed y2o3-doped -si3n4,” *Journal of the European Ceramic Society*, vol. 19, no. 2, pp. 227–237, 1999, [doi:10.1016/s0955-2219\(98\)00184-8](https://doi.org/10.1016/s0955-2219(98)00184-8).
- [149] Ding, J. L. *Journal of Materials Science*, vol. 37, no. 19, pp. 4165–4180, 2002, [doi:10.1023/a:1020044004676](https://doi.org/10.1023/a:1020044004676).
- [150] Laurencin, J., Delette, G., Usseglio-Viretta, F., y Iorio, S. D., “Creep behaviour of porous SOFC electrodes: Measurement and application to ni-8ysz cermet,” *Journal of the European Ceramic Society*, vol. 31, no. 9, pp. 1741–1752, 2011, [doi:10.1016/j.jeurceramsoc.2011.02.036](https://doi.org/10.1016/j.jeurceramsoc.2011.02.036).

- [151] Pathak, S., Steinmetz, D., Kuebler, J., Payzant, E. A., y Orlovskaya, N., “Mechanical behavior of $\text{La}_{0.8}\text{Sr}_{0.2}\text{Ga}_{0.8}\text{Mg}_{0.2}\text{O}_3$ perovskites,” *Ceramics International*, vol. 35, no. 3, pp. 1235–1241, 2009, [doi:10.1016/j.ceramint.2008.06.013](https://doi.org/10.1016/j.ceramint.2008.06.013).
- [152] Baskaran, S., Lewinsohn, C. A., Chou, Y.-S., Qian, M., Stevenson, J. W., y Armstrong, T. R. *Journal of Materials Science*, vol. 34, no. 16, pp. 3913–3922, 1999, [doi:10.1023/a:1004683025114](https://doi.org/10.1023/a:1004683025114).
- [153] Martynczuk, J., Arnold, M., y Feldhoff, A., “Influence of grain size on the oxygen permeation performance of perovskite-type $(\text{Ba}_{0.5}\text{Sr}_{0.5})(\text{Fe}_{0.8}\text{Zn}_{0.2})\text{O}_3$ membranes,” *Journal of Membrane Science*, vol. 322, no. 2, pp. 375–382, 2008, [doi:10.1016/j.memsci.2008.05.064](https://doi.org/10.1016/j.memsci.2008.05.064).
- [154] Zhang, K., Yang, Y. L., Ponnusamy, D., Jacobson, A. J., y Salama, K. *Journal of Materials Science*, vol. 34, no. 6, pp. 1367–1372, 1999, [doi:10.1023/a:1004518719410](https://doi.org/10.1023/a:1004518719410).
- [155] Wang, H., Tablet, C., Feldhoff, A., y Caro, J., “Investigation of phase structure, sintering, and permeability of perovskite-type $\text{Ba}_{0.5}\text{Sr}_{0.5}\text{Co}_{0.8}\text{Fe}_{0.2}\text{O}_3$ membranes,” *Journal of Membrane Science*, vol. 262, no. 1-2, pp. 20–26, 2005, [doi:10.1016/j.memsci.2005.03.046](https://doi.org/10.1016/j.memsci.2005.03.046).
- [156] Wang, L., Dou, R., Bai, M., Li, Y., Hall, D., y Chen, Y., “Characterisation of microstructure and hardness of perovskite-structured $\text{Ba}_{0.5}\text{Sr}_{0.5}\text{Co}_{0.8}\text{Fe}_{0.2}\text{O}_3$ under different sintering conditions,” *Journal of the European Ceramic Society*, vol. 36, no. 7, pp. 1659–1667, 2016.
- [157] Yang, J., Zhao, H., Liu, X., Shen, Y., y Xu, L., “Bismuth doping effects on the structure, electrical conductivity and oxygen permeability of $\text{Ba}_{0.6}\text{Sr}_{0.4}\text{Co}_{0.7}\text{Fe}_{0.3}\text{O}_3$ ceramic membranes,” *International Journal of Hydrogen Energy*, vol. 37, no. 17, pp. 12694–12699, 2012, [doi:10.1016/j.ijhydene.2012.06.013](https://doi.org/10.1016/j.ijhydene.2012.06.013).
- [158] Kang, B.-K., Lee, H.-C., Heo, Y.-W., Kim, J.-J., Kim, J. Y., y Lee, J.-H., “Thermal expansion behavior of La-doped $(\text{Ba}_{0.5}\text{Sr}_{0.5}\text{Co}_{0.8}\text{Fe}_{0.2})\text{O}_3$ cathode material,” *Ceramics International*, vol. 39, no. 7, pp. 8267–8271, 2013, [doi:10.1016/j.ceramint.2013.04.012](https://doi.org/10.1016/j.ceramint.2013.04.012).
- [159] Kharton, V., Viskup, A., Naumovich, E., y Tikhonovich, V., “Oxygen permeability of $\text{LaFe}_{1-x}\text{Ni}_x\text{O}_3$ solid solutions,” *Materials Research Bulletin*, vol. 34, no. 8, pp. 1311–1317, 1999, [doi:10.1016/s0025-5408\(99\)00117-8](https://doi.org/10.1016/s0025-5408(99)00117-8).
- [160] Wei, B., Lü, Z., Jia, D., Huang, X., Zhang, Y., y Su, W., “Thermal expansion and electrochemical properties of Ni-doped $\text{GdBaCo}_2\text{O}_5$ double-perovskite type oxides,” *International Journal of Hydrogen Energy*, vol. 35, no. 8, pp. 3775–3782, 2010, [doi:10.1016/j.ijhydene.2010.01.079](https://doi.org/10.1016/j.ijhydene.2010.01.079).
- [161] Chou, Y.-S., Stevenson, J. W., Armstrong, T. R., y Pederson, L. R., “Mechanical properties of $\text{La}_{1-x}\text{Sr}_x\text{Co}_{0.2}\text{Fe}_{0.8}\text{O}_3$ mixed-conducting perovskites made by the combustion synthesis technique,” *Journal of the American Ceramic Society*, vol. 83, no. 6, pp. 1457–1464, 2000, [doi:10.1111/j.1151-2916.2000.tb01410.x](https://doi.org/10.1111/j.1151-2916.2000.tb01410.x).

- [162] Erchak, M., Fankuchen, I., y Ward, R., “Reaction between ferric oxide and barium carbonate in the solid phase. identification of phases by x-ray diffraction1,” *Journal of the American Chemical Society*, vol. 68, no. 10, pp. 2085–2093, 1946, [doi:10.1021/ja01214a063](https://doi.org/10.1021/ja01214a063).
- [163] Lucchini, E., Meriani, S., y Minichelli, D., “An x-ray study of two phases of BaFeO_{3-x},” *Acta Crystallographica Section B Structural Crystallography and Crystal Chemistry*, vol. 29, no. 6, pp. 1217–1219, 1973, [doi:10.1107/s0567740873004255](https://doi.org/10.1107/s0567740873004255).
- [164] Hook, H. J. V., “Oxygen stoichiometry in the compound BaFeO_{3-x},” *The Journal of Physical Chemistry*, vol. 68, no. 12, pp. 3786–3789, 1964, [doi:10.1021/j100794a041](https://doi.org/10.1021/j100794a041).
- [165] Matsunaga, N., Rogers, D. W., y Zavitsas, A. A., “Pauling’s electronegativity equation and a new corollary accurately predict bond dissociation enthalpies and enhance current understanding of the nature of the chemical bond,” *The Journal of Organic Chemistry*, vol. 68, no. 8, pp. 3158–3172, 2003.
- [166] Mori, S., “Magnetic properties of several phases of barium orthoferrate, BaFeO_x,” *Journal of the Physical Society of Japan*, vol. 28, no. 1, pp. 44–50, 1970, [doi:10.1143/jpsj.28.44](https://doi.org/10.1143/jpsj.28.44).
- [167] Taketani, E., Matsui, T., Fujimura, N., Morii, K., Taketani, E., Matsui, T., Fujimura, N., y Morii, K., “Effect of oxygen deficiencies on magnetic properties of epitaxial grown BaFeO_{3-x} films on,” *IEEE Transactions on Magnetics*, vol. 40, no. 4, pp. 2736–2738, 2004, [doi:10.1109/tmag.2004.830168](https://doi.org/10.1109/tmag.2004.830168).
- [168] Spaldin, N. A. y Mathur, N. D., “Magnetic materials: fundamentals and device applications,” *Physics Today*, vol. 56, no. 12, pp. 62–63, 2003.
- [169] Hücker, M., Chung, K., Chand, M., Vogt, T., Tranquada, J., y Buttrey, D., “Oxygen and strontium codoping of La₂NiO₄: Room-temperature phase diagrams,” *Physical Review B*, vol. 70, no. 6, p. 064105, 2004.
- [170] Niu, Y., Zhou, W., Sunarso, J., Liang, F., Zhu, Z., y Shao, Z., “A single-step synthesized cobalt-free barium ferrites-based composite cathode for intermediate temperature solid oxide fuel cells,” *Electrochemistry Communications*, vol. 13, no. 12, pp. 1340–1343, 2011, [doi:10.1016/j.elecom.2011.08.007](https://doi.org/10.1016/j.elecom.2011.08.007).
- [171] Kolchugin, A., Pikalova, E., Bogdanovich, N., Bronin, D., Pikalov, S., Plaksin, S., Ananyev, M., y Eremin, V., “Structural, electrical and electrochemical properties of calcium-doped lanthanum nickelate,” *Solid State Ionics*, vol. 288, pp. 48–53, 2016, [doi:10.1016/j.ssi.2016.01.035](https://doi.org/10.1016/j.ssi.2016.01.035).
- [172] Akbari-Fakhrabadi, A., Meruane, V., Jamshidijam, M., Gracia-Pinilla, M., Garcia, R., y Orellana, M., “Structural and mechanical properties of La_{0.6}Sr_{0.4}M_{0.1}Fe_{0.9}O_{3-x} (M: Co, Ni and Cu) perovskites,” *Ceramics International*, vol. 43, no. 2, pp. 2089–2094, 2017, [doi:10.1016/j.ceramint.2016.10.185](https://doi.org/10.1016/j.ceramint.2016.10.185).
- [173] Akbari-Fakhrabadi, A., Toledo, E., Canales, J., Meruane, V., Chan, S., y Gracia-

- Pinilla, M., “Effect of sr 2 and ba 2 doping on structural stability and mechanical properties of la 2 NiO 4,” *Ceramics International*, vol. 44, no. 9, pp. 10551–10557, 2018, [doi:10.1016/j.ceramint.2018.03.077](https://doi.org/10.1016/j.ceramint.2018.03.077).
- [174] Huang, B., Steinbrech, R., y Malzbender, J., “Direct observation of ferroelastic domain effects in LSCF perovskites,” *Solid State Ionics*, vol. 228, pp. 32–36, 2012, [doi:10.1016/j.ssi.2012.08.025](https://doi.org/10.1016/j.ssi.2012.08.025).
- [175] Araki, W., Takeda, K., y Arai, Y., “Mechanical behaviour of ferroelastic lanthanum metal oxides LaMO₃ (m = co, al, ga, fe),” *Journal of the European Ceramic Society*, vol. 36, no. 16, pp. 4089–4094, 2016, [doi:10.1016/j.jeurceramsoc.2016.07.006](https://doi.org/10.1016/j.jeurceramsoc.2016.07.006).
- [176] Akbari-Fakhrabadi, A., Rodríguez, O., Rojas, R., Meruane, V., y Pishahang, M. H., “Ferroelastic behavior of LaCoO₃: A comparison of impression and compression techniques,” *Journal of the European Ceramic Society*, vol. 39, no. 4, pp. 1569–1576, 2019, [doi:10.1016/j.jeurceramsoc.2018.11.008](https://doi.org/10.1016/j.jeurceramsoc.2018.11.008).
- [177] Lugovy, M., Slyunyayev, V., Orlovskaya, N., Verbylo, D., y Reece, M. J., “Room-temperature creep of LaCoO₃-based perovskites: Equilibrium strain under compression,” *Physical Review B*, vol. 78, no. 2, 2008, [doi:10.1103/physrevb.78.024107](https://doi.org/10.1103/physrevb.78.024107).
- [178] Chen, Z., “Mechanical Properties of La_{0.6}Sr_{0.4}Co_{0.2}Fe_{0.8}O_{3-d} Fuel Cell Electrodes,” arXiv:1502.02149 [cond-mat], 2015, <http://arxiv.org/abs/1502.02149> (visitado el 2021-10-05). arXiv: 1502.02149.
- [179] Kaur, P. y Singh, K., “Review of perovskite-structure related cathode materials for solid oxide fuel cells,” *Ceramics International*, vol. 46, no. 5, pp. 5521–5535, 2020, [doi:10.1016/j.ceramint.2019.11.066](https://doi.org/10.1016/j.ceramint.2019.11.066).
- [180] Ortiz-Vitoriano, N., Bernuy-López, C., de Larramendi, I. R., Knibbe, R., Thydén, K., Hauch, A., Holtappels, P., y Rojo, T., “Optimizing solid oxide fuel cell cathode processing route for intermediate temperature operation,” *Applied energy*, vol. 104, pp. 984–991, 2013.
- [181] Zhao, Y., Xia, C., Jia, L., Wang, Z., Li, H., Yu, J., y Li, Y., “Recent progress on solid oxide fuel cell: Lowering temperature and utilizing non-hydrogen fuels,” *international journal of hydrogen energy*, vol. 38, no. 36, pp. 16498–16517, 2013.
- [182] Raffaele, R., Anderson, H. U., Sparlin, D. M., y Parris, P. E., “Transport anomalies in the high-temperature hopping conductivity and thermopower of sr-doped la (cr, mn) o 3,” *Physical Review B*, vol. 43, no. 10, p. 7991, 1991.
- [183] Khan, W., Naqvi, A. H., Gupta, M., Husain, S., y Kumar, R., “Small polaron hopping conduction mechanism in fe doped lamno₃,” *The Journal of chemical physics*, vol. 135, no. 5, p. 054501, 2011.
- [184] Dong, F., Chen, Y., Chen, D., y Shao, Z., “Surprisingly high activity for oxygen reduction reaction of selected oxides lacking long oxygen-ion diffusion paths at intermediate temperatures: a case study of cobalt-free bafeo_{3-δ},” *ACS Applied Materials & Inter-*

- faces, vol. 6, no. 14, pp. 11180–11189, 2014.
- [185] Dong, F., Ni, M., He, W., Chen, Y., Yang, G., Chen, D., y Shao, Z., “An efficient electrocatalyst as cathode material for solid oxide fuel cells: $\text{BaFe}_{0.95}\text{Sn}_{0.05}\text{O}_{3-\delta}$,” *Journal of Power Sources*, vol. 326, pp. 459–465, 2016.
- [186] Liu, H., Zhu, K., Liu, Y., Li, W., Cai, L., Zhu, X., Cheng, M., y Yang, W., “Structure and electrochemical properties of cobalt-free perovskite cathode materials for intermediate-temperature solid oxide fuel cells,” *Electrochimica Acta*, vol. 279, pp. 224–230, 2018.
- [187] Wang, J., Saccoccio, M., Chen, D., Gao, Y., Chen, C., y Ciucci, F., “The effect of a-site and b-site substitution on BaFeO_3 : An investigation as a cathode material for intermediate-temperature solid oxide fuel cells,” *Journal of Power Sources*, vol. 297, pp. 511–518, 2015, [doi:10.1016/j.jpowsour.2015.08.016](https://doi.org/10.1016/j.jpowsour.2015.08.016).
- [188] Ranløv, J. y Nielsen, K., “Crystal structure of the high-temperature protonic conductor SrCeO_3 ,” *Journal of Materials Chemistry*, vol. 4, no. 6, pp. 867–868, 1994.
- [189] Gędziorowski, B., Świerczek, K., y Molenda, J., “ $\text{La}_{1-x}\text{BaxCo}_{0.2}\text{Fe}_{0.8}\text{O}_{3-\delta}$ perovskites for application in intermediate temperature sofc,” *Solid State Ionics*, vol. 225, pp. 437–442, 2012.
- [190] Bastidas, D. M., Tao, S., y Irvine, J. T., “A symmetrical solid oxide fuel cell demonstrating redox stable perovskite electrodes,” *Journal of Materials Chemistry*, vol. 16, no. 17, pp. 1603–1605, 2006.
- [191] Martínez-Coronado, R., Aguadero, A., Pérez-Coll, D., Troncoso, L., Alonso, J., y Fernández-Díaz, M., “Characterization of $\text{La}_{0.5}\text{Sr}_{0.5}\text{Co}_{0.5}\text{Ti}_{0.5}\text{O}_{3-\delta}$ as symmetrical electrode material for intermediate-temperature solid-oxide fuel cells,” *international journal of hydrogen energy*, vol. 37, no. 23, pp. 18310–18318, 2012.
- [192] Yang, Z., Xu, N., Han, M., y Chen, F., “Performance evaluation of $\text{La}_{0.4}\text{Sr}_{0.6}\text{Co}_{0.2}\text{Fe}_{0.7}\text{Nb}_{0.1}\text{O}_{3-\delta}$ as both anode and cathode material in solid oxide fuel cells,” *international journal of hydrogen energy*, vol. 39, no. 14, pp. 7402–7406, 2014.
- [193] Zhou, Q., Wei, W., Guo, Y., y Jia, D., “ $\text{LaSrMnCoO}_{5+\delta}$ as cathode for intermediate-temperature solid oxide fuel cells,” *Electrochemistry communications*, vol. 19, pp. 36–38, 2012.
- [194] Yamamoto, O., “Solid oxide fuel cells: fundamental aspects and prospects,” *Electrochimica Acta*, vol. 45, no. 15-16, pp. 2423–2435, 2000.
- [195] Mogensen, M., Lindegaard, T., Hansen, U. R., y Mogensen, G., “Physical properties of mixed conductor solid oxide fuel cell anodes of doped CeO_2 ,” *Journal of the Electrochemical Society*, vol. 141, no. 8, p. 2122, 1994.
- [196] Ishihara, T., Matsuda, H., y Takita, Y., “Doped LaGaO_3 perovskite type oxide as a new oxide ionic conductor,” *Journal of the American chemical society*, vol. 116, no. 9,

pp. 3801–3803, 1994.

- [197] He, W., Fan, J., Zhang, H., Chen, M., Sun, Z., y Ni, M., “Zr doped bafeo $3-\delta$ as a robust electrode for symmetrical solid oxide fuel cells,” *International Journal of Hydrogen Energy*, vol. 44, no. 60, pp. 32164–32169, 2019.
- [198] Gou, Y., Li, G., Ren, R., Xu, C., Qiao, J., Sun, W., Sun, K., y Wang, Z., “Pr-doping motivating the phase transformation of the bafeo $3-\delta$ perovskite as a high-performance solid oxide fuel cell cathode,” *ACS Applied Materials & Interfaces*, vol. 13, no. 17, pp. 20174–20184, 2021.
- [199] Lv, X., Chen, H., Zhou, W., Li, S.-D., y Shao, Z., “A co 2-tolerant srco 0.8 fe 0.15 zr 0.05 o 3- δ cathode for proton-conducting solid oxide fuel cells,” *Journal of Materials Chemistry A*, vol. 8, no. 22, pp. 11292–11301, 2020.
- [200] Xu, C., Sun, K., Yang, X., Ma, M., Ren, R., Qiao, J., Wang, Z., Zhen, S., y Sun, W., “Highly active and co 2 -tolerant sr 2 fe 1.3 ga 0.2 mo 0.5 o $6-\delta$ cathode for intermediate-temperature solid oxide fuel cells,” *Journal of Power Sources*, vol. 450, p. 227722, 2020.
- [201] Simner, S. P., Bonnett, J. F., Canfield, N. L., Meinhardt, K. D., Sprenkle, V. L., y Stevenson, J. W., “Optimized lanthanum ferrite-based cathodes for anode-supported sofc,” *Electrochemical and Solid-State Letters*, vol. 5, no. 7, p. A173, 2002.
- [202] Dong, G., Yang, C., He, F., Jiang, Y., Ren, C., Gan, Y., Lee, M., y Xue, X., “Tin doped prbaf $e 2 o 5+$ δ anode material for solid oxide fuel cells,” *RSC advances*, vol. 7, no. 37, pp. 22649–22661, 2017.
- [203] Taskin, A., Lavrov, A., y Ando, Y., “Achieving fast oxygen diffusion in perovskites by cation ordering,” *Applied Physics Letters*, vol. 86, no. 9, p. 091910, 2005.
- [204] Myung, J.-h., Neagu, D., Miller, D. N., y Irvine, J. T., “Switching on electrocatalytic activity in solid oxide cells,” *Nature*, vol. 537, no. 7621, pp. 528–531, 2016.
- [205] Laguna-Bercero, M., “Recent advances in high temperature electrolysis using solid oxide fuel cells: A review,” *Journal of Power sources*, vol. 203, pp. 4–16, 2012.
- [206] Choi, M.-B., Singh, B., Wachsman, E. D., y Song, S.-J., “Performance of la 0.1 sr 0.9 co 0.8 fe 0.2 o $3-\delta$ and la 0.1 sr 0.9 co 0.8 fe 0.2 o $3-\delta$ -ce 0.9 gd 0.1 o 2 oxygen electrodes with ce 0.9 gd 0.1 o 2 barrier layer in reversible solid oxide fuel cells,” *Journal of Power Sources*, vol. 239, pp. 361–373, 2013.
- [207] Afzal, R. A., Park, K.-Y., Cho, S.-H., Kim, N.-I., Choi, S. R., Kim, J. H., Lim, H.-T., y Park, J.-Y., “Oxygen electrode reactions of doped BiFeO 3 materials for low and elevated temperature fuel cell applications,” *RSC Adv.*, vol. 7, no. 75, pp. 47643–47653, 2017, [doi:10.1039/c7ra08671g](https://doi.org/10.1039/c7ra08671g).
- [208] Jiang, S., Love, J., y Apateanu, L., “Effect of contact between electrode and current collector on the performance of solid oxide fuel cells,” *Solid State Ionics*, vol. 160,

no. 1-2, pp. 15–26, 2003.

- [209] Oh, D., Gostovic, D., y Wachsman, E. D., “Mechanism of $\text{La}_{0.6}\text{Sr}_{0.4}\text{Co}_{0.2}\text{Fe}_{0.8}\text{O}_3$ cathode degradation,” *Journal of Materials Research*, vol. 27, no. 15, pp. 1992–1999, 2012.
- [210] Cai, Z., Kubicek, M., Fleig, J., y Yildiz, B., “Chemical heterogeneities on $\text{La}_{0.6}\text{Sr}_{0.4}\text{CoO}_3$ - δ thin films correlations to cathode surface activity and stability,” *Chemistry of materials*, vol. 24, no. 6, pp. 1116–1127, 2012.
- [211] Katsiev, K., Yildiz, B., Balasubramaniam, K., y Salvador, P. A., “Electron tunneling characteristics on $\text{La}_{0.7}\text{Sr}_{0.3}\text{MnO}_3$ thin-film surfaces at high temperature,” *Applied Physics Letters*, vol. 95, no. 9, p. 092106, 2009.
- [212] Caillol, N., Pijolat, M., y Siebert, E., “Investigation of chemisorbed oxygen, surface segregation and effect of post-treatments on $\text{La}_{0.8}\text{Sr}_{0.2}\text{MnO}_3$ powder and screen-printed layers for solid oxide fuel cell cathodes,” *Applied Surface Science*, vol. 253, no. 10, pp. 4641–4648, 2007.
- [213] Baumann, F. S., Fleig, J., Konuma, M., Starke, U., Habermeier, H.-U., y Maier, J., “Strong performance improvement of $\text{La}_{0.6}\text{Sr}_{0.4}\text{Co}_{0.8}\text{Fe}_{0.2}\text{O}_3$ - δ sofc cathodes by electrochemical activation,” *Journal of The Electrochemical Society*, vol. 152, no. 10, p. A2074, 2005.
- [214] Sharma, V., Mahapatra, M., Singh, P., y Ramprasad, R., “Cationic surface segregation in doped LaMnO_3 ,” *Journal of Materials Science*, vol. 50, no. 8, pp. 3051–3056, 2015.
- [215] Chen, Y., Nie, X., Wang, B., Xia, C., Dong, W., Wang, X., Wang, H., y Zhu, B., “Tuning $\text{La}_{0.6}\text{Sr}_{0.4}\text{Co}_{0.2}\text{Fe}_{0.8}\text{O}_3$ - δ perovskite cathode as functional electrolytes for advanced low-temperature sofc,” *Catalysis Today*, vol. 355, pp. 295–303, 2020.
- [216] Huang, J., Mao, Z., Liu, Z., y Wang, C., “Development of novel low-temperature sofc with co-ionic conducting sdc-carbonate composite electrolytes,” *Electrochemistry Communications*, vol. 9, no. 10, pp. 2601–2605, 2007.
- [217] Zhu, B., Fan, L., y Lund, P., “Breakthrough fuel cell technology using ceria-based multi-functional nanocomposites,” *Applied energy*, vol. 106, pp. 163–175, 2013.
- [218] Simner, S. P., Bonnett, J. F., Canfield, N. L., Meinhardt, K. D., Shelton, J. P., Sprenkle, V. L., y Stevenson, J. W., “Development of lanthanum ferrite sofc cathodes,” *Journal of power sources*, vol. 113, no. 1, pp. 1–10, 2003.
- [219] Niu, Y., Zhou, W., Sunarso, J., Ge, L., Zhu, Z., y Shao, Z., “High performance cobalt-free perovskite cathode for intermediate temperature solid oxide fuel cells,” *Journal of Materials Chemistry*, vol. 20, no. 43, pp. 9619–9622, 2010.
- [220] Yan, L., Ding, H., Zhu, Z., y Xue, X., “Investigation of cobalt-free perovskite $\text{Ba}_{0.95}\text{La}_{0.05}\text{FeO}_3$ - δ as a cathode for proton-conducting solid oxide fuel cells,” *Journal of Power Sources*, vol. 196, no. 22, pp. 9352–9355, 2011.

- [221] Shao, Z., Zhang, C., Wang, W., Su, C., Zhou, W., Zhu, Z., Park, H. J., y Kwak, C., “Electric power and synthesis gas co-generation from methane with zero waste gas emission,” *Angewandte Chemie International Edition*, vol. 50, no. 8, pp. 1792–1797, 2011.
- [222] Švarcová, S., Wiik, K., Tolchard, J., Bouwmeester, H. J., y Grande, T., “Structural instability of cubic perovskite $\text{Ba}_{0.9}\text{Sr}_{0.1}\text{Ti}_{0.9}\text{Fe}_{0.1}\text{O}_{3-\delta}$,” *Solid State Ionics*, vol. 178, no. 35-36, pp. 1787–1791, 2008.
- [223] Shao, Z. y Tadé, M. O., “Cathodes for it-sofcs,” en *Intermediate-Temperature Solid Oxide Fuel Cells*, pp. 59–126, Springer, 2016.
- [224] Naumovich, E., Patraakeev, M., Kharton, V., Yaremchenko, A., Logvinovich, D., y Marques, F., “Oxygen nonstoichiometry in $\text{La}_{2-x}\text{Ni}_x\text{O}_{4-\delta}$ ($x = \text{Cu, Co}$) under oxidizing conditions,” *Solid state sciences*, vol. 7, no. 11, pp. 1353–1362, 2005.
- [225] Zhou, W., Shao, Z., Ran, R., y Cai, R., “Novel $\text{Sr}_{0.2}\text{Co}_{0.8}\text{O}_{3-\delta}$ as a cathode material for low temperature solid-oxide fuel cell,” *Electrochemistry communications*, vol. 10, no. 10, pp. 1647–1651, 2008.
- [226] Lim, C., Sengodan, S., Jeong, D., Shin, J., y Kim, G., “Investigation of the Fe doping effect on the B-site of the layered perovskite $\text{Pr}_{0.8}\text{Ca}_{0.2}\text{Co}_{2}\text{O}_{5-\delta}$ for a promising cathode material of the intermediate-temperature solid oxide fuel cells,” *International Journal of Hydrogen Energy*, vol. 44, no. 2, pp. 1088–1095, 2019.
- [227] Irshad, M., Idrees, R., Siraj, K., Shakir, I., Rafique, M., ul Ain, Q., y Raza, R., “Electrochemical evaluation of mixed ionic electronic perovskite cathode $\text{La}_{1-x}\text{Co}_x\text{O}_{3-\delta}$ for it-sofc synthesized by high temperature decomposition,” *International Journal of Hydrogen Energy*, vol. 46, no. 17, pp. 10448–10456, 2021.
- [228] Schultz, A. M., Brown, T. D., Buric, M. P., Lee, S., Gerdes, K., y Ohodnicki, P. R., “High temperature fiber-optic evanescent wave hydrogen sensors using La-doped SrTiO_3 for sofc applications,” *Sensors and Actuators B: Chemical*, vol. 221, pp. 1307–1313, 2015.
- [229] Meyer, R. y Waser, R., “Resistive donor-doped SrTiO_3 sensors: I, basic model for a fast sensor response,” *Sensors and Actuators B: chemical*, vol. 101, no. 3, pp. 335–345, 2004.
- [230] Kim, J., Choi, S., Jun, A., Jeong, H. Y., Shin, J., y Kim, G., “Chemically stable perovskites as cathode materials for solid oxide fuel cells: La-doped $\text{Ba}_{0.5}\text{Sr}_{0.5}\text{Co}_{0.8}\text{Fe}_{0.2}\text{O}_{3-\delta}$,” *ChemSusChem*, vol. 7, no. 6, pp. 1669–1675, 2014.
- [231] Müller, P., Störmer, H., Dieterle, L., Niedrig, C., Ivers-Tiffée, E., y Gerthsen, D., “Decomposition pathway of cubic $\text{Ba}_{0.5}\text{Sr}_{0.5}\text{Co}_{0.8}\text{Fe}_{0.2}\text{O}_{3-\delta}$ between 700° C and 1000° C analyzed by electron microscopic techniques,” *Solid State Ionics*, vol. 206, pp. 57–66, 2012.
- [232] Hayashi, H., “Structural consideration on the ionic conductivity of perovskite-type

- oxides,” *Solid State Ionics*, vol. 122, no. 1-4, pp. 1–15, 1999, [doi:10.1016/s0167-2738\(99\)00066-1](https://doi.org/10.1016/s0167-2738(99)00066-1).
- [233] Zhogin, I., Nemudry, A., Glyanenko, P., Kamenetsky, Y. M., Bouwmeester, H., y Ismagilov, Z., “Oxygen diffusion in nanostructured perovskites,” *Catalysis today*, vol. 118, no. 1-2, pp. 151–157, 2006.
- [234] Savinskaya, O., Nemudry, A., y Lyakhov, N., “Synthesis and properties of $\text{srfe}_{1-x}\text{m}_x\text{o}_{3-z}$ ($m = \text{mo}, \text{w}$) perovskites,” *Inorganic Materials*, vol. 43, no. 12, pp. 1350–1360, 2007.
- [235] Zhou, Q., Zhang, L., y He, T., “Cobalt-free cathode material $\text{srfe}_{0.9}\text{nb}_{0.1}\text{o}_{3-\delta}$ for intermediate-temperature solid oxide fuel cells,” *Electrochemistry Communications*, vol. 12, no. 2, pp. 285–287, 2010.
- [236] Popov, M., Starkov, I., Bychkov, S., y Nemudry, A., “Improvement of $\text{ba}_{0.5}\text{sr}_{0.5}\text{co}_{0.8}\text{fe}_{0.2}\text{o}_{3-\delta}$ functional properties by partial substitution of cobalt with tungsten,” *Journal of Membrane Science*, vol. 469, pp. 88–94, 2014.
- [237] Artimonova, E., Savinskaya, O., y Nemudry, A., “Effect of b-site tungsten doping on structure and oxygen permeation properties of $\text{srco}_{0.8}\text{fe}_{0.2}\text{o}_{3-\delta}$ perovskite membranes,” *Journal of the European Ceramic Society*, vol. 35, no. 8, pp. 2343–2349, 2015.
- [238] Belenkaya, I., Matvienko, A., y Nemudry, A., “Phase transitions and microstructure of ferroelastic $\text{miec oxide srco}_{0.8}\text{fe}_{0.2}\text{o}_{2.5}$ doped with highly charged nb/ta (v) cations,” *Journal of Materials Chemistry A*, vol. 3, no. 46, pp. 23240–23251, 2015.
- [239] Cascos, V., Martínez-Coronado, R., y Alonso, J., “New nb -doped $\text{srco}_{1-x}\text{nb}_x\text{o}_{3-\delta}$ perovskites performing as cathodes in solid-oxide fuel cells,” *International journal of hydrogen energy*, vol. 39, no. 26, pp. 14349–14354, 2014.
- [240] Zhou, Q., He, T., He, Q., y Ji, Y., “Electrochemical performances of labacufo_{5+x} and labacuco_{5+x} as potential cathode materials for intermediate-temperature solid oxide fuel cells,” *Electrochemistry Communications*, vol. 11, no. 1, pp. 80–83, 2009.
- [241] Lei, N., Ma, P., Yu, B., Li, S., Dai, J., y Jiang, G., “Anion-intercalated supercapacitor electrode based on perovskite-type $\text{srb}_{0.875}\text{nb}_{0.125}\text{o}_3$ ($b = \text{mn}, \text{co}$),” *Chemical Engineering Journal*, vol. 421, p. 127790, 2021.
- [242] Yao, C., Zhang, H., Liu, X., Meng, J., Meng, J., y Meng, F., “A niobium and tungsten co-doped $\text{srfe}_{0.3-\delta}$ perovskite as cathode for intermediate temperature solid oxide fuel cells,” *Ceramics International*, vol. 45, no. 6, pp. 7351–7358, 2019.
- [243] Jiang, S., Sunarso, J., Zhou, W., Shen, J., Ran, R., y Shao, Z., “Cobalt-free $\text{srnbnx}_{1-x}\text{o}_{3-\delta}$ ($x = 0.05, 0.1$ and 0.2) perovskite cathodes for intermediate temperature solid oxide fuel cells,” *Journal of Power Sources*, vol. 298, pp. 209–216, 2015.
- [244] Porras-Vazquez, J. M., Pike, T., Hancock, C. A., Marco, J. F., Berry, F. J., y Slater,

- P. R., "Investigation into the effect of si doping on the performance of srfeo 3- δ sofc electrode materials," *Journal of Materials Chemistry A*, vol. 1, no. 38, pp. 11834–11841, 2013.
- [245] Watanabe, K., Takauchi, D., Yuasa, M., Kida, T., Shimanoe, K., Teraoka, Y., y Yamazoe, N., "Oxygen permeation properties of co-free perovskite-type oxide membranes based on bafe1- y zr y o3- δ ," *Journal of the Electrochemical Society*, vol. 156, no. 5, p. E81, 2009.
- [246] Xu, D., Dong, F., Chen, Y., Zhao, B., Liu, S., Tade, M. O., y Shao, Z., "Cobalt-free niobium-doped barium ferrite as potential materials of dense ceramic membranes for oxygen separation," *Journal of membrane science*, vol. 455, pp. 75–82, 2014.
- [247] Wang, S., Xu, J., Wu, M., Song, Z., Wang, L., Zhang, L., Yang, J., Long, W., y Zhang, L., "Cobalt-free perovskite cathode bafe0. 9nb0. 1o3- δ for intermediate-temperature solid oxide fuel cell," *Journal of Alloys and Compounds*, vol. 872, p. 159701, 2021.
- [248] Chen, K., He, S., Li, N., Cheng, Y., Ai, N., Chen, M., Rickard, W. D., Zhang, T., *et al.*, "Nb and pd co-doped la0. 57sr0. 38co0. 19fe0. 665nb0. 095pd0. 05o3- δ as a stable, high performance electrode for barrier-layer-free y2o3-zro2 electrolyte of solid oxide fuel cells," *Journal of Power Sources*, vol. 378, pp. 433–442, 2018.
- [249] Ding, H., Virkar, A. V., Liu, M., y Liu, F., "Suppression of sr surface segregation in la 1- x sr x co 1- y fe y o 3- δ : a first principles study," *Physical Chemistry Chemical Physics*, vol. 15, no. 2, pp. 489–496, 2013.
- [250] Kuyyalil, J., Newby Jr, D., Laverock, J., Yu, Y., Cetin, D., Basu, S., Ludwig, K., y Smith, K., "Vacancy assisted sro formation on la0. 8sr0. 2co0. 2fe0. 8o3- δ surfaces—a synchrotron photoemission study," *Surface Science*, vol. 642, pp. 33–38, 2015.
- [251] Meffert, M., Störmer, H., y Gerthsen, D., "Dopant-site determination in y-and sc-doped (ba0. 5sr0. 5)(co0. 8fe0. 2) o3- δ by atom location by channeling enhanced microanalysis and the role of dopant site on secondary phase formation," *Microscopy and Microanalysis*, vol. 22, no. 1, pp. 113–121, 2016.
- [252] Rached, H., Bendaoudia, S., y Rached, D., "Investigation of iron-based double perovskite oxides on the magnetic phase stability, mechanical, electronic and optical properties via first-principles calculation," *Materials Chemistry and Physics*, vol. 193, pp. 453–469, 2017.
- [253] Eibschütz, M., Shtrikman, S., y Treves, D., "Mössbauer studies of fe 57 in orthoferrites," *Physical review*, vol. 156, no. 2, p. 562, 1967.
- [254] Mahadevan, P., Shanthi, N., y Sarma, D., "Electronic structure of and from ab initio spin-polarized calculations," *Journal of Physics: Condensed Matter*, vol. 9, no. 15, p. 3129, 1997.
- [255] Arakawa, T., Kurachi, H., y Shiokawa, J., "Physicochemical properties of rare earth perovskite oxides used as gas sensor material," *Journal of materials science*, vol. 20,

no. 4, pp. 1207–1210, 1985.

- [256] Carotta, M. C., Butturi, M. A., Martinelli, G., Sadaoka, Y., Nunziante, P., y Traversa, E., “Microstructural evolution of nanosized lafeo3 powders from the thermal decomposition of a cyano-complex for thick film gas sensors,” *Sensors and Actuators B: Chemical*, vol. 44, no. 1-3, pp. 590–594, 1997.
- [257] Atkinson, A., “Chemically-induced stresses in gadolinium-doped ceria solid oxide fuel cell electrolytes,” *Solid State Ionics*, vol. 95, no. 3-4, pp. 249–258, 1997.
- [258] Hendriksen, P. V., Larsen, P. H., Mogensen, M., Poulsen, F. W., y Wiik, K., “Prospects and problems of dense oxygen permeable membranes,” *Catalysis Today*, vol. 56, no. 1-3, pp. 283–295, 2000.
- [259] Montross, C. S., Yokokawa, H., Dokiya, M., y Bekessy, L., “Mechanical properties of magnesia-doped lanthanum chromite versus temperature,” *Journal of the American Ceramic Society*, vol. 78, no. 7, pp. 1869–1872, 1995.
- [260] Paulik, S., Baskaran, S., y Armstrong, T., “Mechanical properties of calcium-and strontium-substituted lanthanum chromite,” *Journal of materials science*, vol. 33, no. 9, pp. 2397–2404, 1998.
- [261] Mizusaki, J., Sasamoto, T., Cannon, W., y Bowen, H. K., “Electronic conductivity, seebeck coefficient, and defect structure of lafeo3,” *Journal of the American Ceramic Society*, vol. 65, no. 8, pp. 363–368, 1982.
- [262] ten Elshof, J. E., Bouwmeester, H. J., y Verweij, H., “Oxygen transport through la1-xrxfeo3- δ membranes. i. permeation in air/he gradients,” *Solid State Ionics*, vol. 81, no. 1-2, pp. 97–109, 1995.
- [263] Kleveland, K., Orlovskaya, N., Grande, T., Moe, A. M. M., Einarsrud, M.-A., Breder, K., y Gogotsi, G., “Ferroelastic behavior of la_{1-x}co_xo₃-based ceramics,” *Journal of the American Ceramic Society*, vol. 84, no. 9, pp. 2029–2033, 2001.
- [264] Aizu, K., “Possible species of “ferroelastic” crystals and of simultaneously ferroelectric and ferroelastic crystals,” *Journal of the Physical society of Japan*, vol. 27, no. 2, pp. 387–396, 1969.
- [265] Fossdal, A., Einarsrud, M.-A., y Grande, T., “Mechanical properties of lafeo3 ceramics,” *Journal of the european ceramic society*, vol. 25, no. 6, pp. 927–933, 2005.
- [266] Okamura, T., Shimizu, S., Mogi, M., Tanimura, M., Furuya, K., y Munakata, F., “Elastic properties of sr-and mg-doped lanthanum gallate at elevated temperature,” *Journal of power sources*, vol. 130, no. 1-2, pp. 38–41, 2004.
- [267] Stevenson, J. W., Armstrong, T. R., Pederson, L. R., Li, J., Lewinsohn, C., y Baskaran, S., “Effect of a-site cation nonstoichiometry on the properties of doped lanthanum gallate,” *Solid State Ionics*, vol. 113, pp. 571–583, 1998.
- [268] Sammes, N. M., Keppeler, F. M., Näfe, H., y Aldinger, F., “Mechanical properties of

- solid-state-synthesized strontium-and magnesium-doped lanthanum gallate,” *Journal of the American Ceramic Society*, vol. 81, no. 12, pp. 3104–3108, 1998.
- [269] Khandy, S. A., Islam, I., Gupta, D. C., Khenata, R., Laref, A., y Rubab, S., “Dft understandings of structural properties, mechanical stability and thermodynamic properties of BaCo_3 perovskite,” *Materials Research Express*, vol. 5, no. 10, p. 105702, 2018.
- [270] Huang, B., Malzbender, J., y Steinbrech, R., “Thermo-mechanical properties of $\text{La}_2\text{NiO}_4 + \delta$,” *Journal of materials science*, vol. 46, no. 14, pp. 4937–4941, 2011.
- [271] Orlovskaya, N., Kleveland, K., Grande, T., y Einarsrud, M.-A., “Mechanical properties of LaCoO_3 based ceramics,” *Journal of the European Ceramic Society*, vol. 20, no. 1, pp. 51–56, 2000.
- [272] Lipinska-Chwalek, M., Malzbender, J., Chanda, A., Baumann, S., y Steinbrech, R., “Mechanical characterization of porous $\text{Ba}_{0.5}\text{Sr}_{0.5}\text{Co}_{0.8}\text{Fe}_{0.2}\text{O}_{3-\delta}$,” *Journal of the European Ceramic Society*, vol. 31, no. 15, pp. 2997–3002, 2011.
- [273] Wang, L., Dou, R., Li, Y., Lu, H., Bai, M., Hall, D., y Chen, Y., “Microstructure and mechanical properties of $\text{Ba}_{0.5}\text{Sr}_{0.5}\text{Co}_{0.8}\text{Fe}_{0.2}\text{O}_{3-\delta}$ perovskite-structured oxides doped with different contents of ni,” *Materials Science and Engineering: A*, vol. 658, pp. 280–288, 2016, [doi:10.1016/j.msea.2016.02.008](https://doi.org/10.1016/j.msea.2016.02.008).
- [274] Hassan, D., Janes, S., y Clasen, R., “Proton-conducting ceramics as electrode/electrolyte materials for SOFC’s—part i: preparation, mechanical and thermal properties of sintered bodies,” *Journal of the European Ceramic Society*, vol. 23, no. 2, pp. 221–228, 2003.
- [275] Hashim, S., Mohamed, A., y Bhatia, S., “Oxygen separation from air using ceramic-based membrane technology for sustainable fuel production and power generation,” *Renewable and Sustainable Energy Reviews*, vol. 15, no. 2, pp. 1284–1293, 2011.
- [276] Teraoka, Y., Zhang, H.-M., Furukawa, S., y Yamazoe, N., “Oxygen permeation through perovskite-type oxides,” *Chemistry Letters*, vol. 14, no. 11, pp. 1743–1746, 1985.
- [277] Teraoka, Y., Nobunaga, T., y Yamazoe, N., “Effect of cation substitution on the oxygen semipermeability of perovskite-type oxides,” *Chemistry Letters*, vol. 17, no. 3, pp. 503–506, 1988.
- [278] Prado, F., Grunbaum, N., Caneiro, A., y Manthiram, A., “Effect of La^{3+} doping on the perovskite-to-brownmillerite transformation in $\text{Sr}_{1-x}\text{La}_x\text{Co}_{0.8}\text{Fe}_{0.2}\text{O}_{3-\delta}$ ($0 \leq x \leq 0.4$),” *Solid State Ionics*, vol. 167, no. 1-2, pp. 147–154, 2004.
- [279] Shao, Z., Xiong, G., Tong, J., Dong, H., y Yang, W., “Ba effect in doped $\text{Sr}(\text{Co}_{0.8}\text{Fe}_{0.2})\text{O}_{3-\delta}$ on the phase structure and oxygen permeation properties of the dense ceramic membranes,” *Separation and Purification Technology*, vol. 25, no. 1-3, pp. 419–429, 2001.
- [280] Tong, J., Yang, W., Cai, R., Zhu, B., y Lin, L., “Novel and ideal zirconium-based dense

- membrane reactors for partial oxidation of methane to syngas,” *Catalysis Letters*, vol. 78, no. 1, pp. 129–137, 2002.
- [281] Kharton, V., Viskup, A., Kovalevsky, A., Jurado, J., Naumovich, E., Vecher, A., y Frade, J., “Oxygen ionic conductivity of ti-containing strontium ferrite,” *Solid State Ionics*, vol. 133, no. 1-2, pp. 57–65, 2000.
- [282] Zhu, X., Wang, H., y Yang, W., “Novel cobalt-free oxygen permeable membrane,” *Chemical communications*, no. 9, pp. 1130–1131, 2004.
- [283] Adler, S. B., “Factors governing oxygen reduction in solid oxide fuel cell cathodes,” *Chemical reviews*, vol. 104, no. 10, pp. 4791–4844, 2004.
- [284] Fang, W., Liang, F., Cao, Z., Steinbach, F., y Feldhoff, A., “A mixed ionic and electronic conducting dual-phase membrane with high oxygen permeability,” *Angewandte Chemie International Edition*, vol. 54, no. 16, pp. 4847–4850, 2015.
- [285] Lu, Y., Zhao, H., Chang, X., Du, X., Li, K., Ma, Y., Yi, S., Du, Z., Zheng, K., y Świerczek, K., “Novel cobalt-free bafe $1-x$ gd x o $3-\delta$ perovskite membranes for oxygen separation,” *Journal of Materials Chemistry A*, vol. 4, no. 27, pp. 10454–10466, 2016.
- [286] Hwang, J., Rao, R. R., Giordano, L., Katayama, Y., Yu, Y., y Shao-Horn, Y., “Perovskites in catalysis and electrocatalysis,” *Science*, vol. 358, no. 6364, pp. 751–756, 2017.
- [287] Sengodan, S., Choi, S., Jun, A., Shin, T. H., Ju, Y.-W., Jeong, H. Y., Shin, J., Irvine, J. T., y Kim, G., “Layered oxygen-deficient double perovskite as an efficient and stable anode for direct hydrocarbon solid oxide fuel cells,” *Nature materials*, vol. 14, no. 2, pp. 205–209, 2015.
- [288] Pelosato, R., Cordaro, G., Stucchi, D., Cristiani, C., y Dotelli, G., “Cobalt based layered perovskites as cathode material for intermediate temperature solid oxide fuel cells: A brief review,” *Journal of Power Sources*, vol. 298, pp. 46–67, 2015.
- [289] Kim, G., Wang, S., Jacobson, A., Reimus, L., Brodersen, P., y Mims, C., “Rapid oxygen ion diffusion and surface exchange kinetics in prbaco 2 o $5+x$ with a perovskite related structure and ordered a cations,” *Journal of Materials Chemistry*, vol. 17, no. 24, pp. 2500–2505, 2007.
- [290] Chen, D., Ran, R., Zhang, K., Wang, J., y Shao, Z., “Intermediate-temperature electrochemical performance of a polycrystalline prbaco 2 o $5+\delta$ cathode on samarium-doped ceria electrolyte,” *Journal of Power Sources*, vol. 188, no. 1, pp. 96–105, 2009.
- [291] Deng, Z., Smit, J., Niu, H., Evans, G., Li, M., Xu, Z., Claridge, J., y Rosseinsky, M., “B cation ordered double perovskite ba 2 co 0.5 nb 0.5 o $6-\delta$ as a potential sofc cathode,” *Chemistry of Materials*, vol. 21, no. 21, pp. 5154–5162, 2009.
- [292] Zhou, W., Sunarso, J., Chen, Z.-G., Ge, L., Motuzas, J., Zou, J., Wang, G., Julbe, A., y Zhu, Z., “Novel b-site ordered double perovskite ba 2 bi 0.1 sc 0.2 co 1.7 o $6-x$ for

- highly efficient oxygen reduction reaction,” *Energy & Environmental Science*, vol. 4, no. 3, pp. 872–875, 2011.
- [293] Wang, Y., Liu, T., Fang, S., y Chen, F., “Syngas production on a symmetrical solid oxide h₂o/co₂ co-electrolysis cell with sr₂fe_{1.5}mo_{0.5}o₆–sm_{0.2}ce_{0.8}o_{1.9} electrodes,” *Journal of Power Sources*, vol. 305, pp. 240–248, 2016.
- [294] Shin, T. H., Myung, J.-H., Verbraeken, M., Kim, G., y Irvine, J. T., “Oxygen deficient layered double perovskite as an active cathode for co₂ electrolysis using a solid oxide conductor,” *Faraday Discussions*, vol. 182, pp. 227–239, 2015.
- [295] Tang, J., Zou, Z., y Ye, J., “Efficient photocatalysis on babio₃ driven by visible light,” *The Journal of Physical Chemistry C*, vol. 111, no. 34, pp. 12779–12785, 2007.
- [296] Weng, B., Xiao, Z., Meng, W., Grice, C. R., Poudel, T., Deng, X., y Yan, Y., “Bandgap engineering of barium bismuth niobate double perovskite for photoelectrochemical water oxidation,” *Advanced Energy Materials*, vol. 7, no. 9, p. 1602260, 2017.
- [297] Ge, J., Yin, W.-J., y Yan, Y., “Solution-processed nb-substituted babio₃ double perovskite thin films for photoelectrochemical water reduction,” *Chemistry of Materials*, vol. 30, no. 3, pp. 1017–1031, 2018.
- [298] Sun, N., Liu, H., Yu, Z., Zheng, Z., y Shao, C., “The la_{0.6}sr_{0.4}coo₃ perovskite catalyst for li-o₂ battery,” *Solid State Ionics*, vol. 268, pp. 125–130, 2014.
- [299] Liu, G., Chen, H., Xia, L., Wang, S., Ding, L.-X., Li, D., Xiao, K., Dai, S., y Wang, H., “Hierarchical mesoporous/macroporous perovskite la_{0.5}sr_{0.5}coo_{3-x} nanotubes: a bifunctional catalyst with enhanced activity and cycle stability for rechargeable lithium oxygen batteries,” *ACS applied materials & interfaces*, vol. 7, no. 40, pp. 22478–22486, 2015.
- [300] Lu, F., Sui, J., Su, J., Jin, C., Shen, M., y Yang, R., “Hollow spherical la_{0.8}sr_{0.2}mno₃ perovskite oxide with enhanced catalytic activities for the oxygen reduction reaction,” *Journal of Power Sources*, vol. 271, pp. 55–59, 2014.
- [301] Jung, K.-N., Jung, J.-H., Im, W. B., Yoon, S., Shin, K.-H., y Lee, J.-W., “Doped lanthanum nickelates with a layered perovskite structure as bifunctional cathode catalysts for rechargeable metal–air batteries,” *ACS applied materials & interfaces*, vol. 5, no. 20, pp. 9902–9907, 2013.
- [302] Zhao, Y., Liu, T., Shi, Q., Yang, Q., Li, C., Zhang, D., y Zhang, C., “Perovskite oxides la_{0.4}sr_{0.6}co_xmn_{1-x}o₃ (x= 0, 0.2, 0.4) as an effective electrocatalyst for lithium–air batteries,” *Green Energy & Environment*, vol. 3, no. 1, pp. 78–85, 2018.
- [303] Niihara, K., “A fracture mechanics analysis of indentation-induced palmqvist crack in ceramics,” *Journal of materials science letters*, vol. 2, no. 5, pp. 221–223, 1983.
- [304] Akbari-Fakhrabadi, A., Meruane, V., Jamshidijam, M., Gracia-Pinilla, M., Garcia, R., y Orellana, M., “Structural and mechanical properties of la_{0.6}sr_{0.4}mo_{0.1}fe_{0.9}o_{3-δ}

(m: Co, ni and cu) perovskites,” *Ceramics international*, vol. 43, no. 2, pp. 2089–2094, 2017.

- [305] Akbari-Fakhrabadi, A., Toledo, E., Canales, J., Meruane, V., Chan, S., y Gracia-Pinilla, M., “Effect of sr²⁺ and ba²⁺ doping on structural stability and mechanical properties of la₂nio_{4+δ},” *Ceramics International*, vol. 44, no. 9, pp. 10551–10557, 2018.